Aspects of the Standard Model Landscape and Post Vacuum Transition Dynamics

Rudin Petrossian-Byrne

Balliol College

University of Oxford

A thesis submitted for the degree of

Doctor of Philosophy

Hillary 2023

Statement of Originality

This thesis is wholly the work of the author except where stated. No part of this thesis has been submitted for any other qualification. Sections based on collaborative work are listed below.

Chapter 2 and section 3.2 of Chapter 3 are based on *QCD, Flavour and the De Sitter Swampland* (2020), arXiv number 2006.01144, by J. March-Russell and R. Petrossian-Byrne.

In chapter 3, section 3.3 is based on unpublished collaborative work between the author and Prof. John March-Russell.

Chapter 4 is based on *Reflections on Bubble Walls* (2022), arxiv number 2212.10572, by Isabel Garcia Garcia, Giacomo Koszegi, and Rudin Petrossian-Byrne.

Some parts of 1.3 are based on *Quantisation across bubble walls and friction* (2023), arxiv number 2310.06972, by Aleksandr Azatov, Giulio Barni, Rudin Petrossian-Byrne and Miguel Vanvlasselaer.

Abstract

The Standard Model (SM) of particle physics coupled to gravity is a phenomenologically successful effective field theory (EFT) with a number of input parameters which are arbitrary - if not severely tuned from an IR perspective - but are presumably fixed by an underlying UV theory. Several open problems guide the pursuit of new physics just beyond its borders which might or might not exist. On the other hand, the SM along with any additions, is expected to be eventually embedded within a framework that includes quantum gravity. How vast is the landscape of effective field theories - the SM one of them - which can be consistently derived therefrom and what conditions establish its boundary is currently unknown and a topic of intense research. The Standard Model landscape is defined as the space of EFTs obtained from the structure of the SM while allowing its input parameters to scan all possible values, and should correspond to exploring our neighbourhood of a supposed UV landscape.

In this thesis I review in detail the structure of the SM, and the successful standard cosmological history based on it. I then explore the SM landscape by varying Yukawa couplings, the QCD theta parameter and the Higgs mass squared parameter, focusing on whether the ensuing vacuum potentials admit long-lived meta-stable states with positive vacuum energy, a property which is conjectured to be incompatible with quantum gravity, and thus partially explain the puzzling hierarchies observed.

The only known setting to probe the existence of de Sitter meta-stable states is the possibility that during its cosmological history, the universe as a whole was once in a meta-stable state and proceeded to decay through the nucleation of bubbles of true vacuum in a first order phase transition. This can lead to observable signals such as a stochastic gravitational wave background, with a number many dedicated detectors planned to come online over the next decades. Making contact between theoretical predictions and potential signals however requires a better understanding of friction forces acting on the expanding bubbles. In this thesis I highlight the singularly peculiar reflective properties of longitudinally polarised vector particles and discuss their significant source of friction.

Contents

Dedicated to my late grandmother, Amalia Der Avanessian.

Acknowledgements

I am deeply grateful to John March-Russell, my supervisor, first of all for believing in me. For doing his utmost to support my success. For making time for me when he had none. For his honest advice and guidance, enthusiasm and support in some very tough times. Your many lessons, often condensed into incisive phrases will continue to serve me well as I go off into the world. I hope to continue to work with you for many years to come.

I consider myself very lucky and indebted to the trustees and funders of the Clarendon and Foley-Bèjar scholarships at the University of Oxford and Balliol College respectively, for providing the financial means to pursue my doctorate at Oxford.

I would like to thank my wonderful collaborators Isabel Garcia Garcia and Giacomo Kosezgi. Without her insight for the best application and his discipline of calculation the work described in the final chapter of this thesis would not have gone far.

Though stretching back some years, I would like to mention David Lynn and James Donnellan, my flat-and-course-mates during my undergraduate years. When it comes to physics, you might feel like I was the one helping you through much of those years, but I have come to realise how your good company and banter was crucial in keeping me sane and allowed me to work as hard, efficiently and happily as I did.

Finally, as I move on to the next stage of my life, I would like to acknowledge the cultural value of my doctoral experience. Because whether I will ever make any contribution to the field of any importance at all remains to be seen, but it is in some sense secondary to upholding the spirit imperceptibly acquired through the example of exceptional colleagues and hours of careful thought. For the pursuit of truth, from chasing an obstinate factor of 2 in some meaningless calculation to the grandest questions, seems to me first and foremost a beautifully humbling affair. Perhaps the best lesson learnt is that what you would like to be true, or even what you think would be good to be true, has nothing to do with what might actually be true. And you are the easiest person to fool.

Chapter 1

Introduction

1.1 The Standard Model and Beyond

By the Standard Model of particle physics we refer to the theory of fundamental microscopic physics that was established theoretically in the 1970s. In layman's terms, the SM is a list of the known 'things' in our world that can be taken to be elementary, their essential properties and the fundamental rules by which they interact. Its claim to truth lies first and foremost in its power to make quantitative predictions that agree with experiments within the current uncertainties of measurement *despite* our best efforts to find it amiss. Its much celebrated degree of success is measured by the vast and diverse range of those tests - often coupled with extraordinary precision - ranging from low energy atomic, to our most powerful particle accelerators, to astrophysical probes as well as its consistency with observations of the past history of our universe at large (see section 1.2).

1.1.1 Basic elements

The list of known elementary particles that happen to exist in our world are a set of (Weyl) fermions - primarily interacting through a number of vector bosons - and an additional scalar field, the Higgs boson, responsible for selecting the vacuum. As we will see, the fermions are grouped into *leptons*, such as the electron e [1], and *quarks* such the 'up' u and 'down' d [2] whose bound states form protons and neutrons and pions (as well as other hadronic states).

The vectors are associated to generators of the *gauge group* of the SM: a Lie group of *local* (meaning arbitrarily space-time dependent) transformations often referred to

[1] as well as its heavier cousins the muon μ and tau τ, plus a (left-handed) neutrino ν each.
[2] and heavier cousins charm & strange c, s and top & bottom t, b.

as gauge symmetries, although they are not proper symmetries of the theory in the sense of relating physically inequivalent states but rather field re-definitions describing redundancies of the field description. To every gauge symmetry there is associated however a proper symmetry when the transformation is taken to be *global* - i.e. space-time independent.

For the SM the gauge group comes in the form of a direct product of three separate groups

$$G_{\rm SM} = SU(3)_c \times SU(2)_W \times U(1)_Y \ , \tag{1.1}$$

where the first stands for colour, the second for weak and the third for hypercharge. The gauge boson associated to the Abelian $U(1)_Y$ will be denoted B_μ, while those associated to the non-Abelian groups live in the adjoint representation of the corresponding algebra, meaning they are packaged as a general element of the algebra itself,

$$W_\mu = W_\mu^i \frac{\sigma^i}{2} \ , \qquad G_\mu = G_\mu^a \frac{\lambda^a}{2} \ , \tag{1.2}$$

where λ^a and σ^i are the eight Gell-Mann and three Pauli matrices respectively - generators of the $\mathfrak{su}(2)$ and $\mathfrak{su}(3)$ algebras respectively. [3]

The fermionic fields are organised in three generations - three identical copies - as characterized by their transformations with respect to the three different sectors of the gauge group. Assigning a generation index i to each copy, these are

$$\ell^i \equiv \begin{pmatrix} e_L^i \\ \nu_L^i \end{pmatrix} \ , \ e_R^i \ , \qquad Q_L^i \equiv \begin{pmatrix} u_L^i \\ d_L^i \end{pmatrix} , \ u_R^i \ , d_R^i \ , \qquad \text{where} \quad i = 1,2,3 \ , \tag{1.3}$$

where again we have made a separation between leptons and quarks. Each u^i, d^i field listed lives in a fundamental representation of $SU(3)_c$ - I am and will continue to suppress these colour indices. Q_L^i and ℓ^i, along with the Higgs field H transform as $SU(2)_W$ doublets. These representations, as well as the $U(1)$ charge assignments are summarized for convenience in fig. 1.1.

1.1.2 The Lagrangian

Not all interacting quantum mechanical theories admit a local Lagrangian description. [4] The SM does. What this means is that the theory has a weakly coupled description

[3] Generally the generators T_r^x of the representation r of a Lie algebra satisfy $\mathrm{Tr} T_r^x T_r^y = C(r)\, \delta^{xy}$. It is conventional in particle physics to choose $C(r) = 1/2$ when r is the fundamental representation.

[4] For example, strongly interacting conformal field theories, which don't possess a weak coupling limit

Field\Group	$SU(3)_c$	$SU(2)_W$	$U(1)_Y$	$U(1)_{em}$
$\ell^i \equiv \begin{pmatrix} e^i_L \\ \nu^i_L \end{pmatrix}$	1	2	-1	$\begin{pmatrix} 0 \\ -1 \end{pmatrix}$
e^i_R	1	1	-2	-1
$Q^i_L \equiv \begin{pmatrix} u^i_L \\ d^i_L \end{pmatrix}$	3	2	$+1/3$	$\begin{pmatrix} +2/3 \\ -1/3 \end{pmatrix}$
u^i_R	3	1	$+4/3$	$+2/3$
d^i_R	3	1	$-2/3$	$-1/3$
H	1	2	1	0

Figure 1.1: Matter content of the SM and their representations with respect to the gauge group heading each column. For the non-Abelian groups, '1' signifies the trivial singlet representation. The '3' and '2' stand for the fundamental representations of $SU(3)$ and $SU(2)$ respectively. For the Abelian $U(1)$ groups what is tabulated are the associated charges. Color indices have been suppressed. Figure adapted from [1].

at some energy scale. There will be more to say about this later. The Standard Model Lagrangian is given by

$$\begin{aligned}\mathcal{L}_{SM} = &-\frac{1}{4}B_{\mu\nu}B^{\mu\nu} - \frac{1}{2}\mathrm{Tr}W_{\mu\nu}W^{\mu\nu} - \frac{1}{2}\mathrm{Tr}G_{\mu\nu}G^{\mu\nu} \\ &+ i\overline{Q}^j_L \not{D} Q^j_L + i\overline{u}^j_R \not{D} u^j_R + i\overline{d}^j_R \not{D} d^j_R + i\overline{\ell}^j \not{D} \ell^j + i\overline{e}^j_R \not{D} e^j_R \\ &+ D_\mu H^\dagger D^\mu H - V_H(|H|) \\ &+ Y^{ij}_u \overline{Q}^i_L i\sigma^2 H^* u^j_R + Y^{ij}_d \overline{Q}^i_L H d^j_R + Y^{ij}_l \overline{\ell}^i H e^j_R \ .\end{aligned} \tag{1.4}$$

I will presently proceed to somewhat unpack this expression line by line, with subsequent subsections dedicated to further details. I will also highlight what are the SM input parameters - those constants which are not calculable from principle at present but have to be taken from experimental measurement.

The first line above represents the kinetic terms for the gauge bosons, written in terms of the rank-2 anti-symmetric 'field strength' tensors

$$\begin{aligned} W_{\mu\nu} &= \partial_\mu W_\nu - \partial_\nu W_\mu - ig[W_\mu, W_\nu] \ , \\ G_{\mu\nu} &= \partial_\mu G_\nu - \partial_\nu G_\mu - ig_s[G_\mu, G_\nu] \ , \\ B_{\mu\nu} &= \partial_\mu B_\nu - \partial_\nu B_\mu \ , \end{aligned} \tag{1.5}$$

and the trace operation acts over algebra elements. Notice that the field strengths for the weak and strong gauge bosons contain the coupling constants g, g_s reflecting

the well-known fact that non-Abelian gauge theories are intrinsically self-interacting. These, along with the hypercharge coupling g', are the input parameters of the gauge sector.

The second line represents the kinetic terms for the fermionic matter fields as well as their interactions with the gauge bosons. These are neatly condensed in simple format by using the *gauge covariant derivative*[5] $D_\mu = \partial_\mu - ig^x A^x_\mu T^x$ where T^x are the generators of the gauged group in the representation appropriate to the field that D_μ is acting on. As an example, for the left-handed quark doublet Q^i_L

$$D_\mu Q^i_L = \left(\partial_\mu - ig'\frac{1}{2}q_Y B_\mu - igW^j_\mu\frac{\sigma^j}{2} - ig_s G^a_\mu\frac{\lambda^a}{2}\right)Q^i_L \tag{1.6}$$

where the factor of $q_Y = 1/6$ is the hypercharge of Q^i_L.

The third line describes the Higgs boson, the only elementary scalar field in the SM. Its kinetic term and coupling to gauge bosons is again captured simultaneously via covariant derivative. The potential $V_H(|H|)$ is a function of the gauge singlet quantity $H^\dagger H$. We will have much more to say about this in section 1.1.3.

The fourth and final line are the Yukawa couplings between the Higgs boson and the fermionic matter fields. The three Yukawa matrices $Y_{u,d,l}$ account for most of the input parameters in the SM. Although not often highlighted in this way, these terms can be thought of as a new fundamental force between matter states in addition to the usual four taught in school.

Notice that as written in eq. (1.4) none of the fermionic degrees of freedom have any mass terms. This is because eq. (1.4) is not actually the correct field basis to describe our world, as discussed in the next section. The physics of the SM can be separated into two qualitatively different sectors, which will be the subject of section 1.1.3 and section 1.1.5.

1.1.3 The Electroweak Sector

I will continue this introduction to the SM by first discussing in more detail the dynamics associated to the $SU(2)_W \times U(1)_Y$ part of the gauge group known as the 'electroweak' sector. Its characteristic length scales $\sim (10^2\,\mathrm{GeV})^{-1}$ are the smallest in the SM. Moreover, in contrast to $SU(3)_c$, it affects both leptons and quarks.

[5]The term is justified by a geometric interpretation.

The first thing to notice is that the theory is *chiral* - it distinguishes between left and right-handed fields. In fact, the $SU(2)_W$ part of the group *only* talks to the left-handed quarks and leptons. By this I mean that only the u_L^i, d_L^i and e_L^i, ν_L^i are in non-trivial representations as can be seen from fig. 1.1. This simple fact means that parity is 'maximally' violated in microscopic interactions. This came as an extraordinary shock when it was first discovered in beta decay [2].

In addition to the fermionic matter, we have a scalar field in the doublet representation of $SU(2)_W$ - the Higgs boson - which plays a fundamental role in the theory of electroweak interactions, in that it is responsible for spontaneously breaking $SU(2)_W \times U(1)_Y$ down to $U(1)_{\text{em}}$. This follows from the fact that the gauge invariant quantity $H^\dagger H$, as we will motivate further down, has a non-zero vacuum expectation value (vev) in the true vacuum of the theory:

$$\langle H^\dagger H \rangle = \frac{v^2}{2} \ , \qquad \text{where} \quad v \approx 246.22\,\text{GeV} \ . \tag{1.7}$$

Because of this non-trivial background, we cannot make sense of perturbation theory in terms of the Higgs field as written in the basis eq. (1.4). We must rather expand H around a field configuration H_0 satisfying eq. (1.7) and thus successfully treat its fluctuations as perturbative quantum fields. There is not a unique H_0 however, but rather a three-parameter continuous family of vacua - labelled by different H_0 - related by the $SU(2)_W$ transformations. Our embarrassment in choosing which specific H_0 to expand around is the manifestation of *spontaneous symmetry breaking* (SSB). Although the theory is invariant under a symmetry group, a choice of vacuum has to be made, which breaks the symmetry. Despite the fact that all choices lead to equivalent physics (by symmetry), the vacuum is no longer invariant under those transformations. A very common choice is

$$H_0 = \frac{1}{\sqrt{2}} \begin{pmatrix} 0 \\ v \end{pmatrix} \ , \quad \Longrightarrow \quad H = \frac{1}{\sqrt{2}} \begin{pmatrix} h_1 + i h_2 \\ v + h + i h_3 \end{pmatrix} \ , \tag{1.8}$$

where the h_i are the three massless 'Nambu-Goldstone boson' (NGB) field directions, while h describes the massive Higgs boson proper - the one discovered at the LHC . As is well known, Goldstone's theorem predicts that in theories with SSB there exist a number of massless scalar fields equal to the number of symmetry generators broken by the vacuum. Examining the action of $SU(2)_W \times U(1)_Y$ on H_0 it easy to see the surviving generator is

$$Q = \frac{\sigma^3}{2} + Y \ , \tag{1.9}$$

which defines the familiar $U(1)$ of electromagnetism. Thus arise the electric charge assignments in fig. 1.1. In theories of SSB of gauge theories the massless scalars of Goldstone's theorem are not actual physical dof but are 'eaten' by the gauge bosons associated to the broken generators. In the process, those gauge bosons become massive and the total number of dof remains constant, as it should. The new mass terms are found in the Higgs kinetic term

$$\begin{aligned}\mathcal{L}_{\rm SM} &\supset D_\mu H^\dagger D^\mu H \qquad (1.10)\\ &\supset \frac{1}{8}v^2\left(g^2 W^1_\mu W^{1,\mu} + g^2 W^2_\mu W^{2,\mu} + g^2 W^3_\mu W^{3,\mu} - 2gg' W^3_\mu B^\mu + g'^2 B_\mu B^\mu\right)\\ &= \frac{1}{2}\left(m_W^2 W^*_\mu W^\mu + m_Z^2 Z_\mu Z^\mu\right) \qquad (1.11)\end{aligned}$$

where in going to the third line I have diagonalised the mass matrix, defining the Z_μ boson and familair photon A_μ in terms of the weak angle $\tan\theta_W = g'/g$ as

$$\begin{aligned} Z_\mu &= \cos\theta_W W^3_\mu - \sin\theta_W B_\mu \ ,\\ A_\mu &= \cos\theta_W W^3_\mu + \sin\theta_W B_\mu \ ,\end{aligned} \qquad (1.12)$$

as well as thee electrically charged $W_\mu = (W^1_\mu + iW^2_\mu)/\sqrt{2}$ vector boson, and defined their masses in terms of the original parameters.

$$m_W^2 = \frac{1}{2}g^2v^2 \ , \qquad m_Z^2 = \frac{1}{2}v\sqrt{g^2+g'^2} \ . \qquad (1.13)$$

The electromagnetic coupling associated to the surviving photon A_μ instead is given by $e = g\sin\theta_W$.

Expanding around the Higgs vev, mass for all the fermions (except the neutrinos) emerge from the Yukawa interactions in eq. (1.4)

$$\mathcal{L}_{\rm SM} \supset -\frac{v}{\sqrt{2}}\left(Y_u^{ij}\overline{u}^i_L u^j_R + Y_d^{ij}\overline{d}^i_L d^j_R + Y_l^{ij}\overline{e}^i_L e^j_R\right) + \text{h.c.} \ . \qquad (1.14)$$

Each of the mass matrices Y in principle are completely arbitrary. They can be diagonalised via bi-unitary transformations. Focusing on the quarks, the change of basis is

$$u^i_{L,R} \to U^{ij}_{L,R} u^j_{L,R} \ , \qquad d^i_{L,R} \to D^{ij}_{L,R} d^j_L \ , \qquad (1.15)$$

$$Y_u \to \mathbb{Y}_u = U_L^\dagger Y_u U_R \ , \qquad Y_u \to \mathbb{Y}_d = D_L^\dagger Y_d D_R \ , \qquad (1.16)$$

where $U_{L,R}$ and $D_{L,R}$ are unitary matrices and $\mathbb{Y}_{u,d}$ are real and diagonal. While the analogous diagonalisation of Y_ℓ for the leptons leaves the rest of $\mathcal{L}_{\rm SM}$ invariant,[6] this

[6]This fundamentally a consequence of neutrinos being massless in the SM.

is not so for the quarks, resulting in the inter-generation mixing reappearing in the weak interactions

$$\mathcal{L}_{\rm SM} \supset \frac{g}{\sqrt{2}} V^{ij}_{\rm CKM} \overline{u}^i \gamma^\mu W^*_\mu d^j \ + \ \text{h.c.} \tag{1.17}$$

where $V_{\rm CKM} = U_L^\dagger D_L$ is the *Cabibbo-Kobayashi-Maskawa* (CKM) matrix. The latter is characterised by four independent angles, one of which is the only known source of CP-violation in the SM. The basis of eq. (1.17), is referred to as the 'mass basis' (in virtue of the mass matrix being diagonal) while the previous one (where flavour interactions are diagonal) is the 'flavour basis'.

The Higgs potential: We have discussed the consequences of the non-zero Higgs vev. In practice, the vacuum is selected by the minimum of the Higgs potential $V_H(|H|)$ so that the statement of eq. (1.7) is equivalent to

$$V_H(|H|) \qquad \text{has a minimum at} \qquad |H| = v/\sqrt{2} \tag{1.18}$$

I have thus far delayed the discussion of the explicit form of V_H because, beyond this crucial role in spontaneous symmetry breaking, the Higgs potential is currently the least experimentally constrained and theoretically understood ingredient of known particle physics. In the context of the Standard Model, the usual Landau-Ginzburg form is implied

$$V_H(|H|) = -m_H^2 H^\dagger H + \lambda (H^\dagger H)^2 = \lambda \left(H^\dagger H - \frac{v^2}{2} \right)^2 \ , \tag{1.19}$$

where $v = m_H/\sqrt{\lambda}$. This indeed is fixed if we demand renormalizability of the SM. Notice a 'cubic' $|H|^3$ term would naively be renormalizable but would introduce non-analyticity to the potential, essentially making the theory strongly coupled at the origin [3]. After expanding around a proper vacuum eq. (1.8) the potential of the physical Higgs is of the form

$$V_H = \frac{1}{2} m_H^2 h^2 + k_3 \frac{m_H^2}{2v^2} h^3 + k_4 \frac{1}{4} \frac{m_H^2}{2v^2} h^4 + \dots \ , \tag{1.20}$$

where I have parameterised possible deviations of the cubic and quartic self-interactions from those fixed by SM potential of eq. (1.19) by the dimensionless coefficients k_3, k_4 as is the convention, where $k_3 = k_4 = 1$ corresponds to the SM. m_H has been measured at the LHC with the present precision of $125.25 \pm 0.17\,\text{GeV}$, while v is known very accurately via Fermi's constant from weak decays. In fig. 1.2 I graphically compare the usually quoted potential of eq. (1.19) with the actual experimental bounds.[7] The

[7] This way of thinking about the Higgs potential arose from discussions between the author and Nathaniel Craig and will appear more rigorously in forthcoming work.

potential for BSM hints coming from precise measurements of the Higgs self-coulings is a topic of growing interest [4, 5].

1.1.4 Beta functions

A fundamental fact in perturbative quantum field theory is that interaction couplings are not fixed numbers but should be thought of as functions of renormalization scale μ - loosely, the characteristic energy scale of processes we wish to describe. This 'running' of a coupling is captured by its beta function.

The one-loop beta function for the gauge coupling $\mathfrak{g}(\mu)$ of a gauge theory based on the non-Abelian group $\mathbb{G}$ with n_f (n_s) active[8] Weyl fermions (complex scalars) in representation r is given by

$$\frac{d\mathfrak{g}^2}{d\ln\mu^2} = -\frac{\mathfrak{g}^4}{(4\pi)^2}\left(\frac{11}{3}C_2(\mathbb{G}) - \frac{2}{3}n_f C(r) - \frac{1}{3}n_s C(r)\right) , \tag{1.21}$$

where $C_2(\mathbb{G})$ is the quadratic Casimir operator for the adjoint representation of the group.[9] The same expression can be applied to the abelian $U(1)$, with $C_2 \to 0$ and for each separate contribution $C(r) \to q^2/2$, where q is the charge of the field.

It is thus straightforward to compute the one loop beta functions for the SM gauge couplings above the scale of electroweak symmetry breaking

$$\frac{dg'^2(\mu)}{d\ln\mu^2} = \frac{g'^4}{(4\pi)^2}\frac{41}{10} , \tag{1.22}$$

$$\frac{dg^2(\mu)}{d\ln\mu^2} = -\frac{g^4}{(4\pi)^2}\frac{19}{6} , \tag{1.23}$$

$$\frac{dg_s^2(\mu)}{d\ln\mu^2} = -\frac{g^4}{(4\pi)^2}7 . \tag{1.24}$$

where particular attention should be payed to the difference in signs. The beta functions require an initial condition - the value of the couplings at a particular scale μ_0 - which is extracted from experiment. For example, at the top mass $m_t \approx 173\,\text{GeV}$ we have the values [9]

$$g'(\mu = m_t) = 0.35830 , \tag{1.25}$$

$$g(\mu = m_t) = 0.64779 , \tag{1.26}$$

$$g_s(\mu = m_t) = 1.16660 . \tag{1.27}$$

[8] Meaning their mass is $\lesssim \mu$.

[9] Defined by $T^x_{\text{adj}}T^x_{\text{adj}} = C_2(\mathbb{G})\mathbb{1}$. For $SU(N)$, we have $C_2(G) = N$.

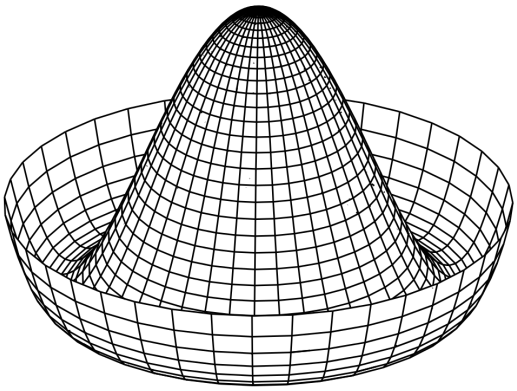

(a)

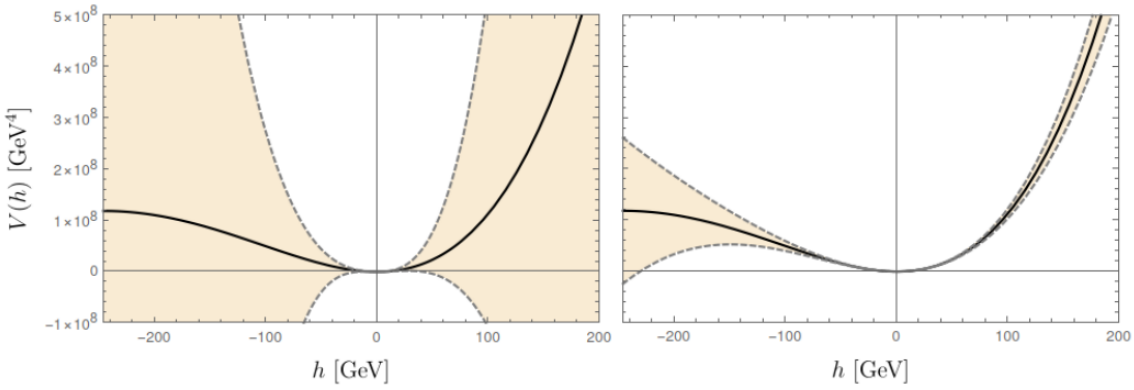

(b)

Figure 1.2: Above is the usual 'Mexican-hat' schematic picture for the Higgs potential. In reality, our knowledge of the exact shape of $V_H(h)$ is currently quite limited. Combining the latest CMS and ATLAS measurements [6] gives $k_3 \approx 4 \pm 10$ at present. The 'High Luminosity' (HL) upgrade of the LHC is projected to increase sensitiviy to $k_3 \approx 1 \pm 0.5$ [7]. A direct measurement of k_4 at accelerators for now seems hopeless (see however [8] for the possibility of indirect constraints at future colliders.) and the only absolute bound (naively) comes from unitary. Fixing $k_4 = 1$, the uncertainty in the potential arsing from k_3 alone is shown at present (left panel) and at HL (right panel).

Consider first the positive sign in the running of the hypercharge coupling $g'(\mu)$. Its obvious consequence is that the strength of the coupling grows with energy - in the UV. It is easy to integrate eq. (1.22) and find that g' blows up at some large finite scale. What this means is that the theory is becoming strongly coupled and already before it blows up when $g'^2 \sim 4\pi$ the perturbative result we are integrating should no longer be valid. Not much fuss is usually made of this as it lies above the Planck scale.[10]

The negative sign of the beta functions for g, g_s on the other hand means that these couplings are growing in the IR. However, at scales when g is still small, the Higgs mechanism described in section 1.1.3 means that g is no longer the proper coupling to track further down. The combination of g and g' giving the coupling of the surviving abelian $U(1)_{\rm em}$ then shrinks in the UV until the scale of the lightest charged particle - the electron - and remains constant thereafter.

The colour coupling g_s on the other hand continues to grow in the IR, where it indeed becomes strongly coupled. This will be the subject of the following section.

1.1.5 QCD

In this section I shall focus on the dynamics of the $SU(3)_c$ colour sector of the gauge group known as quantum chromo-dynamics (QCD). Only quarks partake in its interactions, so we shall ignore all other degrees of freedom and study the quark sector after the SSB of EW interactions has taken place. I will start by introducing new notation to describe the left and right-handed quarks in terms of a single multiplet

$$q_L = (u_L, d_L, c_L, s_L, t_L, b_L)^T \ , \tag{1.28}$$

and similarly for q_R. In these terms the QCD Lagrangian is neatly packaged as

$$\mathcal{L}_{\rm QCD} = i\, \overline{q}_L \not{D}_c q_L + i\, \overline{q}_R \not{D}_c q_R - \overline{q}_L M_q q_R + \text{h.c.} \tag{1.29}$$

where M_q is the quark mass matrix and I have stressed that $\not{D}_c = \gamma^\mu(\partial_\mu - i g_s G_\mu)$ only contains gluons.

As mentioned at the end of section 1.1.4, the negative sign of the QCD beta function means the coupling grows in the IR. Integrating eq. (1.24) and defining the true perturbative coupling $\alpha_s = g_s^2/(4\pi)^2$ gives

$$\alpha_s(\mu) = \frac{\alpha_s^0}{1 + 14(\alpha_s^0/2\pi)\ln(\mu/\mu_0)} \tag{1.30}$$

[10] Moreover, new physics is generally expected to kick in well below $M_{\rm pl}$.

which relates the coupling at arbitrary scale μ to the coupling $\alpha_s^0 = \alpha_s(\mu_0)$ at an initial fixed scale μ_0. Choosing $\mu_0 = m_t$ as in eq. (1.25) we can see that QCD becomes strongly coupled $\alpha_s \sim 1$ at a scale $\Lambda_{\rm QCD} \equiv \mu \approx 100\,{\rm MeV}$. Beyond this point, the description of QCD dynamics in terms of quarks becomes hopelessly non-perturbative. Indeed, we do not observe free (color-charged) quarks around us but rather their color-singlet bound states of three quarks (baryons, such as protons and neutrons) and two quarks (mesons, such as pions). In this sense, the strong force is said to be *confining*.

On top of confinement, the vacuum of QCD exhibits *chiral condensation*, captured by the non-zero vev of the following quark bilinear

$$\langle \overline{q}_R^j q_L^i \rangle = C_0 \delta^{ij} \ , \tag{1.31}$$

where $C_0 \sim \Lambda_{\rm QCD}^3$. If we momentarily ignore in eq. (1.29) the mass terms of the three lightest quarks u, d, s (for which it makes sense to treat their mass as perturbations on top of the QCD dynamics , set by the scale of $\Lambda_{\rm QCD}$), QCD has a symmetry group given by

$$G_{\rm QCD} = SU(3)_L \times SU(3)_R \times U(1)_V \ , \tag{1.32}$$

where $SU(3)_{L,R}$ acts on the left and right handed fields independently, $U(1)_V$ is a vectorially acting[11] common phase redefinition, while its axial counterpart $U(1)_A$ does not appear since it is anomalous (i.e. broken at the quantum theory level, which can be seen for instance by the non-invariance of the path integral measure). The chiral condensate is said to induce (spontaneous) *chiral symmetry breaking* by the fact that, the vacuum section 1.1.5 is not invariant under the entirety of $G_{\rm QCD}$, but breaks it down to the vectorially acting subgroup $H_{\rm QCD}$

$$G_{\rm QCD} \to H_{\rm QCD} = SU(3)_V \ . \tag{1.33}$$

Thus, again by Goldstones theorem, we expect 8 Nambu-Goldstone bosons in the IR of the theory. Although some of the symmetry transformations of $G_{\rm QCD}$ are gauged in the SM by the weak interactions, they are spontaneously broken by the Higgs potential at the much higher scales of v, so that in practice $G_{\rm QCD}$ should now be thought of as a purely global symmetry. Therefore these NGBs are indeed real and identified with the lightest spectrum of mesons. The small explicit breaking of $G_{\rm QCD}$

[11] In the sense of acting identically on left and right handed fields. In contrast, for axial transformations the transformation on right handed fields is the inverse of the transformation on left-handed fields.

by the non-zero mass terms for u, d, s in eq. (1.29) means these PNGBs (P for *Pseudo*) are not exactly massless. Further details of this will be developed in chapter 2.

In section 3.3 we will discuss in depth what happens if the Higgs were not present and QCD was the sole responsible for the breaking of $SU(2)_W \times U(1)_Y$.

Before moving on I will discuss an extra term which might have appeared in the SM lagrangian but does not. We shall be particularly interested in its use in chapter 2 when we start exploring worlds with slightly different physics.

The Theta term. Gell-Mann is said to have coined the phrase 'anything that is not forbidden by symmetry is mandatory'. Therefore, given the symmetries of the SM as a whole, we would seem compelled to add the following parity and CP violating term

$$\mathcal{L}_{\rm SM} \overset{?}{\supset} \frac{g_s^2}{32\pi^2}\theta\, G_{\mu\nu}\tilde{G}^{\mu\nu} \tag{1.34}$$

where $\tilde{G}^{\mu\nu} = \epsilon^{\mu\nu\rho\sigma}G_{\rho\sigma}$ is the dual field strength tensor and θ_0 is a new coupling - an angle . Although eq. (1.34) can be written as a total derivative and therefore has no classical effect, in quantum mechanics it does contribute non-perturbatively - for example, to an eletric dipole moment (EDM) for the neutron [10]. One theoretical reason for not including eq. (1.34) in our Lagrangians eqs. (1.4) and (1.29) is that there is always a basis where it can be set to zero, moving the phase θ_0 into the quark mass matrix (the Yukawa matrices in the basis of eq. (1.4)), specifically into $\mathrm{Arg}(\mathrm{det}M)$. The basis-independent P and CP violating parameter in QCD is

$$\overline{\theta} \;=\; \mathrm{Arg}\left(e^{i\theta_0}\mathrm{det}M\right) \underset{\text{if det } M\neq 0}{=} \theta_0 + \mathrm{Arg}\left(\mathrm{det}M\right)\;, \tag{1.35}$$

where I have written it first in a slightly unconventional way to highlight that if any of the quarks were massless ($\mathrm{det}M = 0$) then $\overline{\theta} = 0$. The evidence strongly opposes this however. The experimental non-observation of a neutron EDM [6] sets a very tight constraint on the size of $\overline{\theta}$

$$\overline{\theta} < 10^{-11}\;, \tag{1.36}$$

which, in light of eq. (1.35) would imply a bizarre cancellation between two seemingly independent phases and sources of P, CP violation whose (naturally expected) values would be $\mathcal{O}(1)$, especially since this is observed for the CP violating phase in the CKM matrix.

1.1.6 Effective Field Theory

We saw in section 1.1.5 that the description of QCD dynamics in terms of quarks became impossibly non-perturbative at low energies. We also saw however that the IR spectrum of the theory included a set of 8 PNGBs, the lightest bound states of quarks. We shall see that it is possible to write down a weakly coupled *Effective Field Theory* (EFT) for these degrees of freedom despite our ignorance of strongly coupled QCD.

The point of an EFT is precisely to describe the dynamics of a theory at energies below a certain *cut-off* Λ, by using only those degrees of freedom that are light (with respect to Λ) and therefore active. From a field theory point of view, one starts by identifying the proper dof and symmetries. One then proceeds to write down all Lagrangian terms consistent with those symmetries, including non-renormalisable interactions, with unknown coefficients of expected size order one, suppressed by the appropriate powers of Λ to make dimensionful sense. Despite thus being *technically* non-renormalisabile, loop diagrams can be computed and physical parameters are renormalised, as long as a so-called mass-independent renormalisation scheme is adopted, the prime examples of which are the MS and $\overline{\text{MS}}$ schemes.

1.1.7 Beyond the Standard Model

The theory described in the sections above along with the classical theory of general relativity (GR) (see section 1.2) is the current rock on which we base our science. The pursuit of *new physics*, in addition to the micro-physics elements described above, is the field of *Beyond the Standard Model* (BSM) theory. Despite the great success of the SM, there are several open problems suggesting the existence of BSM physics.

One should make a distinction between physical problems associated with the failure of the SM to include observed phenomena and aesthetic problems of the theory. We first address the former.

Experimental Shortcomings

It is important to realize that the following shortcomings do not mean that the SM is wrong. Rather they point to the fact that it is *incomplete*; an invitation for soon-to-be graduating physics doctorates to work and think hard.

Neutrino oscillations. Neutrinos are massless in the SM. Thus, the basis of generation diagonal weak interactions can also be thought of as their mass basis, unlike with quarks as we saw in section 1.1.3 (which resulted in the CKM matrix). On the other hand, the detection of neutrinos produced in the sun, Earth's atmosphere and man-made nuclear reactors have demonstrated that neutrinos produced at source in definite weak eigenstates (ν_L^i above), after travelling macroscopic distances can register as different weak eigenstate at detection. The observations indicate that three distinct neutrino mass eigenstates exist,[12] each picking up a slightly different phase under time evolution. Therefore, a linear combination of the latter corresponding to a definite weak eigenstate at some initial time will oscillate between all the ν_L^i as a function of distance travelled. It is still an open question whether massive neutrinos are Majorana or Dirac and how to accommodate them into the SM.

Dark Matter. The most serious shortcoming of the SM plus GR is the current inability to explain the observation that the amount of matter in galaxies - as measured by gravitational effects - is roughly 5 times larger than what can be estimated judging by all luminous matter detected by astronomers. The inferred existence of a cold, inert, abundance of *dark* matter (DM) is now supported by galaxy rotation curves, strong and weak gravitational lensing as well as synergy with large scale cosmological structure formation and the CMB, as mentioned further on in section 1.2. Note that while DM dominates the galaxy's overall mass, it is spread thinly over a large spherical 'halo' so that locally in our surroundings inside the galactic disk baryonic matter is far more abundant. Beyond its gravitational presence there is no evidence towards any non-gravitational interactions. The failure of the SM is to provide a candidate microscopic particle with the right properties. A lot of BSM physics has thus been motivated by studying possible DM candidates and their production mechanisms in the early universe. In chapter 4 we will encounter one candidate: the *dark photon*, an extra massive vector field very weakly coupled to the SM.

Standard Model Hints of Beyond

Some features of the SM, despite being perfectly predictive, offend the principle of *naturalness*, which, in general terms, disfavours unexplained hierarchies of scales and couplings. A distinction is made for the value of a parameter y when the theory recovers a symmetry in the limit where the parameter in question is set to zero. This is because quantum corrections will shift the value of $y(\mu_0)$ (in the sense of

[12] With current upper bound $m \lesssim 1\,\text{eV}$ [6].

section 1.1.4) at some reference scale by corrections proportional to $y(\mu)$ itself. Such a parameter is said to be 'technically natural'. Large hierarchies in these still beg for an explanation but should be considered less puzzling than when no restorable symmetry is present.

The highest energy scale in fundamental physics naively is the Planck scale $M_{\rm pl} = 1.2 \times 10^{19}\,\text{GeV}$. In the SM, there are two scales, many orders below $M_{\rm pl}$, driving the physics: the EW scale v of eq. (1.7) and the QCD strong scale determined by eq. (1.30). The latter is technically natural because the beta function is proportional to the coupling itself. The logarithmic running of $\alpha_s(\mu)$ found in eq. (1.30) means that given an underlying scale, such as $M_{\rm pl}$, where the α_s is perturbative, it becomes ~ 1 at a scale exponentially smaller.[13]

The electroweak hierarchy problem: As we saw in section 1.1.3, in the SM the EW scale is set by the Higgs mass term $v = m_H/\sqrt{\lambda} \approx 246\,\text{GeV}$. The unnaturalness of the m_H^2 term arises in BSM theories with new ingredients at energies $\Lambda \gg v$ that couple to the Higgs. Interactions between these heavy particles and H generically lead to quadratically divergent quantum corrections to the Higgs mass term which naively would set $m_H^2 \sim \Lambda^2$. The qualitative difference of the Higgs mass term, in contrast to the QCD scale, can be seen in its beta function not being proportional to m_H^2 itself. For example, the contribution from an active heavy complex scalar of mass $\mathbb{M} \gg m_H$ marginally coupled to the Higgs with coupling $\mathbb{y}$ is

$$\frac{dm_H^2(\mu)}{d\ln\mu^2} = \frac{\mathbb{y}}{(4\pi)^2}\mathbb{M}^2\ , \qquad (\mu > \mathbb{M})\ , \tag{1.37}$$

with contributions differing only by $\mathcal{O}(1)$ numbers for other dof. Assuming an initial condition $m_H^2(\Lambda_{\rm UV})$ at some scale $\Lambda_{\rm UV} \gg \mathbb{M}$, integrating the beta function down to the EW scale gives

$$m_H^2(v) = m_H^2(\Lambda_{\rm UV}) - \frac{\mathbb{y}}{8\pi^2}\mathbb{M}^2\ln\left(\Lambda_{\rm UV}/M\right)\ . \tag{1.38}$$

Thus in order for $m_H(v) \ll \mathbb{M}$ one requires a fine-tuned cancellation between the UV initial condition and the quantum correction to to an increasing order of precision as the scale of the new physics $\Lambda \sim \mathbb{M}$ becomes larger.

The general expectation of new physics, coupled with the naturalness principle strongly suggesting its scale could not be too far from the EW scale, formed a target for BSM for a long time, pointing squarely at the *energy frontier* of more powerful colliders as the path to progress.

[13] This dynamical generation of a mass scale, such as $\Lambda_{\rm qcd}$ from an order one dimensionless coupling is known as 'dimensional transmutation'.

The strong CP problem: We have already encountered in section 1.1.5 a different apparent puzzling cancellation to at least one part in 10^{-11} eq. (1.35). The current leading solution to this conundrum is essentially to promote the parameter θ to field $a(x)/f_a$ - called the axion - which is the PNGB of a spontaneously broken $U(1)_{\rm PQ}$ at some large scale $\sim f_a$. The particle is typically very light $m_a \approx \Lambda^2_{\rm QCD}/f_a$ but also very weakly coupled to the SM. As these are the opposite characteristics of particles at the energy frontier described above, the axion is the prime suspect in the pursuit of new physics at the so-called *intensity frontier*.

1.2 The Standard Cosmological History and Beyond

Given the known laws of physics today, as embodied in the SM of section 1.1, plus whichever completions remain to be discovered at higher energy and/or weaker coupling, we are still faced with the physical but qualitatively different question of 'how did we get here?' [11]. The field of Cosmology attempts to address this question in a quantitative way.

Strictly speaking, the history of the Universe is not a controlled repeatable experiment which we can test against our scientific theory.[14] However, it also not *just* an exercise in telling a story consistent with the known laws for the satisfaction of our musing curiosity and retrospective anxiety. In the modern era of fundamental physics, cosmology has more and more become a complementary - and often leading - tool to constrain and guide our quest for physics beyond the Standard Model The theory is successful enough that adding BSM elements can spoil it in unacceptable ways. Or, the other way around, particularly elegant solutions to cosmological problems can further motivate the existence of certain BSM theories. In addition, many cosmological observables and potential signals are beyond the grasp of our current technology but will not be in the future.[15] This delay in data acquisition allows competing theories to make distinguishable predictions for those observables and prove their worth or misery.

An interesting case is that of dark matter. Although its true microscopic nature remains a mystery as described in section 1.1.7, its purely gravitational presence is a key element in the standard theory of the early universe; as we will see, its

[14] At least for those of us who live in it and for a fraction of a moment at that.

[15] As well as improvements in the precision and accuracy of measurements of existing observables of course.

name even takes after it. More precisely, its role - along with contributing its energy density to the total - is to kick start the growth of small overdensities, the seeds of all self-gravitating structures which eventually become galaxies and clusters thereof. Simulations consistently show incompatibility between observations and structure formation involving baryonic matter alone. Thus, the theory of the history of the universe can be taken both as further independent evidence for the existence of dark matter, *and* as an opportunity - due to its critical role - to further study its nature.

The Big Bang and ΛCDM. Two fundamental statements lay the foundations for the theory of the universe. Firstly, the observation initially made by Edwin Hubble, that everything beyond our local neighbourhood of gravitationally bound galaxies appears to be moving away from us, properly interpreted as space itself expanding. Secondly, the assumption that at very large scales, put roughly at $\gtrsim 300\,\mathrm{Mpc}$, the universe starts to look homogeneous and isotropic, as best indicated by the observed statistical isotropy[16] of the *Cosmic Microwave Background* (CMB) and the success of structure formation theories based on the assumption of a homogeneous and isotropic universe with tiny (statistically homogeneous and isotropic) initial perturbations.

In the following sections I shall describe what has come to establish itself as the standard history, which, by inverting the observed expansion today, traces the current universe and its current energy density back to a rapidly expanding and fiery stage known as the *hot Big Bang*, the subject of section 1.2.3, a *plasma* state of temperatures at least a few MeV, when neither atoms nor nuclei existed yet but electrons, neutrons and protons were unbound. The greatest validations of the Big Bang theory comes from two sources: 1) the 1962 discovery and subsequent analyses of the CMB, a near-thermal spectrum of microwave radiation with temperature $T_0 \approx 2.7$ K coming from every corner of the sky, which has been travelling undisturbed apart from redshifting since the universe first became transparent to light (the epoch of so-called *recombination* at then temperature $T \approx 0.1$ eV); and 2) the success of the theory of *Big Bang Nucleosynthesis* (BBN) in describing the observed light-element ratios as they result from the initial $T \approx 1$ MeV plasma.

The standard theory in its latest form is nowadays referred to as ΛCDM, which emphasises the late-time roles of cold dark matter (as mentioned above) and 'dark energy', essentially the energy density of our current vacuum $\rho_0 \approx 3.7 \times 10^{-47}\,\mathrm{GeV}$. The latter is the latest major addition to cosmology, initially born out the observation that the Hubble expansion is accelerating at the present, apparently due to

[16] With, possibly, some caveats on the very largest scales due to cosmic variance uncertainties in the lowest multipole moments of the CMB fluctuations.

an approximately constant vacuum energy being dominant at the present time (see eq. (1.44)). This inferred measurement of the vacuum energy presents the most severe fine-tuning problem (in the language of section 1.1.7). We will return to the subject of this vacuum energy, and whether it is actually a constant, in later sections of this thesis.

The study of cosmology requires understanding gravity and the structure of space and time at the largest scales for which the appropriate theory is that of General relativity (GR), to which we turn to next.

1.2.1 General Relativity for Cosmology

General Relativity is first and foremost a theory-framework for the statement that the laws of physics should be independent of coordinate system. More precisely, fundamental equations should be organised as equalities between tensorially identical objects in the language of differential geometry. The metric tensor $g_{\mu\nu}$ defines the concept of distance (between two events / coordinate points) that of course enters into all force laws. Given a system of coordinates $\{x^\tau\}$ which spans a space-time manifold, the invariant distance infinitesimal (line element) is given by

$$ds^2 = g_{\mu\nu}(x^\tau)dx^\mu dx^\nu \ . \tag{1.39}$$

Generalising Newton's law of inertia, test particles are assumed to follow geodesics of the metric in the absence of net forces. The great conceptual break with Newton is that, in this language, gravity is not a force at all but simply the presence of intrinsic curvature in the space-time described by eq. (1.39); *free-fall is geodesic motion.* Said curvature is captured by the Riemann tensor $R_{\mu\nu\rho\sigma}(x^\tau)$, which has a well known form in terms of the metric components and its derivatives [12]. Finally, the sourcing of gravity (curvature) by matter is dictated by the Einstein field equation

$$R_{\mu\nu} - \frac{1}{2}\left(g_{\mu\nu}R + \Lambda_{\rm c}\right) = 8\pi G_{_N}\, T_{\mu\nu} \tag{1.40}$$

where $R_{\mu\nu} = R^\sigma_{\mu\sigma\nu}$ is the Ricci tensor, $R = R^\mu_\mu$ the Ricci scalar,[17] $\Lambda_{\rm c}$ is a (cosmological) constant - included because it is not forbidden[18] - and $T_{\mu\nu}$ is the energy-momentum tensor of matter. Thus Einstein gives Newton's constant $G_{_N} = 1/M_{\rm pl}^2$ a new home.

[17] Not to be confused with the general chiral transformation on right-handed fields of sections 1.1.6 and 3.3. The context should be self-explanatory.

[18] See for example Lovelock's Theorem [13].

To describe a homogeneous and isotropic universe we should start with the most general metric with the same level of symmetry. These are given by the Friedmann-Lemaitre-Robertson-Walker (FLRW) space-times, which can be described by the line element

$$ds^2 = dt^2 - a^2(t)\left(\frac{dr^2}{1 - k\, r^2/r_c^2} + r^2 d\Omega^2\right) \tag{1.41}$$

where $a(t)$ is the so-called 'scale-factor' capturing the relative measure of distance between space-like separated points as a function of time[19] t and is usually normalised to $a(t_0) = 1$, with t_0 present time. k is a discrete geometric parameter with three possible values $-1, 0, 1$ describing an open, flat or closed universe respectively at the largest scales and r_c is the corresponding radius of curvature (when $|k| = 1$).

1.2.2 Expansion

The simple metric eq. (1.41) has a single undetermined function $a(t)$ whose evolution is driven by the matter content of the universe via the dynamical law of gravity eq. (1.40). To a very good approximation the different forms of matter in the universe can be taken to be in the form of a (homogeneous & isotropic) perfect fluid with total energy density $\rho(t)$ and pressure $p(t)$ related by the constraint $\nabla_\mu T^{\mu\nu} = 0$. Given the symmetries, Einstein's equation boils down to the Friedmann equation

$$H \equiv \frac{\dot{a}}{a} = \sqrt{\frac{8\pi}{3} G_N \rho_{\rm tot}(t) + \frac{k}{a^2}}\ , \tag{1.42}$$

where we have defined the Hubble parameter $H(t)$ giving a measure of the rate of expansion of the universe at a given time. Specifying the equation of state $p = p(\rho)$ of the matter we wish to describe, one can solve for $\rho = \rho(a(t))$, giving

$$\rho(t) = \rho(t_{\rm ref}) \begin{cases} 1\ , & \text{vacuum energy} \\ (a(t)/a(t_{\rm ref}))^{-4}\ , & \text{radiation (relativistic matter)} \\ (a(t)/a(t_{\rm ref}))^{-3}\ , & \text{dust (cold matter)} \end{cases} \tag{1.43}$$

where $\rho(t_{\rm ref})$ is the energy density at some reference time $t_{\rm ref}$ and I have listed the three important types of matter for cosmology (each will have its moment dominating the energy budget of the universe). It should be obvious why the energy density of the vacuum remains constant with expansion. For dust, which we will henceforth refer to simply as 'matter', $\rho = n\, m$ and the scaling simply reflects the dilution of number

[19] The coordinate t corresponds to the time measured by a so called 'fundamental observer' living on a geodesic corresponding to the rest frame of the cosmic matter, observing the universe to be homogeneous and isotropic at every moment.

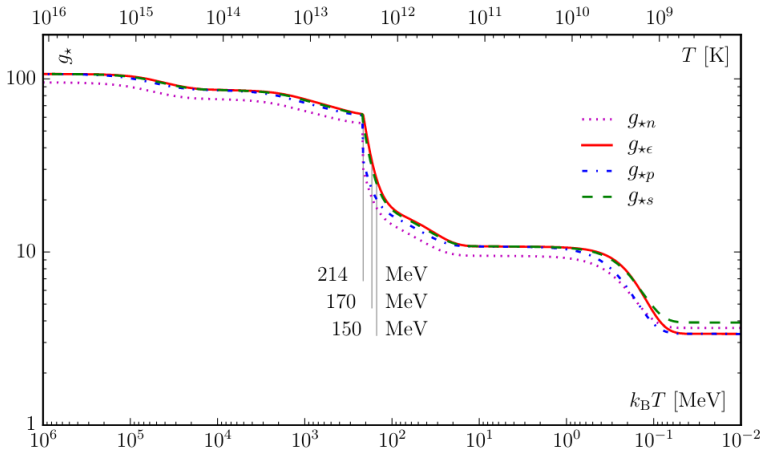

Figure 1.3: Effective degrees of freedom $g_*(T)$ in the standard model as a function of temperature. Figure taken from [14].

density n. For radiation - on top of the latter dilution - there is an additional 'redshift' scale-factor of the energy that can heuristically be thought of a the 'stretching' of its wavelength.[20] Notice, it is possible for massive particles to be relativistic at one stage, loose energy by redshifting until their momentum is comparable to their mass and thus scale as matter from then onwards.

As our universe is observed to be flat today and the scaling of both matter and radiation energy densities means that they dominate the right side of the Friedmann equation even more in the past, I will from now on set $k = 0$. eq. (1.43) allows one to easily solve the Friedmann equation for periods when a single type of matter dominates the energy density. This gives

$$a(t) \approx a(t_{\rm ref}) \begin{cases} e^{Ht}\,, & \text{V.D. (inflation)} \\ t^{-1/2}\,, & \text{R.D.} \\ t^{-2/3}\,, & \text{M.D.} \end{cases} \tag{1.44}$$

where V.D., R.D. and M.D. stand for vacuum, radiation and matter domination respectively.

1.2.3 Hot Big Bang

It is a marvellous - as well as convenient - thing that the whole observable universe was once in a hot plasma state well described by thermal equilibrium. Thus, to first approximation, its state was completely characterised by a single thermodynamic quantity, the temperature T, its makeup determined by the known particle content

[20] For a proper discussion the reader is directed to [1].

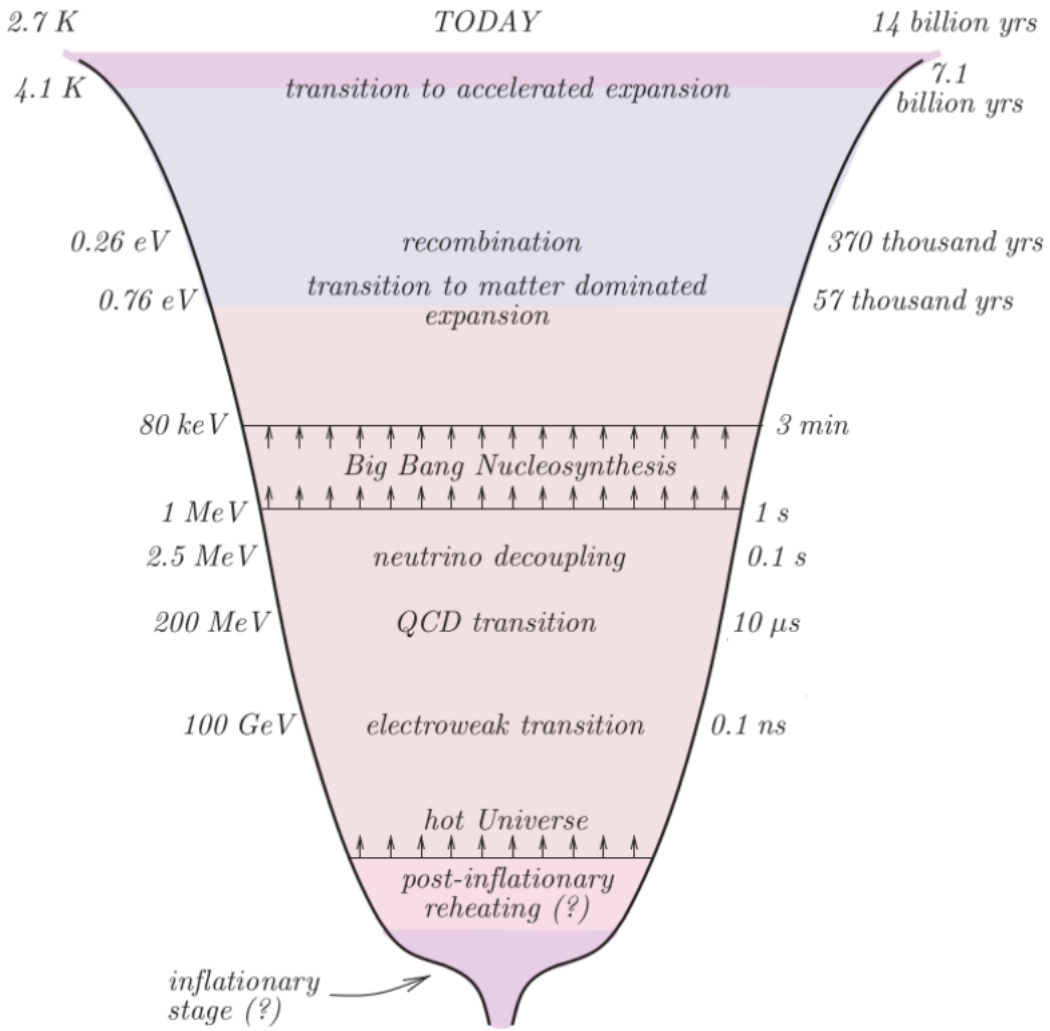

Figure 1.4: Timeline of the standard cosmological history of the universe. Good evidence exists for our present state deriving from a plasma of temperatures $\gtrsim 1-3\,\mathrm{MeV}$. At temperatures above this the QCD and EW phase transitions occur. Although each were once suspected to be of first order, with potential observational signals as per subject of section 1.3 and chapter 4, there is now strong evidence that they are both crossovers. Before the hot phase - though at what scale is still unknown - it is generally believed that a period inflation was responsible for setting the right initial conditions for subsequent evolution. There is some tension however between this and conjectures mentioned in section 2.1 regarding quasi-de Sitter phases motivated by quantum gravity. Figure adapted from [1].

of nature[21] plus chemical potentials associated to the conserved quantities of their microscopic interactions.

The plasma has sufficient energy only to significantly excite those particles whose mass is $m < T$, otherwise the number density is Boltzmann suppressed $n \propto \exp(\mu - m)/T$, where μ is a possible chemical potential. Although the largest temperatures for which we have evidence are around a few MeV, it is natural to believe that T could have started at much higher values. For T above the electroweak scale of eq. (1.7), all SM particles are massless and active. The energy density is that of radiation in thermal equilibrium

$$\rho_{\rm SM} = \frac{\pi^2}{45} g_*(T) T^4 \ , \tag{1.45}$$

where g_* counts the number of *effective relativistic degrees of freedom* in the plasma; $g_* = 106.75$ for the full SM spectrum, while fig. 1.3 shows the explicit dependence on temperature. More specifically, allowing for multiple decoupled sectors,

$$g_*(T) = \sum_{\rm b} g_b \left(\frac{T_b}{T}\right)^4 + \frac{7}{8} \sum_f g_f \left(\frac{T_f}{T}\right)^4 \tag{1.46}$$

where the indices b and f sum over bosonic and fermionic dof respectively, $g_{b,f}$ count helicities as usual and $T_{b,f}$ are the respective decoupled temperatures. Note that in presence of different temperatures the reference T is always given by the sector connected to the SM photons.

As discussed in the previous section, the universe is actually expanding - more and more rapidly as we go back in time. Consequently the gas is cooling: T is changing. The statement of equilibrium is thus an *instantaneous* feature applicable to a particular particle species as long as the interaction rate Γ at the characteristic energies involved - also a function of time - for the relevant equilibrating process satisfies $\Gamma \gg H$, where $H(t)$ is the Hubble parameter measuring the rate of expansion as defined in eq. (1.42). When the contrary becomes true, the particle - or at least the process in question - is said to have 'frozen out' of equilibrium. An important example is that of neutrino decoupling, the most weakly coupled SM particles. Taking characteristic energies to be of order $\sim T$ and number densities $\sim T^3$, the integrated cross section for electron-neutrino scattering is $\sigma_{e\nu} \sim G_F^2 T^2$ and the corresponding interaction rate is $\Gamma_{e\nu} \sim G_F^2 T^5$, where $G_F \approx 1.27 \times 10^{-5}\,\mathrm{GeV}^{-2}$ is Fermi's constant of the weak interactions. Comparing this to the Hubble rate in radiation domination

[21] which was the subject of section 1.1

$H \sim T^2/M_{\rm pl}$ it is easy to find the neutrino freeze-out temperature

$$\begin{aligned} & \Gamma_{e\nu}(T_\nu^{\rm dc}) \overset{!}{\sim} H(T_\nu^{\rm dc}) \\ \Longrightarrow \quad & T_\nu^{\rm dc} \sim (G_F^2 M_{\rm pl})^{-1/3} \sim 3\,{\rm MeV} \qquad \text{(neutrino freeze-out)} \ . \end{aligned} \tag{1.47}$$

After this the neutrinos become completely inert and simply 'free-stream' till the present, forming a cosmic relic far beyond our current detection reach.

It is important to note that $g_*(T)$ evolves non-trivially as the temperature evolves below the mass of heavy particles[22] and freeze-out temperatures, spoiling the simple scaling $\propto a^{-3}$ of radiation energy density given in eq. (1.43), valid for a perfectly adiabatically evolving thermal bath of same dofs. An often more convenient quantity is the entropy density

$$s = \frac{2\pi^2}{45} g_{*,s}(T) T^3 \ , \tag{1.48}$$

where $g_{*,s}(T)$ is given by a formula just like eq. (1.46), except for the power in temperature ratios going like 3 rather than 4. Its evolution for the SM is also shown in fig. 1.3. Unlike ρ, throughout the standard thermal history of the universe $s(T)$ does actually follow the simple a^{-3} scaling to a very good approximation.[23] Since $s\, a^3 = $ constant, we have a relatively simple relation between scale factor and temperature

$$a(t) = a(t_{\rm ref}) \frac{T_{\rm ref}}{T} \left(\frac{g_{*,s}(T_{\rm ref})}{g_{*,s}(T)} \right) \ . \tag{1.49}$$

Underlying the established thermal history is the asymmetric abundance of baryons versus anti-baryons (plus electrons versus positrons by overall charge neutrality), eventually reflecting the present observation that our world is almost entirely made up of the former .[24] At temperatures below $\lesssim 100\,{\rm GeV}$ there are no known active (i.e. not exponentially slowly occurring) baryon violating processes[25] thus the asymmetry is to be taken as an initial condition - a chemical potential in practice, as mentioned above. The size of the asymmetry is best captured by the time invariant quantity

$$\Delta_B \equiv \frac{n_B - n_{\overline{B}}}{s} \approx 0.88 \times 10^{-10} \ , \tag{1.50}$$

[22] For example, in descending order, t, h, Z, W, b, τ, ...

[23] Fundamentally this is a consequence of Liouville's theorem for phase space. See [15] for the curved space-time generalisation.

[24] With such little naturally occurring antimatter that it took a theorist in 1931 to point out it might be there.

[25] Above the EW phase transition non-perturbative SM processes involving B and L anomalous non-conservation lead to fast, $\Gamma/Vol \sim T^4$, violation of B, L, and $(B+L)$ numbers, though not $(B-L)$. Below the EW phase transition the anomalous non-conservation rate is dominated by sphaleron configurations, with a very large exponential Boltzmann suppression when $T \ll m_W$.

where n_B and $n_{\overline{B}}$ are the number density of baryons and anti-baryons respectively. The dynamical origin of Δ_B - known as *baryogenesis* - is one of the most serious outstanding questions in cosmology and also of particle physics since the SM on its own is insufficient to explain the size of Δ_B, despite the presence of baryon number violation at large temperatures. The reason is that the Sakharov conditions for baryogenesis require not only B-number violation but also simultaneous CP-violation and departure from thermal equilibrium, and in these last two regards the SM is insufficient during the epoch when B-violation is active. At the time of writing this thesis there is no compelling BSM baryogenesis theory supported by evidence. I will thus continue to take eq. (1.50) as an initial condition.

Moving on, at temperatures below neutrino decoupling, the relativistic SM plasma is made of only electrons, positrons and photons, while the three neutrino generations free-stream, nonetheless maintaining the thermal spectrum imprinted[26] when $T \sim T_\nu^{\rm dc}$, though redshifted due to expansion. In addition, there are also net abundances of protons and neutrons - the parents of all present baryonic matter today - as set by the asymmetry Δ_B. These are the protagonists of the first step of the cosmic tale for which we have direct evidence.

($\sim 1\,$MeV) Big Bang Nucleosynthesis (BBN): During BBN, temperatures drop low enough so that bound nuclear states which are formed by the binding of free neutrons and protons are no longer quickly broken back up by collisions with the bath. Thus, by the end of BBN the first light elements (in the form of ions) emerge with relative abundances dictated by the calculable physics at the time. The temperatures at which this occurs $\lesssim 1\,$MeV correspond to timescales of the order of minutes as shown in fig. 1.4, which is comparable to the lifetime of free neutrons ≈ 15 minutes. Thus, one should expect appreciably more protons than neutrons in the universe. Indeed, when the dust settles[27] BBN theory predicts that $\sim 75\%$ of baryonic mass energy is still in the form of free protons - which we can now symbolically think of as hydrogen ions - while almost all of the remaining $\sim 25\%$ is comprised of two protons and two neutrons pairing up into α-particles,[28] also known as helium-4. Fractions of order $\sim 10^{-5}$ of the total are instead deuterium and helium-3, 10^{-10} are lithium-7 with even smaller trace amounts of heavier elements. These predictions of the standard theory, as a function of the baryon-to-photon ratio at the time, can be

[26] Also Liouville.

[27] Pun intended.

[28] Famous of course in nuclear physics for having a particularly large binding energy per nucleon among light elements.

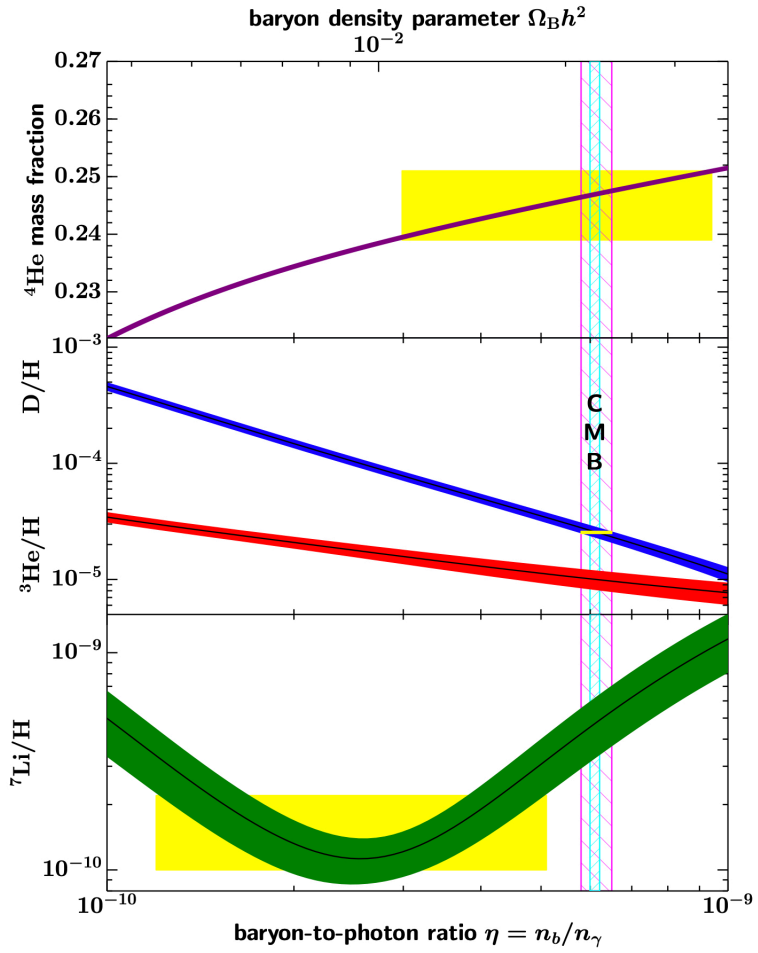

Figure 1.5: BBN predictions of the light element abundances as a function of the baryon-to-photon ratio (bands indicate 95% CL intervals). Yellow boxes are observationally inferred primordial element abundances. Vertical band is CMB measurement of baryon-to-photon ratio (with and without BBN D/H ratio determination included). Figure taken from [16].

tested against the chemical composition of matter - determined from the analysis of absorbtion spectra - in low-metallicity regions of the Universe where it is believed to be (approximately) primordial, despite subsequent evolution - see fig. 1.5.

($\sim 0.1\,\mathrm{eV}$) Recombination and transition to matter domination: well after BBN is complete, the temperature has dropped below the scale of the electron mass $m_e \approx 0.5\,\mathrm{MeV}$ so that the symmetric part of the electron - positron abundance annihilates leaving a Boltzmann suppressed asymmetric component related to eq. (1.50) by electric charge neutrality. Photons still remain in equilibrium with the electrons and light nuclei, and the universe remains radiation dominated but only photons and decoupled neutrinos are relativistic.

Recombination is the transition that occurs around $0.3 - 0.2\,\text{eV}$ from the state described above to one where the once-free electrons become captured by the ions, forming the first neutral atoms of mostly hydrogen and helium, and interactions between matter and photons freeze out, leaving the latter completely decoupled and free streaming thereon, all the way to the present time. This is the CMB discovered in 1964 by Penzias and Wilson. Notice that recombination occurs quite below the naively right scale of the binding energy of the ground state of hydrogen ($13.6\,\text{eV}$). The decoupling is delayed by a combination of the small number density of baryons and the effect of high energy photons at the tail of the distribution reionising the atoms even as $T \ll 13.6\,\text{eV}$ [1].

In the meantime, during the same epoch - around $\sim 0.8\,\text{eV}$ - the total mass energy in (mostly dark) matter becomes larger than that in radiation - the photons and decoupled neutrinos. In the subsequent era of matter domination, the most interesting dynamics concern the linear growth with scale factor of small over-densities $\delta\rho/\rho$ and the eventual formation of self-gravitating structures, surely a fascinating topic for a different thesis.

1.2.4 Cosmological constraints: Dark radiation

The sequence of events described in section 1.2.3 is sensitive to the addition of new elements so that several non-trivial constraints are obtained from the physics of BBN and recombination, as well as structure formation, though the latter is not as pertinent to this thesis. I will focus here on the constraint most relevant to chapter 4.

Dark Radiation: The physics of primordial nucleosynthesis and recombination depends on the temperature of the visible sector[29] as well as the expansion rate at the corresponding time, determined by the *total* energy density via the Friedmann equation. Thus, there cannot be much more *dark radiation* around the temperatures of $T \sim 1\,\text{MeV}$ and $0.1\,\text{eV}$ without spoiling the predictions of standard cosmology.

Before quantifying the bounds on extra dark radiation we must understand the contribution from the SM. When the symmetric part of the electron and positron abundances annihilate below $T \sim 0.5\,\text{MeV}$, as mentioned in section 1.2.3, the neutrinos have already decoupled, so all the former's mass energy goes primarily into into heating up the photon bath. Then onward the neutrinos have a slightly lower temperature $T_\nu = (4/11)^{1/3} T$. Thus, using the definition of eq. (1.46), the total energy

[29] By this I mean the thermodynamic sector in contact with the SM photons.

density of radiation ρ_r in the universe after e^+e^- annihilation is

$$\rho_r = \left[1 + \frac{7}{8}\left(\frac{4}{11}\right)^{4/3} N_{\rm eff}\right]\rho_\gamma \tag{1.51}$$

where I have normalised contributions in terms of the energy density in photons ρ_γ and $N_{\rm eff} = 3.046$ accounts for the three neutrino species. Notice this is not exactly three because in reality neutrino decoupling is not instantaneous and occurs at slightly different times for the different energies in the thermal spectrum, so that some e^+e^- energy is indeed transferred to them.

Any additional dark radiation that might be present is quoted as a deviation in $N_{\rm eff}$, that is

$$\Delta N_{\rm eff} = \frac{8}{7}\left(\frac{11}{4}\right)^{4/3}\frac{\rho_{\rm dr}}{\rho_\gamma} \tag{1.52}$$

This is the quantity to be compared with the exclusions set by BBN $\Delta N_{\rm eff} \lesssim 0.464$ and from the CMB $\Delta N_{\rm eff} \lesssim 0.284$ at their respective epochs [17].

1.2.5 Inflation, or what made the big bang?

Turning the clock backwards on expansion, the scale factor $a(t) \to 0$ in finite time. In this limit the metric eq. (1.41) becomes singular as does the energy density in radiation[30] according to eq. (1.43). This is a real curvature singularity, as can be seen by the blow up of curvature invariants. Of course, when the scales involved start becoming comparable to the Planck scale a full theory of quantum gravity is necessary. The current predominant belief however is that a qualitative change occurs well before $\rho \sim M_{\rm pl}^4$ is reached, still in the realm of field theory.

An early period of exponential expansion, known as *inflation*, was first proposed to solve various supposed problems of the Hot Big Bang theory.[31] This is usually achieved by a sufficiently flat scalar field potential leading to an approximately vacuum dominated universe while the vev of this field slowly rolls along.

Note that none of the 'problems' of the Big Bang concerned an explicit disagreement with observation. Rather, inflation was born as a dynamical explanation for the peculiar initial conditions of the Big Bang. For example, the fact that the maximum traversable distance (for light) $H^{-1} \sim t$ grows faster than the physical size between manifold points $a(t) \sim t^{1/2}$ or $\sim t^{2/3}$ (depending on R.D. or M.D.) means that the

[30] Strictly speaking, far before $M_{\rm pl}$, Hubble becomes so large that no SM interaction rates can keep up so that the assumption of equilibrium breaks down.

[31] See the introduction of [18] for a comprehensive list.

CMB light we receive from different parts of the sky - giving us a photograph of the universe at the time of recombination - actually comes from $\sim$ 10000 different patches that were causally disconnected from each other at the time of last scattering.[32] Yet the CMB is isotropic to one part in $\sim 10^{-5}$. This and similar qualms are resolved if we imagine our entire observable universe as deriving from a tiny, causally connected patch, stretched to exponentially large proportions $a \sim e^{H_I t}$, where H_I is the (constant) Hubble parameter during inflation. The duration of inflation is most conveniently measured in number of efoldings $N_e = H_I t$ and the minimum necessary is given by [19]

$$N_e^{(\mathrm{tot})} > N_e^{(min)} \approx 67 + \ln(M_{\mathrm{pl}}/T_{\mathrm{reh}}). \tag{1.53}$$

where T_{reh} is the temperature of the universe at the start of the Big Bang phase.

On top of providing a dynamical explanation for the large-scale uniformity and simplicity of the universe, the inflationary paradigm also successfully predicts the correct spectrum of primordial density perturbations. These have their origin in the quantum mechanical fluctuations of the inflaton field vev, which are stretched to scales beyond the horizon $> H^{-1}$ and become 'frozen' and classical.

The greatest unknown at the present is the scale of inflation H_I, which could be anywhere above $\gtrsim 10^{-24}\,\mathrm{GeV}$ (just allowing reheating to $\sim$ MeV temperatures suitable for BBN), while an upper bound can be placed for the simplest case of single field slow-role inflation at $H_I \lesssim 10^{14}\,\mathrm{GeV}$ from the non-observation of tensor modes in the CMB [6].

1.3 Phase transitions in the early Universe

Fig.1.4 shows the timeline of the physics of the standard cosmological history of the universe, for which there is significant support. As mentioned already in section 1.2, this presents a singular laboratory, where one can search for evidence of BSM physics. I will now discuss the generic, well-motivated, BSM possibility that, at some time during this history, the universe as a whole underwent the non-equilibrium dynamics of a first order phase transition (FOPT).

Systems changing temperature will often undergo a phase transition - a qualitative change of state, such as water turning into vapour above 100 $^\circ C$ (at sea-level pressure). Boiling water is the most familiar example of a FOPT, which in general terms is characterised by a discontinuity in heat capacity. In field theory this corresponds to a jump in the expectation value of some field order parameter - call it

[32] The angular size of the apparent causally connected region at CMB decoupling is ~ 0.03 radians.

ϕ. The situation is as depicted in fig. 1.6. At some point an effective potential[33] $V_{eff}(\phi, T)$ exists with two local minima and respective vacuum energy densities V_- and V_+, separated by some potential barrier. This is to be contrasted with a second order phase transition schematically drawn in fig. 1.7 and a smooth cross-over (which involves no discontinuity in any thermodynamic variable).

FOPTs were long ago proposed as a possibility during the hot big-bang phase of the universe [21–23]. In the past, it was entertained that even within the SM of particle physics there might be as many as two: chiral symmetry breaking/confinement in QCD at temperatures $T \sim 150$ MeV and the spontaneous breaking of electroweak (EW) symmetry at $T \sim 160$ GeV. Both are now understood to be smooth crossovers [24, 25]. It is interesting to note that from the currently known laws of physics there is *no conclusively established meta-stable vacuum for any temperature* at zero chemical potential[34].

By contrast, FOPTs are ubiquitous in beyond the SM (BSM) theories. This can be understood firstly in light of a vast richness of important phenomenological consequences, among which baryogenesis, the production of heavy dark matter, primordial black holes and gravitational waves (GWs), to name a few. In particular, the EW phase transition is easily made first order in many BSM models [27–38] and the consequent out-of-equilibrium dynamics (in conjunction with B violation in the SM) still make for an attractive theory of baryogenesis. Perhaps most importantly from a phenomenological perspective, the advent of gravitational wave detectors has re-energised interest in these violent phenomena with the prospect of upcoming experiments possibly detecting a stochastic gravitational wave background relic [23,39,40]. Thus even FOPTs occurring in potential hidden sectors decoupled from the SM and its thermal history become of interest [41, 42].

1.3.1 Bubble Nucleation

In a FOPT the 'false' vacuum $\langle\phi\rangle = 0$ is unstable to thermal fluctuations and/or quantum mechanical vacuum tunnelling. In both cases, the transition to the 'true' vacuum occurs locally, through the nucleation and subsequent expansion of bubbles.

[33] Here I have in mind a completely general, properly approximated, effective potential including thermal and quantum loop corrections. For details on how to calculate this, see for example [20].

[34] A possible counterexample is the instability in the Higgs effective potential for central values of SM parameters when extrapolated to very large field range [26]. However, this is sensitive to possible - though unknown - UV physics, over many orders of magnitude, so that we certainly cannot count it as 'conclusive'.

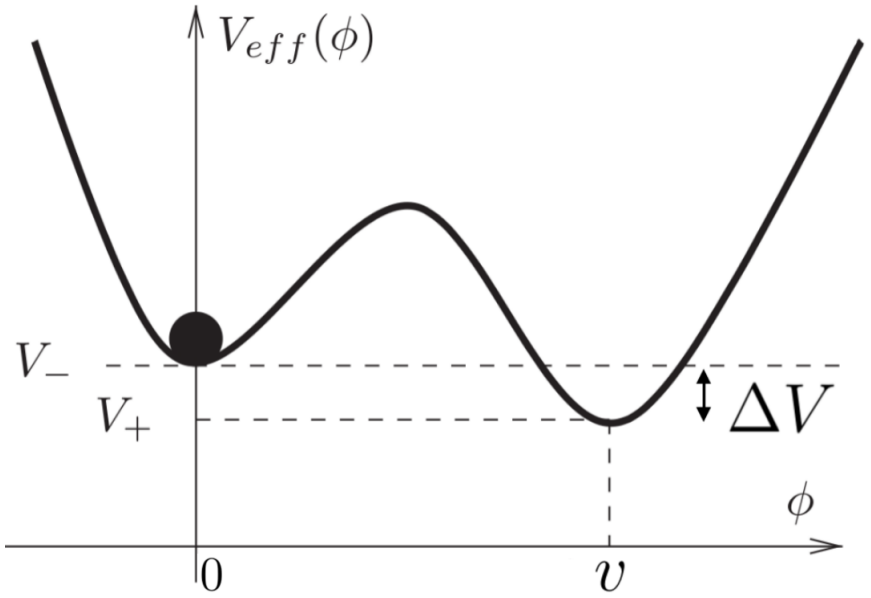

Figure 1.6: Schematic of an effective potential $V_{eff}(\phi, T)$ at some fixed temperature, as a function of order parameter ϕ, which can lead to a first order phase transition. The universe as a whole may get stuck in the $\langle\phi\rangle = 0$ meta-stable state with vacuum energy density an amount ΔV larger than the true vacuum. Figure adapted from [1].

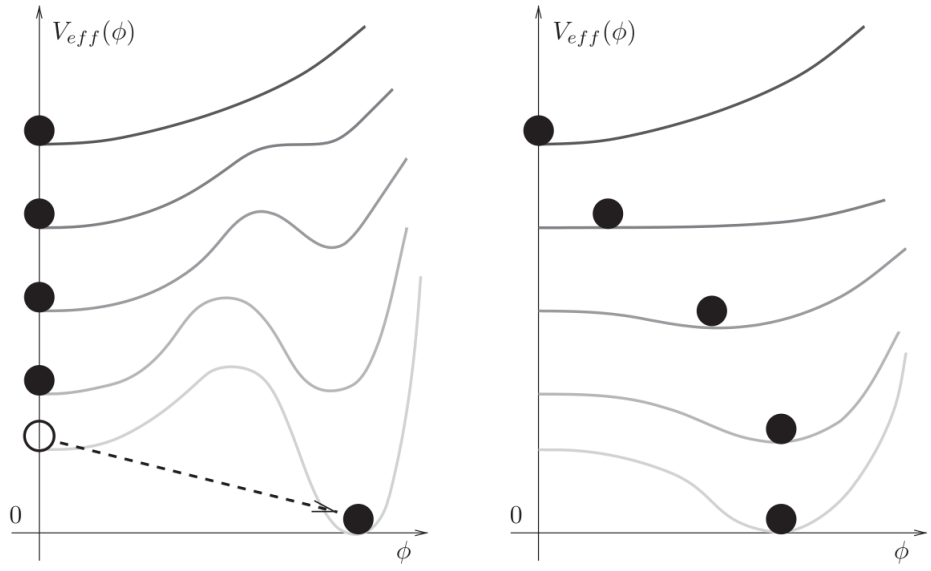

Figure 1.7: Snapshots of the effective potential at different temperatures, with T decreasing downwards. The left (right) figure shows the schematic evolution of a potential in a first (second) order phase transition. The black ball represents the state of the universe. Figure taken from [1] .

An expanding bubble of true vacuum is a spherically symmetric solution $\phi(r,t)$ of the field equations for the order parameter

$$\partial_t^2\phi - \frac{1}{r^2}\partial_r\left(r^2\partial_r\phi\right) = -V'_{eff}(\phi)\ , \tag{1.54}$$

which interpolates between the false vacuum at $\phi(r\to\infty,t)\to 0$ and the true vacuum at its centre $\phi(0,t\to\infty)\to v$.

One can show on general grounds that there is a minimum size of the bubble for which it is energetically favourable to expand. Denoting the radius and wall width of the bubble as R and L respectively and working for simplicity in the *thin wall* approximation $R \gg L$ in which these are well distinguished, the total free energy $F = E - TS$ associated to a static bubble configuration is the sum of two separate parts

$$F(R) = 4\pi R^2\sigma - \frac{4\pi}{3}R^3\Delta V \tag{1.55}$$

where $\Delta V \equiv V_- - V_+$ as defined in fig. 1.6 and σ is the surface tension of the bubble wall. The vacuum energy difference favours larger R, whereas the energy cost of the interpolating wall favours smaller radius. $F(R)$ has a single, unstable, positive extremum at $R_c = 2\sigma/\Delta V$, defined as the radius of the *critical bubble*. Bubbles with radius smaller than this critical size will shrink and disappear while if $R > R_c$, the bubble grows.

Nucleation The critical bubble configuration exists beyond the thin wall limit described above for both transitions mediated by thermal fluctuations and quantum tunnelling. The probability of nucleating such a bubble per unit time per unit volume in both cases is given by an expression of the form

$$\Gamma_n = A\ e^{-B}\ . \tag{1.56}$$

The exponent B is the free energy of the critical bubble configuration in the thermal case , while for tunnelling it is the action evaluated for the 'bounce' instanton solution of the Euclidean version of the classical equation of motion eq. (1.54). In both cases the prefactor is formally a determinant over field fluctuations around the respective classical configuration, with very roughly, $A \sim T^4$ for thermal transitions while $A \sim v^4$ for tunnelling. Of course, in certain cases bubble formation can be dominated by a more complicated combination of thermal fluctuation and tunneling.

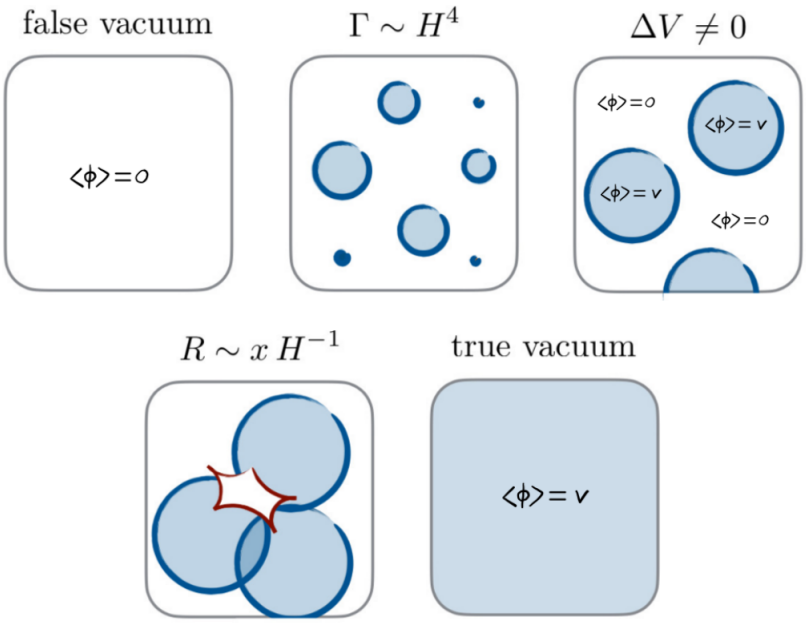

Figure 1.8: Progression of events during a FOPT in an expanding universe. Bubbles are nucleated significantly when $\Gamma_n \sim H^4$, they expand due to the vacuum difference pressure $\Delta P \neq 0$ until collisions occur at a typical radius xH^{-1} and percolate the entire universe to the true vacuum.

1.3.2 Collision and Percolation

In an expanding universe, even when the true vacuum becomes energetically favourable and bubbles are nucleating, the universe is not guaranteed to transition to the new phase. This is because the rate Γ_n needs to be large enough so that enough bubbles are nucleated that they collide before being diluted away. Loosely, this yields the requirement [43]

$$\Gamma_n \sim H^4 \ , \tag{1.57}$$

that is, at least one bubble is nucleated in a Hubble volume per Hubble time. These bubbles then expand and collide before, for a successful FOPT, percolating and finally converting all the false vacuum phase into true vacuum.[35] The bubble expansion and collision dynamics are of great interest as they are far from equilibrium processes with gravitational wave signatures and they can in principle be crucial for baryogenesis. Fig.1.8 describes the progression of events during a successful FOPT in the early universe

[35]In principle a close to measure zero fraction of the false vacuum could remain as compact soliton-like objects.

1.4 Landscapes and Swamps

In section 1.1 we saw how the SM, despite its success, had several input parameters with arbitrary, often puzzling values. At present we cannot say *why* the masses of the electron and the u, d quarks are what they are, or why they are so much lighter than their higher generation cousins. We discussed in section 1.1.7 a more serious aesthetic puzzle of the mass of the Higgs boson and in section 1.2 we mentioned perhaps the worst fine-tuning problem in science in the cosmological constant.

Presumably some or all of these parameters are explained within an underlying, more fundamental theory, perhaps by the introduction of new elements that simultaneously explain some of the open problems described in section 1.1.7. As it stands however, the SM is a renormalisable theory, and no compelling anomalies point to its breakdown.[36] The latest runs of the LHC have for now instead failed to produce the glaring new physics expected from the rationale of the hierarchy problem.

On the other hand, the SM (along with any BSM additions) is expected to be eventually embedded within a framework that includes quantum gravity (QG) at or below the Planck scale $M_{\rm pl}$ and one might legitimately hope a unified description to be very constraining. This was certainly the expectation in the 80s, when the authors of [44] concluded their presentation of the free heterotic string with the (in)famous remarks

> *" Although much work remains to be done there seem to be no insuperable obstacles to deriving all of known physics from the heterotic string."*

Later, the phenomenological significance of QG was challenged by the apparent discovery of an enormous number of vacua in string theory, our best candidate QG. If the *landscape* of all possible resulting low-energy 'laws of nature' were so vast it could, in principle, include any self-consistent effective field theory (EFT), there would be no definite prediction of QG below the Planck scale.

Large landscapes present other types of opportunities, such as the necessary setting for *anthropic* arguments. When satisfactory dynamical explanations for the value of particularly fine-tuned parameters fail, a viable alternative is the presence of a landscape of different reliasable possibilities where only those fine-tuned instances are amenable to the formation of observers who ask the question in the first place.[37]

[36] Beyond neutrino oscillations which can be added straightforwardly.

[37] The prime example of this is the 'coincidence' of the Earth-Sun distance in our solar system being *just right* for the development of life. The answer to this conspiracy is of course that many many stars with orbiting planets exist in ours and other galaxies and only in those where the distances are in fact *just right* are there observers pondering over their unreasonable luck.

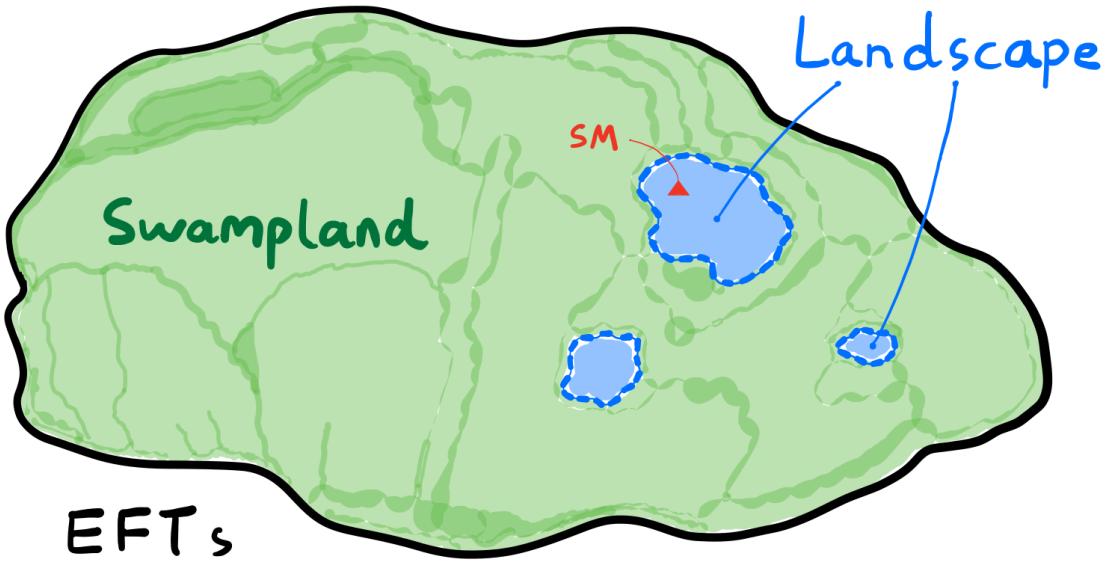

Figure 1.9: A conceptual, sketched map of the theory space of semi-classical effective field theories (EFTs). The solid black line encloses the space of self-consistent EFTs from those which are sick already at the semi-classical level. The subset of consistent EFTs which admit embedding into a theory of quantum gravity is called the Landscape (blue regions with dashed boundaries), while the remaining EFTs are said to be in the Swampland (green region). The relative sizes of the two in this pictorial representation should not be taken seriously. A more precise quantification of this is indeed part of ongoing research and debate. The red triangle marks the Standard Model.

This is the nature of the *anthropic principle*. To date it is the only option seriously discussed for the tiny value of Λ_c.

In more recent years, there has been some push back against the extent of the landscape. It is again becoming increasingly plausible that EFTs descending from QG must satisfy at least *some* non-trivial consistency conditions. The effort to identify (and prove!) the full set is the so-called *Swampland* program [45–47], currently in the form of conjectures with varying degrees of support. The situation is depicted pictorially in fig. 1.9.

In section 1.4.2 I will discuss the conjecture with strongest support at present and briefly mention those which are more consequential despite lacking the same level of rigor. The conjectures I will most focus on will be introduced in section 2.1.
First, however, some general comments on the marriage of relativity and quantum mechanics.

1.4.1 Gravity and quantum mechanics

The established laws of microphysics of section 1.1 and of general relativity in section 1.2.1 can be described by a single action principle

$$S = \int d^4x\sqrt{-g}\left[\frac{1}{16\pi G}\left(-R + 2\Lambda_c\right) + \mathcal{L}_{\rm SM}\right] \ , \tag{1.58}$$

where R is again the Ricci scalar, Λ_c the cosmological constant, $\mathcal{L}_{\rm SM}$ is the SM lagrangian of eq. (1.4) covariantly written by promoting partial derivatives to covariant ones $\partial_\mu \to \nabla_\mu$ and using the general metric $g_{\mu\nu}$ in tensor contractions rather than that of flat Mikowski space.

At present, we are most confident when treating eq. (1.58) semi-classically, keeping $g_{\mu\nu}$ as a classical field background satisfying the Einstein equations with the right hand side given by a classical $T_{\mu\nu}$. The quantisation of perturbative quantum fields in general space-time background already leads to extremely insightful results, such as the derivation of the *Hawking emission* of all existing particles from a black hole of mass M with a thermal spectrum of temperature

$$T = \frac{1}{8\pi GM} \ . \tag{1.59}$$

Backreaction on the metric from quantum effects can be computed by appropriately renormalising $\langle T_{\mu\nu}\rangle$ and adding its contribution (in general perturbatively) to the Einstein equation.

The geometric 'Einstein-Hilbert' part of eq. (1.58) also has a field theory interpretation; infact, it can be shown that its form is the unique lowest dimensional Lagrangian for a massless spin 2 field. It is famously non-renormalisable but one *can* of course actually quantise $g_{\mu\nu}$ within an effective field theory. No compelling UV completion exists to date within the framework of field theory; rather, it is usually expected that the fundamental quantisation of gravity requires a departure from the usual tools of quantum field theory.

Our best candidate for quantum gravity is *String Theory* [48, 49], already mentioned above, in essence a first quantisation theory of $1-$dimensional 'strings' which replace the 'traditional' view of particles as point-like objects. The consistency of the theory requires at least 10 total space-time dimensions. Thus, to make contact with our 4d world, 6 or more of those must be *compactified*. The richness of the string theory landscape arises from the enormous variety of compactifying geometries, as well gauge fields non-trivially wrapped around the compactified dimensions ('fluxes'). In the resulting 4d theory a large number of scalar 'moduli' fields emerge

which parametrise the continuous geometric properties (e.g. total volume) of the compactified space. It is believed that all couplings, such as the Yukawas in eq. (1.4) derive from products of vauum expectation values of moduli.

I will generally avoid delving into any string theory details in this thesis as the work here is focused on exploring IR considerations inspired by very general statements pertaining to a consistent quantum gravity but not fundamentally reliant on the explicit machinery of any theory thereof.

1.4.2 No Global Symmetries and Other Conjectures

The conjecture for which there is most evidence is that *in any theory coupled to gravity there can be no exact global symmetry.*

This statement can be traced back to the 'no-hair' theorems in black hole physics. Glossing over subtleties, this states that black hole solutions to the Einstein field equations are completely characterised by their charges associated to gauge symmetries, such as mass, angular momentum and electromagnetic charges. I will take as the prime example of an apparent global symmetry $B - L$ in the SM but the arguments apply completely in general. No stationary solution of eq. (1.58) exists with field configurations storing the $B - L$ charge. If an observer throws a neutron into a black hole, its mass will increase but no property of the classical spacetime then onwards registers a $+1$ for $B - L$.

Thus global charge does not register at the semiclassical level. If $B - L$ were truly a symmetry however, one would expect at the QM level for the BH states to be labeled by their $B - L$ number. Since it does not register semi-classically one can construct BHs of mass for instance $\sim 10 M_{\rm pl}$ with arbitrary high global charge by throwing in neutrons and then letting it shrink back down by emitting photons. Thus there would be an infinite tower of distinct states at a given mass scale which would renormalise G_N to infinity.

In perturbative string theory any symmetry of the world sheet is automatically gauged so that the conjecture is trivial [50]. Recently a proof was put forward in [51] in the context of AdS/CFT correspondence.

The no global symmetries conjecture does constrain SM parameters - for example, one should not be able to take the up and charm quark masses equal - but rules out only a seemingly measure zero space,[38] so this is not yet by itself a powerful explanatory principle.

[38] Though more likely an exponentially small set, of rough 'size' $\exp(-M_{\rm pl}^2/\Lambda_s^2)$, where Λ_s is a cut-off related to the tension of strings [52].

Closely related, is the *Weak Gravity Conjecture* [53] concerning the limit of small gauge coupling (in which in some sense a global symmetry is recovered), which demands that for any gauge theory there exists at least one particle in the spectrum with mass-charge relation $Q > M$ ensuring that 'gravity is the weakest force' for it.

Modern swampland conjectures have multiplied in number and decreased in rigor in recent years - although they are often interconnected - and the reader is directed to [47] for a review.

In the rest of this thesis I will focus on conjectures constraining the form of the vacuum potential of any theory coupled to gravity. Made explicit by the *swampland de Sitter conjecture* and *trans-Planckian censorship conjecture* described in section 2.1, they are in essence a quantitative formulation of the general difficult with marrying QM mechanics with de Sitter space, corresponding to a stable positive vacuum energy vacuum.

Chapter 2

QCD, Flavour and the Stability of de Sitter

2.1 Introduction

One of the most striking of the conjectured constraints is the *swampland de Sitter conjecture* (SdSC) proposed in [54] and then refined [55–57], which states, in the 4-dimensional case, that the total low-energy potential $V(\{\phi_i\})$ must either satisfy

$$|\nabla V| \geq c\frac{V}{M_{\rm pl}} \tag{2.1}$$

$$\text{or} \qquad \min(\nabla_i \nabla_j V) \leq -c'\frac{V}{M_{\rm pl}^2} \tag{2.2}$$

for $\mathcal{O}(1)$ coefficients $c, c' > 0$, and where ∇ denotes a derivative with respect to all scalar field directions $\{\phi_i\}$. Thus according to this conjecture *potentials possessing meta-stable de Sitter vacua are in the swampland, as are potentials with regions of field space that are too 'flat' if* $V > 0$.

So far the dominant use of this conjecture has been in the cosmological context, for example the analysis of Ref. [58]. It has been argued that a possible early epoch of cosmological inflation is severely constrained, and that the apparent presently-observed cosmological acceleration must be due to a time-evolving quintessence field, $\varphi(t)$, and not a true cosmological constant.

A closely-related conjecture that imposes somewhat weaker restrictions on the potential is the Trans-Planckian Censorship Conjecture (TPCC) [59], a 'global' (in field space) constraint that states that during the expansion of the universe quantum fluctuations that start sub-Planckian must remain smaller than the Hubble horizon and so never freeze-in to become effectively classical. Notably, the TPCC *allows meta-stable de Sitter states if they are sufficiently short-lived.* Specifically, the lifetime τ_V,

of a meta-stable dS state with effective cosmological constant V is bounded above by

$$\tau_V \leq \frac{1}{H_V} \log\left(\frac{M_{\rm pl}}{H_V}\right) = \frac{1}{2}\sqrt{\frac{3M_{\rm pl}^2}{V}} \log\left(\frac{3M_{\rm pl}^4}{V}\right) \tag{2.3}$$

where H_V is the Hubble constant of the meta-stable state.

The validity of the SdSC is controversial, with arguments being made both for and against. It is also possible that a further refinement of the conjecture is necessary beyond fixing the presently unknown, but believed to be $\mathcal{O}(1)$, constants c, c'. For the present purposes I *assume that the SdSC is correct as stated* and explore its possible ramifications for low-energy physics.

Specifically, in this section I will make the surprising claim that it is possible that the SdSC limits the allowed values of the quark masses and QCD-$\overline{\theta}$ parameter. I find that the *observed* values of the quark masses and $\overline{\theta}$-parameter are consistent with the SdSC, but variations away from the observed values lead to IR-calculable potentials which, as functions of the light pseudo-Nambu-Goldstone boson (pNGB) fields, $\pi^a(x)$, possess meta-stable de Sitter vacua. The difference, ΔV, in the value of the potential energy density between the true ground state and these meta-stable states satisfies, $H_0^4 \ll \Delta V \ll M_{\rm pl}^4$, where H_0 is the present value of the Hubble parameter. In addition these meta-stable vacua occur for field values $\langle \pi^a(x) \rangle \lesssim f_\pi \ll M_{\rm pl}$. Because of this large parametric separation in scales, the effective field theory analysis of the meta-stable state structure is under good control. Moreover, I am here making what I believe to be the reasonable statement that if the SdSC makes sense in its current form then it should apply not only to 'fundamental' scalar fields and their potentials but also composite scalar fields and their potentials arising from strong-coupling dynamics. (If this were not the case then a straightforward extension of the results here imply that it would be easy to construct simple strong-coupling hidden sector models that would lead to a very-long-lived de Sitter phase, and thus in practical terms invalidate the constraints on early and late cosmology from the SdSC.)

Thus I make the claim that regions of quark-mass-parameter and $\overline{\theta}$-parameter space might be forbidden by consistency with quantum gravity! Indeed, a connection between quantum gravity consistency and the detailed properties of QCD and the flavor sector of the SM is in fact *already implied* by other better established (though I emphasise not yet proven) swampland conjectures. For example, the Swampland Global Symmetry Conjecture already states that, for the pure SM, it is inconsistent

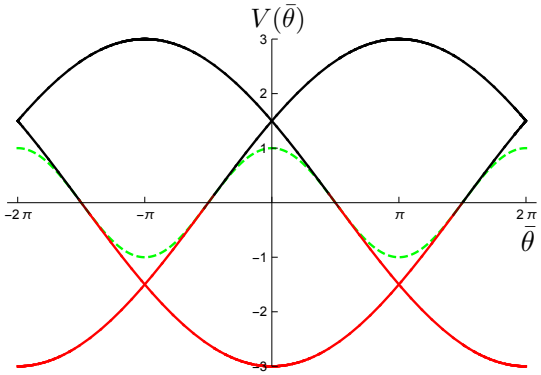

Figure 2.1: The behavior, as a function of $\overline{\theta}$, of the potential energy density of the critical points of the three-light-flavor leading-order chiral Lagrangian when quark masses, m, are equal [62, 63]. Red sections of curves are local minima, dashed green are saddle points, and black sections local maxima. The true ground state, the lowest segment of the red curves, is a 2π-periodic, non-analytic function of $\overline{\theta}$. In the range $\pi/2 < \overline{\theta} < 3\pi/2$ there are two local minima, *with the upper section of the red curve being a meta-stable state split from the ground state by* $\mathcal{O}(m\Lambda_{qcd}^3)$. At $\overline{\theta} = \pi$ the Dashen phenomena [64] occurs, CP is spontaneously broken, and there are two degenerate ground states.

with quantum gravity for any two equally-charged quarks to have Yukawa couplings that simultaneously vanish or be exactly equal.

Although in its own right this statement regarding the violation of global symmetries is a fascinating connection between quantum gravity and low-energy physics, practically speaking this only excludes only a vanishingly small set of the a-priori SM parameter space. (Naively of measure zero, but in fact likely a thicker set of size $\exp(-M_{\rm pl}^2/\Lambda^2)$ where here Λ is a suitable cutoff of the low-energy theory related to the tension of strings [52, 60].) On the other hand *I will argue that the refined swampland de Sitter conjecture plausibly excludes an* $\mathcal{O}(1)$ *subset of the a-priori allowed SM parameter space, and thus is potentially a much more powerful restriction on the low-energy features of the SM.*

2.1.1 The primary idea

As has been known for some time [61–63] and as I will argue in detail in section 2.2, QCD can exhibit for $N > 2$ light quarks both a true ground state *and meta-stable states* as a function of the light pseudo-Nambu-Goldstone boson fields, π^a (here $a = 1, \ldots, N^2 - 1$).

Suppose the QCD- and flavor-sector parameters of the SM which here I collectively

call $\{y_\alpha\}$, which include both heavy and light quark masses and the QCD $\overline{\theta}$-parameter, are allowed to vary from their observed values.[1] Critical points of the QCD-sector potential will move continuously as a function of the $\{y_\alpha\}$ parameters and may change their character, between local minimum, saddle point and local maximum. Let the energy density of these discrete 'branches', labelled by $n = 0, 1, \ldots$, be $V^{(n)}_{\{y_\alpha\}}(\pi^a)$. I choose the convention that at any given value, $\{y_\alpha\}$, of the SM parameters the true ground state branch is $n = 0$ while $n = 1, \ldots$ label the potential functions for the various non-ground-state branches in ascending order of energy density. Note, importantly, that as the SM parameters $\{y_\alpha\}$ vary the number of meta-stable branches can change. Branches can also cross or merge. Thus in general the behavior of the ground state and excited branches is a non-analytic and extravagant function of the parameters $\{y_\alpha\}$. I illustrate this behavior in figure 2.1 for the simple case of three equal mass light quarks as a function of $\overline{\theta}$, and in figure 2.2 for six light quarks divided into two groups of three equal mass quarks, as a function of the mass ratio, and for $\overline{\theta} = 0$.[2]

Most importantly, and as is well known, using the power of chiral Lagrangian techniques the $V^{(n)}_{\{y_\alpha\}}(\pi^a)$ are *IR-computable* functions of the π^a's not depending on details of the UV completion. So as to compare hypothetical worlds on a like-for-like basis, I demand that in the ground state of the SM, so in the branch $V^{(0)}_{\{y_\alpha\}}(\pi^a)$, the total vacuum energy is (close to – I quantify this in section 2.3) zero for each and every choice of $\{y_\alpha\}$. Minimally I do this by tuning a necessarily $\{y_\alpha\}$-dependent additive constant in the potential, which may or may not be, for example, the result of some continuous or discrete neutralization or relaxation mechanism [65–69] as long as it itself is not in conflict with the SdSC and other swampland constraints. We of course do not currently have an accepted good theory of this tuning, but this tuning cannot simultaneously set both the effective vacuum energy density of the meta-stable state(s) and the stable ground state to zero. The working assumption in this thesis is that the SM ground state is the state that must have vacuum energy

[1] For the purposes of this paper I will only consider the quark masses and $\overline{\theta}$-angle as variable parameters, and fix all other SM parameters such as the electromagnetic fine structure constant and the QCD scale Λ_{qcd}. Other 'hidden' parameters are possible too, e.g. the scale of a spontaneous breaking $SU(N_c) \to SU(3)_c$ if we want to smoothly extend consideration to $SU(N_c)$ theories of the QCD-gauge group.

[2] Although, strictly speaking, three quarks of exactly equal mass is a point in parameter space forbidden by the SGSC, it is important to note that the form of the curves is an analytic function of the $\{y_\alpha\}$, so if I move very slightly away from exact equality of masses, or special points like $\overline{\theta} = 0$, the number and properties of the critical points of the potential is almost everywhere unchanged, with the exceptions being points where curves cross. So the situation illustrated in figures 2.1 and 2.2 is a good guide as I explicate in detail in section 2.2.

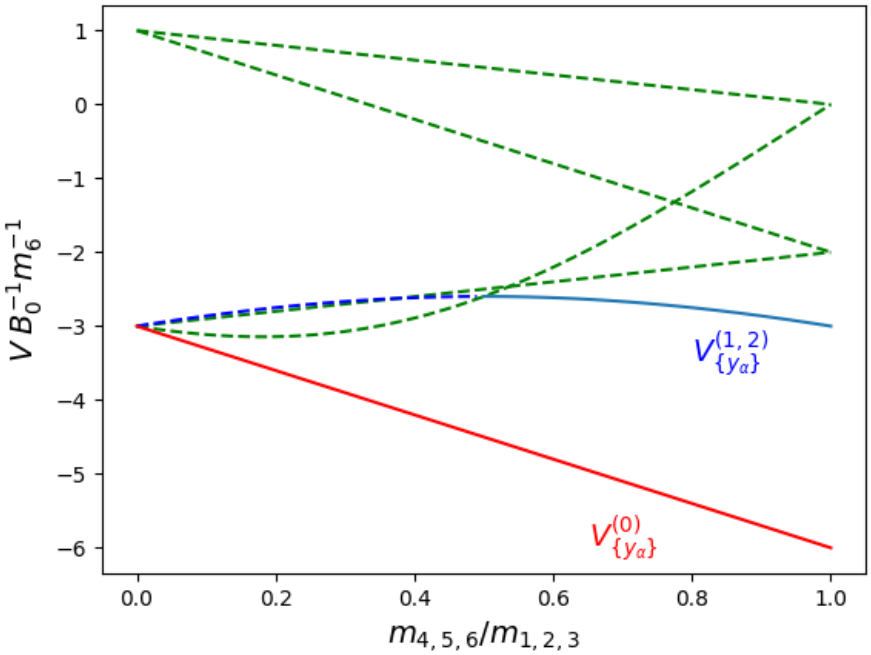

Figure 2.2: An example of meta-stable states appearing in the vacuum structure of QCD at $\overline{\theta} = 0$ as quark masses are varied. Here I divide 6 light quarks into two sets of three equal mass quarks, $m_1 = m_2 = m_3$ and $m_4 = m_5 = m_6$, and continuously vary the mass ratio $0 \leq m_6/m_1 \leq 1$. $V^{(0)}_{\{y_\alpha\}}$ in red corresponds to the global minimum 'branch', while $V^{(1,2)}_{\{y_\alpha\}}$ in blue are a pair of degenerate branches which turn from saddle points (dashed line) to meta-stable states (solid line). Some, but not nearly all, other branches of saddle points are also shown. $B_0 \sim \Lambda^3_{QCD}$ is a parameter of the chiral Lagrangian related to the pNGB mass. The typical difference in energy densities between the ground state and the meta-stable branches is $\sim$ few $\times B_0 m_6 \sim$ few $\times \Lambda^3_{qcd} m_6$.

close to zero. Then, if the SM plus gravity were a complete description of low-energy, $E \lesssim \Lambda_{qcd}$, physics, with no ultra-light feebly-coupled fields present, and given the stated assumptions, the SdSC would immediately forbid those values, $\{y^*_\alpha\}$, of the SM parameters for which meta-stable states exist.

Although the vacuum structure of the strong sector is determined by the N 'light' quarks, $m_q \ll 4\pi f_\pi \sim 4\pi\Lambda_{qcd}$, the value of Λ_{qcd} itself, however, is of course sensitive to the UV initial condition on g_3 as well as, to a lesser extent, the masses of the 'heavy', $M_q \gtrsim 4\pi\Lambda_{qcd}$, quarks, which stop contributing to the running at scales $\mu < M_i$. Concerning this, if $\Lambda_{(n_f)}(g_{3,\mathrm{UV}})$ is the value of the strong scale computed with n_f quarks always active, the effect of a heavy quark mass threshold is, to leading order [70],

$$\Lambda_{(n_f-1)} = \Lambda_{(n_f)}^{(33-2n_f)/(35-2n_f)} M_1^{2/(35-2n_f)} \tag{2.4}$$

where M_1 is the mass of the heaviest quark. So, as the heavy quark masses are lowered, the value of Λ_{qcd} reduces, and in principle more quarks could become light as some of the heavy quark masses are reduced, or vice versa. However this effect is quite weak. In this paper I limit myself to simply considering 'QCD with N light quarks' in its generality, for different mass ratios and vacuum angles, irrespective of what $\Lambda_{qcd}(g_{3,\mathrm{UV}})$ and the M_i are. In reality, it is of course to be expected that these parameters and others are set by UV quantum gravity dynamics and it is certainly possible that one may not freely vary each individually. In fact, if the SdSC were true, the results here make the surprising point that the correlated dependence of the low-energy parameters on the underlying UV parameters must be such so that the values of $\{y_\alpha\}$ I find to be in the swamp could never be attained.

In section 2.2 I delineate, in the case where there are two or more light quarks, $N \geq 2$, the regions of quark mass and $\overline{\theta}$-parameter space which are excluded by this criterion. The region of meta-stable states is determined by a function of the light-quark mass ratios and $|\overline{\theta}|$. For example, in the limit that the two lightest masses become degenerate $m_{N-1} \to m_N$ (my convention is that m_N is the mass of the lightest quark) the results are captured by the following single condition

$$\sum_{i=1}^{N-2} \sin^{-1}\left(\frac{m_N}{m_i}\right) > \pi - |\overline{\theta}|, \qquad \overline{\theta} \in (-\pi, \pi] \ . \tag{2.5}$$

If satisfied, the theory will feature a meta-stable state as derived from the leading order chiral Lagrangian (if the inequality is saturated a higher-order analysis is necessary). The general condition, valid for arbitrary light quark mass ratios, is made precise in section 2.2.

As the number of light quarks increases, larger and larger regions of the parameter space possess meta-stable states and so are excluded. For instance, in the case of all light quark masses equal, I find $N > 4$ possesses meta-stable states for $\overline{\theta} = 0$ ($N = 4$ at $\overline{\theta} = 0$ requires a higher order analysis that I will cover in a later work). This continues to hold for a range of mass ratios away from exact equality. For example in figure 2.2 I show how a branch goes from being a saddle point to a meta-stable state as a particular combination of masses is changed. As $\overline{\theta}$ becomes non-zero the range of ratios $\{m_\alpha/m_\beta\}$ in the swamp increases. The analysis shows that for $|\overline{\theta}| > \pi/2$ even for $N = 3$, close relatives of our world have meta-stable states. For the theory to be 'safe' from the swamp for all $\overline{\theta}$ one requires[3]

$$\frac{1}{m_3} > \frac{1}{m_2} + \frac{1}{m_1} \ , \tag{2.6}$$

a condition curiously satisfied by the SM in the up, down and strange quark masses (see figure 2.7). As well as providing analytic expressions, I develop a diagrammatic method (a 'fan diagram') for identifying meta-stable states, as well as more general critical points.

This analysis summarized above assumes the IR theory is the SM plus gravity, so I have not yet considered the effects of additional ultra-light feebly-coupled fields which may be motivated for two reasons. First, cosmological observations appear to demand that we are presently in an epoch of accelerated cosmological expansion. As mentioned, a net positive cosmological *constant* term is in contradiction with the SdSC,[4] and therefore the approach taken in the literature has been to assume that there exists an ultra-light quintessence field, $\varphi(t)$, which is evolving in a potential with suitable tiny effective vacuum energy density without a local minimum and which (marginally) satisfies the SdSC [58]. If this is correct then we must include the quintessence field in the analysis too.[5] In section 2.3 I address this modification and argue that, unless an extreme fine-tuning is allowed, it is impossible to include a quintessence field in a manner consistent with the SdSC that does not also lead to a collapse into an AdS state on excessivley short timescales. Thus the SdSC still excludes the regions of parameter space with QCD meta-stable states.

[3]The generalisation to N quarks is straightforward, see eq.(2.29).

[4]Given the apparent immense theoretical difficulty and fine-tuning implied by such a tiny positive cosmological term, we do not consider it *definitely* established that the observations are explained by an effective non-zero vacuum energy rather than, say, an apparently highly unusual but not so extremely-fine-tuned alternative cosmology without a positive vacuum energy. For the purposes of this paper I assume that the observational claims of acceleration are correct and, moreover, there *is* at present a tiny positive effective vacuum energy density.

[5]Here I am ignoring the stimulating "Thermal Dark Energy" proposal of [71] which avoids quintessence fields.

Second, I have excluded the possibility of a light QCD axion relaxing the $\overline{\theta}$ angle to zero [72–74]. This is less of an issue as there are non-Peccei-Quinn-Weinberg-Wilczek solutions to the strong-CP problem that do not involve adding new states in the deep IR of the SM [75–79]. Nevertheless, it is interesting to consider the effect of the axion solution to the strong-CP problem on the reasoning here, and which will be addressed in future work.

In section 2.2.6 I turn to the question of whether the case of no light quarks, $N = 0$, namely, pure $SU(3)_c$ Yang-Mills theory, possesses meta-stable states and thus is in the swampland. There are of course two ways this situation could occur: Either all the quark Yukawa couplings could be $\gg 0.01$ with the electroweak vacuum expectation value (vev) fixed. Or, most interestingly, the Yukawa couplings can retain their standard values while the electroweak vev is taken to be $\gg 50\,\text{TeV}$. In this second case this thesis then possibly leads to a new perspective on the hierarchy problem. Fascinatingly, as has been known for a long time, large-N_c analysis of the pure $SU(N_c)$ theory strongly implies an $\mathcal{O}(N_c)$ number of meta-stable states (I review this statement and its refinements in section 2.2.6), though this analysis breaks down for small N_c. Moreover other, related, semi-classical arguments possibly indicate that even $SU(3)$ Yang-Mills theory might have meta-stable states at $\overline{\theta} = 0$. To my knowledge there are no lattice studies of this issue, so it is not definitively known whether pure $SU(3)$ has meta-stable states or not.[6] If we assume that it does, much of the a-priori SM parameter space is eliminated by the SdSC, in particular the limit of large electroweak vev $v_{EW} \gtrsim 50\,\text{TeV}$ is excluded (if quark Yukawa couplings are kept fixed). I again argue that these statements are robust against the addition of a quintessence field unless extreme fine-tuning is allowed. Thus it is possible that the SdSC sheds a significant new light on the hierarchy problem. In section 3.3 I discuss the limit of large positive Higgs m_H^2 parameter in light of the Swampland Program.

I now turn to the details of my analysis.

2.2 meta-stable states of $SU(3)_c$ with $N \geq 2$ light quarks

I here focus on the study of the meta-stable states of the color and quark sector of the SM for two or more light quarks (but not so many that UV asymptotic freedom and IR confinement and $SU(N)_L \times SU(N)_R \to SU(N)_V$ chiral symmetry breaking are lost). In this case we may use the power of chiral Lagrangian techniques to investigate the

[6] JMR and I thank Mike Teper for discussions of this issue.

vacuum and meta-stable state structure of the theory as a function of the light quark masses and the QCD $\overline{\theta}$-angle [61–63, 80]. Written in terms of the Nambu-Goldstone fields packaged as $\Sigma(x) = \exp(2i\pi^a(x)T^a/f_\pi) \in SU(N)$, the relevant terms in the chiral Lagrangian are

$$\mathcal{L} = \frac{f_\pi^2}{4}\mathrm{Tr}\left(\partial_\mu\Sigma^\dagger\partial^\mu\Sigma\right) - B_0\mathrm{Tr}\left(e^{-i\overline{\theta}/N}M_q^\dagger\Sigma + e^{i\overline{\theta}/N}\Sigma^\dagger M_q\right) , \tag{2.7}$$

where M_q is the $N \times N$ quark mass matrix, and $B_0 > 0$ is a mass-dimension three parameter, $\mathcal{O}(\Lambda_{qcd}^3)$, whose precise value can be related to the pion mass. Using field redefinitions it is always possible to take, without loss of generality, the quark mass matrix to be diagonal and real, $M_q = \mathrm{Diag}(m_1, m_2, \ldots, m_N)$, with $m_1 \geq m_2 \geq \ldots \geq m_N$.

2.2.1 Critical points of the potential

As shown in [80] all spacetime-independent extrema of the potential eq.(2.7) can be written in diagonal form

$$\Sigma = e^{i\overline{\theta}/N}\mathrm{Diag}(e^{\phi_1}, e^{\phi_2}, \ldots, e^{\phi_N}) . \tag{2.8}$$

Here an overall $\exp(i\overline{\theta}/N)$ has been factored out for convenience. Special unitarity requires

$$\phi_1 + \cdots + \phi_N + \overline{\theta} = 0 \mod 2\pi. \tag{2.9}$$

Subject to this constraint $(\phi_i + \overline{\theta}/N)f_\pi \equiv \langle\pi^i\rangle$ defines a useful linear-recombination of the vacuum expectation values of the neutral ($SU(N)$ Cartan sub-algebra) pNGB fields. The relevant potential is then

$$V(\phi_i) = -B_0\sum_i^N m_i\cos\phi_i . \tag{2.10}$$

Each angle can thus be associated to a quark mass. Differentiating eq.(2.10) subject to eq.(2.9) gives a condition for a critical point in terms of the tower of identities:

$$\sin\phi_1 = \frac{m_2}{m_1}\sin\phi_2 = \cdots = \frac{m_N}{m_1}\sin\phi_N . \tag{2.11}$$

We see therefore that the angles ϕ_i must be spread out like an ordered fan, as shown in fig. 2.3(a).

Taking $\phi_{i<N}$ as independent, the relevant Hessian determining the nature of the critical points is

$$H_{ij} = \delta_{ij}m_i\cos\phi_i + m_N\cos\phi_N , \tag{2.12}$$

where the second term is common to all entries. From this one sees that a necessary condition for positive-definiteness is $\cos\phi_{i<N} > 0$ as in figure 2.3(b). If we also have $\cos\phi_N > 0$, *the critical point is guaranteed to be a local minimum.* The more general condition is given by[7]

$$\det\left(H_{ij}\right) = \sum_{i}^{N}\prod_{j\neq i}^{N} m_j \cos\phi_j > 0 \ , \tag{2.13}$$

$$\implies C(\phi_N) = 1 + \frac{m_N\cos\phi_N}{m_1\cos\phi_1} + \cdots + \frac{m_N\cos\phi_N}{m_{N-1}\cos\phi_{N-1}} > 0 \ . \tag{2.14}$$

C is chosen to depend on ϕ_N as all other ϕ_i *at a local minimum point* unambiguously follow from eq.(2.11).

2.2.2 meta-stable states at equal quark masses

A particularly simple case in which analytic expressions are straightforward to derive occurs when all masses are equal, $m_i = m$, $\forall i$ (see figure 2.1 for the $N = 3$ case). Then the critical points of the potential eq.(2.10) satisfy $\phi_i = \phi$ or $\pi - \phi$ $\forall i$, for some angle ϕ which is determined by the unitarity constraint.

At a local minimum, all ϕ_i are equal

$$\phi_i = \frac{2\pi n - \overline{\theta}}{N} \equiv \phi \qquad \forall i \ , \tag{2.15}$$

and have positive cosine, so that $n \in \mathbb{Z}$ satisfies

$$-\frac{N}{4} + \frac{\overline{\theta}}{2\pi} < n < \frac{N}{4} + \frac{\overline{\theta}}{2\pi} \ . \tag{2.16}$$

Note that if the boundary values satisfy $\overline{\theta}/2\pi \pm N/4 \in \mathbb{Z}$ this does not reliably lead to extra meta-stable states. This is because the eigenvalues of the Hessian at a local min are $Nm\cos\phi$ (once) and $m\cos\phi$ (with multiplicity $N-2$), which all vanish at such a point and so a higher-order analysis including the $\mathcal{O}(M_q^2)$ and electromagnetic terms in the chiral Lagrangian is necessary to determine if there are shallow local minima in this marginal case. So, to be conservative, I only count those minima strictly satisfying the condition eq.(2.16).

In any case, the value of the potential at the local minima specified by eq.(2.15) subject to eq.(2.16) are

$$V^{(n)} = -NmB_0\cos\left(\frac{2\pi n - \overline{\theta}}{N}\right) \ , \tag{2.17}$$

[7] One way to see this is by studying the characteristic polynomial of the symmetric matrix H_{ij}. The condition eq.(2.13) can be seen to ensure that there are no negative roots (i.e. eigenvalues) by Descartes' rule of signs.

so if meta-stable local minima exist they are typically split in energy density from the ground state by $\mathcal{O}(m\Lambda_{qcd}^3)$, apart from the exceptional case of $\overline{\theta} = \pi$ where there are two degenerate states [63]. Except in tuned cases, $\mathcal{O}(m\Lambda_{qcd}^3)$ is also a good estimate of the splitting between the meta-stable states and the ground state in the general case of unequal masses if the mass parameter is chosen to be that of the lightest non-zero quark mass.

It is amusing to count the number of local minima in this equal quark mass case as $N \geq 2$ and $\overline{\theta}$ vary. For example one finds that at $\overline{\theta} = 0$ the total number of reliably predicted meta-stable minima, N_s (excluding the true ground state), is given as

$$N_s(\overline{\theta} = 0) = 2[N/4]_< \tag{2.18}$$

where $[x]_<$ denotes the integer part of x with magnitude strictly less than $|x|$. So for $N = 2, 3, \ldots, 6$ one finds $N_s = (0, 0, 0, 2, 2)$, and thus that five equal mass light quarks is the first case one definitely finds meta-stable vacua at $\overline{\theta} = 0$. On the other hand for, eg, $\overline{\theta} = \pi/2$, $N_s = [(N+1)/4]_< + [(N-1)/4]_<$, giving $N_s = (0, 0, 1, 1, 2)$, so meta-stable vacua definitely first appear when there are four equal mass light quarks.

The tunnelling rate between these meta-stable states and the ground state (or a lower meta-stable state if there are many) has been calculated in simple limits in Refs. [63, 80]. For example, just away from $\overline{\theta} = \pi$ there are two slightly split vacua with a difference in energy densities given by $\Delta V \sim \sqrt{3} B_0 m|\delta|$ where $\overline{\theta} = \pi + \delta$ and $|\delta| \ll 1$ is assumed. Then the result of a thin-wall false vacuum decay calculation gives a zero-temperature decay rate per unit volume [63] (neglecting sub-leading $\mathcal{O}(1/|\delta|^2)$ terms in the exponent)

$$\frac{\Gamma}{\text{Vol}} \sim \Lambda_{qcd}^4 \exp\left(-D \frac{f_\pi^4}{m B_0 |\delta|^3}\right) , \tag{2.19}$$

with a numerical factor $D \simeq 4 \times 10^3$. Because of this large numerical factor, even for $\delta \not\ll 1$ (as long as δ does not approach $\pi/2$ where the meta-stable state ends) and relatively 'heavy' light quarks with $m \sim \Lambda_{qcd}$, the meta-stable state is predicted to be long lived in this equal quark mass case.

2.2.3 Fan diagrams

Away from the special case of equal masses the analysis is more complicated and analytic formulae are not particularly illuminating. Fortunately, as already indicated, the general conditions in section 2.2.1 lend themselves to a diagrammatic interpretation of critical points, a 'fan' diagram, which is particularly useful for the qualitative identification of meta-stable states for any $\{m_i, \overline{\theta}\}$.

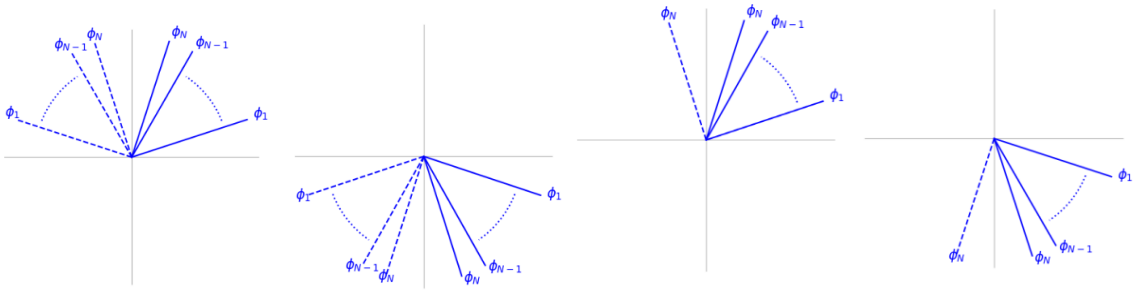

(a) *Critical point* (b) *Local minima*

Figure 2.3: Necessary qualitative arrangements of the ϕ_i at a general critical point and a local minimum. The 'spreadout-ness' of these 'fan diagrams' is determined by ratios m_i/m_j via eq.(2.11). As m_N was chosen to denote the lightest quark, the angle ϕ_N will always be closest to the y axis, with successive angles flattening out towards the x axis with separations determined by the ratios m_i/m_j (if $m_i = m_j$ then $\phi_i = \phi_j$ or $\pi - \phi_j$). Dashed lines in figure (a) denote an equally possible alternative for each individual angle. Thus there are $2 \cdot 2^N$ qualitativelty different arrangements that may constitute a critical point. Generally, only a subset of these will be consistent with the constraint $\sum_i \phi_i = -\overline{\theta} \mod 2\pi$, which determines the absolute value of the ϕ_i. The extra requirement of a local minimum picks out the arrangements in figure (b). Here, for the dashed ϕ_N to be a valid alternative for a local minimum the extra constraint eq.(2.21) must also be satisfied.

A local minimum, if it exists, corresponds to an ordered arrangement of angles as in figure 2.3(b), where the spread between angles is fixed by the respective mass ratios according to eq.(2.11), so as the mass ratios approach unity the separation angles between the corresponding elements of the fan become smaller, and conversely increase as the mass ratios increase.

To find a local minimum one adjusts the value of the 'leading' angle ϕ_N (recall that m_N is the lightest quark), from which all other (subordinate) angles follow via $\phi_i = \sin^{-1}\left(\frac{m_N}{m_i}\sin\phi_N\right)$, until the sum of all ϕ_i hits the 'target' angle demanded by the unitary condition

$$S \equiv \sum_{i=1}^{N} \phi_i = -\overline{\theta} \mod 2\pi \ . \tag{2.20}$$

If the target angle is hit for $|\phi_N| < \pi/2$ the configuration is guaranteed to be a local minimum. Otherwise ($\cos\phi_N < 0$) one also requires eq.(2.14) to ensure minimality, which in this case can be reformulated in a version suited to diagrammatic analysis that only depends on the angles

$$|\tan(\phi_N)| > |\tan(\phi_1)| + \cdots + |\tan(\phi_{N-1})|, \quad \left(\frac{\pi}{2} < \phi_N < \pi\right) \ . \tag{2.21}$$

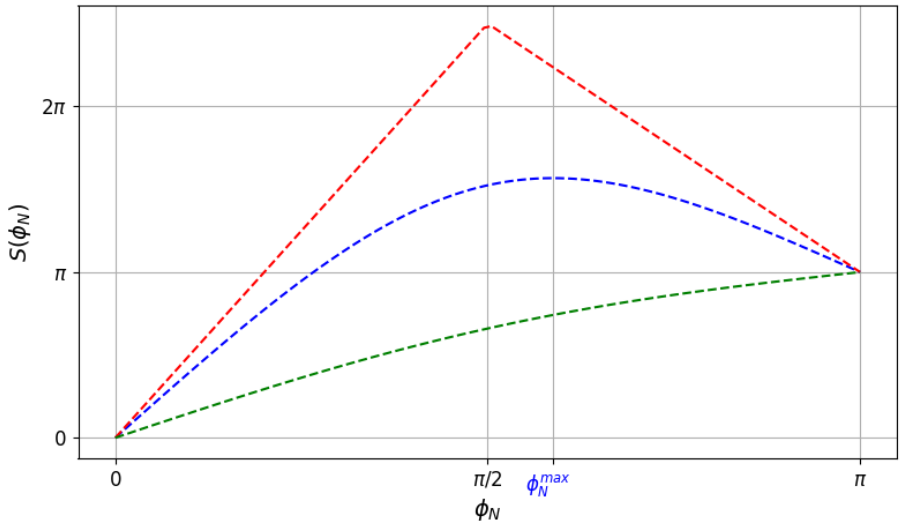

Figure 2.4: The sum of angles S as a function of leading angle $\phi_N \in (0, \pi)$ for different values of quark masses. $S(\phi_N)$ on $\phi_N \in (-\pi, 0)$ is inferred, being an odd function. If S hits the target angle $-\overline{\theta}$ mod 2π while its slope is positive then we have a local minimum. The position of the maximum value of $S(\phi_N)$ is mostly controlled by the two lightest quark masses. The red curve is characteristic of $m_N = m_{N-1}$, when $\phi_N^{max} = \pi/2$ always. As their ratio increases $S(\phi_N)$ goes from having $\phi_N^{max} \in (\pi/2, \pi)$ (blue line) to $\phi_N^{max} = \pi$, achieved at the boundary (green line).

Importantly, fan diagrams are useful because *if for a given set of parameters,* $\{y_\alpha\}$, *two distinct local minimum fan diagrams can be drawn, the theory admits meta-stable states.*

For a quantitative handle it is useful to consider the sum in eq.(2.23) as an explicit function of the leading angle ϕ_N

$$S(\phi_N) = \sin^{-1}\left(\frac{m_N}{m_1}\sin\phi_N\right) + \cdots + \sin^{-1}\left(\frac{m_N}{m_{N-1}\sin\phi_N}\right) + \phi_N \ . \tag{2.22}$$

For all quark masses, S goes from the 'closed fan' configuration $S(0) = 0$ to $S(\pi) = \pi$. Clearly $S(\phi_N)$ is monotonically increasing for $\phi_N \in (0, \pi/2)$ as all other subordinate angles also become larger. After $\phi_N > \pi/2$, however, the latter decrease as ϕ_N increases: the behaviour of $S(\phi_N)$ depends on the mass ratios at hand. Insight is obtained by differentiating eq.(2.22),

$$S'(\phi_N) = C(\phi_N) \ , \tag{2.23}$$

where $C(\phi_N)$ was the function whose positivity implied a local minimum, eq.(2.14), equivalent to eq.(2.21). Thus, the mark of a local minimum is equivalently expressed as

$$S(\phi_N) = -\overline{\theta} \mod 2\pi, \quad S'(\phi_N) > 0. \tag{2.24}$$

Note also that $C'(\phi_N) < 0$ on $(0, \pi)$. Depending on the values of $\{m_i\}$, $S(\phi_N)$ will either always monotonically increase or achieve a maximum $\in (\pi/2, \pi)$ as shown in figure 2.4.

Notice that here my primary concern is the *existence* of (multiple) local minima, rather than their specific location. For any $\theta \in (-\pi, \pi)$ there will always be a first local minimum with $|S(\phi_N^{max})| = |\theta|$. Suppose S achieves its largest value at ϕ_N^{max}. A sufficient condition for the existence of a second minimum is

$$S(\phi_N^{max}) > 2\pi - |\overline{\theta}| \ , \tag{2.25}$$

which ensures the target angle is hit a second time *for some value of* ϕ_N.

2.2.4 meta-stable states at $\overline{\theta} = 0$

For $\overline{\theta} = 0$, the global minimum of the potential corresponds to the trivial 'closed fan' arrangement $\phi_i = 0 \ \forall i$. We will have meta-stable states if there exist other arrangements satisfying

$$S(\overline{\theta}_N) = 2\pi n, \qquad S'(\phi_N) > 0 \ , \tag{2.26}$$

with $n \in \mathbb{Z}/\{0\}$. These will always come *in pairs* as for $\overline{\theta} = 0$ we have a $\phi_j \to -\phi_j$ symmetry. I focus on diagrams with positive angles, unless otherwise stated.

It is natural to start from the case of all masses equal $m_i = m_j$, implying $\phi_i = \phi_j$ for all i, j, already discussed in section 2.2.2. Even with the maximum values $\phi_i = \pi/2$ clearly no appropriate fan diagram may be drawn for $N \leq 3$. For $N = 4$, the diagram $\phi_{1-4} = \pi/2$ saturates eq.(2.13) and so is sensitive to higher order corrections to our effective Lagrangian eq.(2.7), and a deeper analysis is required.

As already mentioned, $N = 5$ is the first case with meta-stable states for $\overline{\theta} = 0$. For all masses equal, this corresponds to the diagram in figure 2.5. Analogous diagrams can be drawn for $N > 5$, explicitly with $\phi_i = 2\pi/N$. Moving away from the equal mass theory point, there will meta-stable states for a range of non-trivial mass ratios, corresponding to spreading of the angles in figure 2.5. For example, if the lightest four quarks are degenerate, then it should be clear from the diagram that the remaining one can be arbitrarily heavier (within the range of validity of the chiral Lagrangian): ϕ_1 can be arbitrarily small, compensated by $\phi_{2,3,4,5}$ moving arbitrarily close to $\pi/2$. A full chart of the swamp (by measure of the SdSC) for arbitrary $\{N, m_i\}$ is identified with the region satisying[8]

$$S(\phi_N^{max}(m_i)) > 2\pi \qquad (\overline{\theta} = 0) \ , \tag{2.27}$$

where the dependence of ϕ_N^{max} on $\{m_i, N\}$ is non-trivial, though easily implementable numerically. A good approximation is obtained by replacing $\phi_N^{max} \to \pi/2$ as suggested in figure 2.4, which gives

$$\sin^{-1}\left(\frac{m_N}{m_1}\right) + \cdots + \sin^{-1}\left(\frac{m_N}{m_{N-1}}\right) \gtrsim \frac{3\pi}{2} \qquad (\overline{\theta} = 0) \ . \tag{2.28}$$

The latter becomes an exact condition in the limit $m_{N-1} \to m_N$, is an underestimate when $m_N \lesssim m_{N-1}$ and again valid when $m_N \ll m_{N-1}$ (in which case there are no meta-stable states).

2.2.5 Non zero $\overline{\theta}$-angle

As $\overline{\theta} \in (-\pi, \pi)$ turns on, the global minimum of the potential moves away from the closed fan to a fan diagram with $\text{sign}(\phi_i) = -\text{sign}(\overline{\theta})$. At least one meta-stable state will be present if there exists also an arrangement with $\text{sign}(\phi_i) = \text{sign}(\overline{\theta})$ as in the example in figure 2.6. Clearly, the bigger $\overline{\theta}$ is, the larger the space of mass ratios with meta-stable states is, as less 'angular power' is necessary to reach the target angle

[8] See eq.(2.25) and surrounding text.

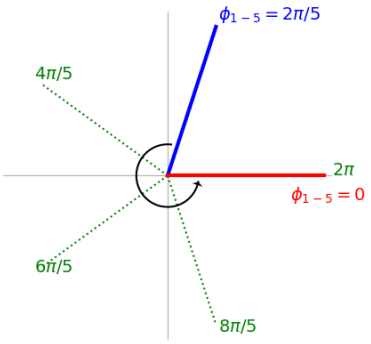

Figure 2.5: QCD at $\overline{\theta} = 0$ with 5 equal mass light quarks has a meta-stable state (blue) as well as the global minimum (red). There is also another (degenerate in V) meta-stable state corresponding to $\phi_{1-5} = -2\pi/5$. This behaviour persists for mass ratios satisfying $S(\phi_5^{max}\{m_i\}) > 2\pi$.

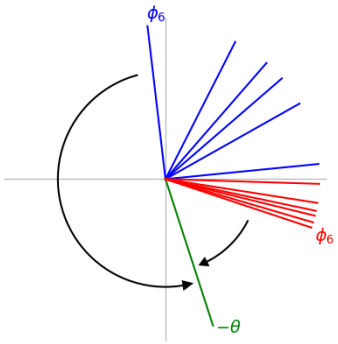

Figure 2.6: Global minimum (red) and meta-stable state (blue) in a 6 light quark theory with $\overline{\theta} = 2\pi/5$ and mass ratios $10 : 2 : 1.5 : 1.3 : 1.1 : 1$. In general, for high N and certain mass ratios, there may also be more minima, corresponding to diagrams whose angle sum makes an extra complete revolution before hitting the target.

$-\overline{\theta}$. This continues until $\overline{\theta} = \pi$, when global and first meta-stable branches become degenerate and in the neighbourhood of which the space of masses $\{m_i\}$ admitting a meta-stable state is at its largest, set by[9]

$$\frac{1}{m_N} < \frac{1}{m_1} + \cdots + \frac{1}{m_{N-1}} \qquad (\overline{\theta} = \pi) \ . \tag{2.29}$$

In particular, the case of *two light quarks* remains safe from meta-stable states for any mass ratio m_1/m_2 and vacuum angle $\overline{\theta}$. The case of *three light quarks* (our world) starts showing meta-stable states after $\overline{\theta} > \pi/2$, starting from the equal masses theory point and expands from there as shown in figure 2.7. It is interesting to note that the SM ratio of light quark masses satisfies

$$\frac{1}{m_u} > \frac{1}{m_d} + \frac{1}{m_s}, \tag{2.30}$$

where $m_{u,d,s}$ are the up, down and strange quark masses respectively, making the theory 'safe' from meta-stable states *for all values of* $\overline{\theta}$. As more quarks are made light, meta-stable states are encountered more and more frequently. Figure 2.8 shows a particular section of parameter space for four light quarks, while figure 2.2 shows

[9]This can be obtained by noting from figure 2.4 that there can be no local minimum other than the global one in the neighbourhood of $\overline{\theta} = \pi$ iff $S'(\pi) = C(\pi) > 0$.

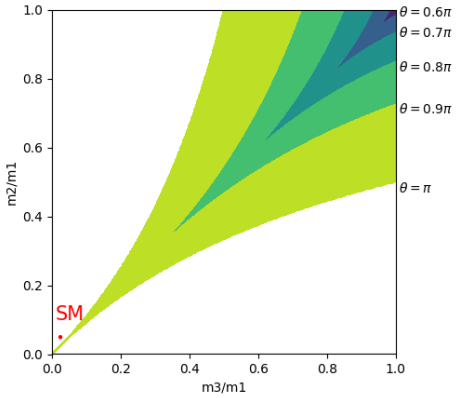

Figure 2.7: For three light quarks, regions with meta-stable states in the mass ratio plane for different values of $\overline{\theta}$ according to the leading order chiral Lagrangian analysis. Our world, with the values of $m_u = 2.16^{+0.49}_{-0.26}\,\text{MeV}$, $m_d = 4.67^{0.48}_{-0.17}\,\text{MeV}$ and $m_s = 93^{+11}_{-5}\,\text{MeV}$ is indicated by the red 'dot'.

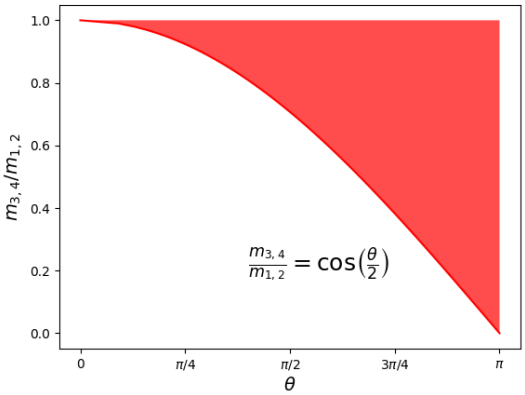

Figure 2.8: For four light quarks, fixing $m_1 = m_2$ and $m_3 = m_4$, the region in red, bordered by the equation in figure, corresponds to theory points with meta-stable states according to the leading order chiral Lagrangian analysis.

a similar slice for the case of six light quarks. Once again, we can write a condition mapping out the swamp (by measure of the SdSC) as

$$S(\phi_N^{max}(m_i)) > 2\pi - |\overline{\theta}| \ , \tag{2.31}$$

which, in its approximated $\phi_N^{max} \to \pi/2$ form, appeared as eq.(2.5).

Finally, it is also noteworthy that the theory points at the centre of the regions of meta-stable states correspond to the lightest quarks being degenerate (equal masses), the ensuing global symmetry thus simultaneously violating another swampland conjecture.

2.2.6 Standard Model with $N = 0$ light quarks

A question prompted by the proceeding analysis is if the $N = 0$ light quark limit is similarly constrained by the SdSC. There are two ways one can achieve this limit. Either all the quark Yukawa couplings can be taken to be $\gg 0.01$ so there are no quarks with masses less than $\sim 4\pi f_\pi \simeq 1\,\text{GeV}$. Or the Yukawa couplings can remain at their standard values while the electroweak vacuum expectation value (vev) is taken to be $\gg 50\,\text{TeV}$. In the second case this thesis possibly leads to a new perspective on the hierarchy problem. This will be the subject of section 3.2.

2.3 Coupling to quintessence

The swampland de Sitter conjecture has immediate relevance to our present environment; we must not currently live in a positive energy density local minimum. As a result, the cosmological constant is eponymously defiant, in that it must not be constant! As I briefly discussed in the Introduction this suggests (but does not uniquely imply) that there is currently some quintessence scalar $\varphi(t)$ contributing a positive energy density which is slowly evolving with time.

It is striking that, when confronted with observed cosmological parameters, simple models of quintessence are on the cusp of tension with the SdSC [58]. In particular, eqs.(2.1) and (2.2) imply that either the slope of the potential in the φ-direction around its present value, φ_0, is bounded below by an amount that depends on the value of the total effective vacuum energy now, $V(\varphi_0, \ldots) \equiv V_0 > 0$, or φ_0 is a local maximum in the φ-direction with curvature around that point being similarly bounded. But the quintessence field must not be so fast evolving that within a fraction of a Hubble time a deep anti-de-Sitter state is reached, and an associated "big crunch" occurs.[10]

Since quintessence may render the known Universe consistent with the swampland conjectures it is natural to consider whether it may also pose a potential significant caveat to the inconsistency of meta-stable QCD states with the conjectures. To this end, let us consider two possibilities

(i) Sequestered quintessence: $V \approx V^{(n)}_{\{y_\alpha\},\mathrm{QCD}}(\pi^a) + \tilde{V}(\varphi)$

(ii) Coupled quintessence: $V = V^{(n)}_{\{y_\alpha\},\mathrm{QCD}}(\pi^a, \varphi)$

where as before $n = 0, 1, \ldots$ labels all the branches. In the second case there is a non-trivial coupling between the QCD and quintessence sectors, and thus also between φ and the SM more generally. For either case there are two further considerations. The first is whether or not a scenario is consistent with the swampland conjectures. The second is whether or not it may be consistent with having a Universe that avoids a big crunch occurring on an extremely short timescale.

[10] Also in our particular Universe one must be consistent with the observational bound on the deviation of the equation of state parameter from $\omega \simeq -1$, though I will *not* need to use this tighter constraint.

2.3.1 Sequestered quintessence

The case of sequestered quintessence is straightforward, as the slope and curvature of the potential in the φ direction are independent of whether the QCD sector is in the ground state or a meta-stable state. This situation is illustrated in figure 2.9, while a case of coupled quintessence is sketched in figure 2.10. Applying the SdSC conditions to the meta-stable state at SM parameter values $\{y^*_\alpha\}$ with large and positive vacuum energy $\Delta V_{\{y^*_\alpha\},\mathrm{QCD}} \sim m_q \Lambda^3_{qcd}$ (here m_q is an appropriate quark mass) gives

$$|\nabla_\varphi \tilde{V}(\varphi)| \geq c\frac{m_q\Lambda^3_{qcd}}{M_{\rm pl}} \quad \text{or} \quad \nabla^2_\varphi \tilde{V}(\varphi) \leq -c'\frac{m_q\Lambda^3_{qcd}}{M^2_{\rm pl}} \tag{2.32}$$

where on the RHS of both inequalities I have dropped the tiny corrections from $V_0 \ll m_q\Lambda^3_{qcd}$. But the sequestered form now implies that in the QCD ground state branch at $\{y^*_\alpha\}$ the slope or curvature is just as large.

Specifically, in the case that the first, slope, condition of eq.(2.32) is satisfied, the φ equation of motion for the ground state branch is (dropping the Hubble friction term, $3H\dot{\varphi}$, as the vacuum energy, V_0, and thus H is now tiny)

$$\ddot{\varphi}(t) \gtrsim c\frac{m_q\Lambda^3_{qcd}}{M_{\rm pl}} \tag{2.33}$$

implying that in a time $\Delta t \equiv \tau/H$ (here I measure time in fractions of the Hubble time $H^{-1} \sim M_{\rm pl}/\sqrt{V_0}$) the quintessence field evolves by an amount $\Delta\varphi \sim \tau^2 c M_{\rm pl} m_q \Lambda^3_{qcd}/V_0 \gg M_{\rm pl}$ unless $\tau \ll 1$ since $m_q\Lambda^3_{qcd} \gg V_0$. Here I have made the conservative assumption that the initial quintessence field velocity, $\dot{\varphi} = 0$. (Note that the Swampland Distance Conjecture [57, 81] states that the effective field theory describing the quintessence plus SM system must irrevocably break down once $\Delta\varphi \gtrsim M_{\rm pl}$. This limits $\tau \lesssim (V_0/m_q\Lambda^3_{qcd})^{1/2}$.) During this evolution the value of the vacuum energy density in the ground state branch becomes

$$V(\varphi_\tau, \ldots) \simeq V_0 - c^2\tau^2\frac{m^2_q\Lambda^6_{qcd}}{V_0} \ . \tag{2.34}$$

Thus as c is $\mathcal{O}(1)$, within a fraction

$$\tau_{AdS} \sim \frac{V_0}{m_q\Lambda^3_{qcd}} \ll 1 \tag{2.35}$$

of a Hubble time the Universe evolves to an anti-de-Sitter state. Taking as an example, the present inferred value of the vacuum energy $V_0 \simeq 10^{-47}\,\mathrm{GeV}^4$, and, conservatively, $m_q = m_u \simeq 3\,\mathrm{MeV}$ gives $\tau_{AdS} \simeq 10^{-43}$, so I would collapse essentially instantaneously!

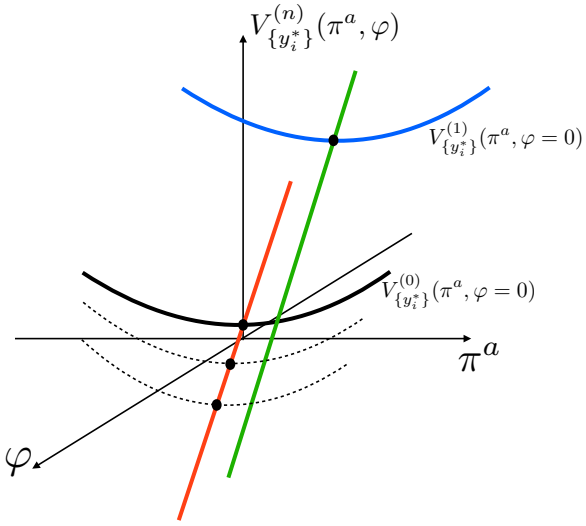

Figure 2.9: Schematic illustration of sequestered quintessence. The black curve gives the form of the ground state branch as a function of the vev's of pNGB fields π^a at a value of the quintessence field $\varphi = 0$, while the blue curve shows the first meta-stable branch possessing minimum (in absence of φ) shifted in π^a. Both curves are at the same values of all SM parameters $\{y^*_\alpha\}$. The green curve shows the bottom of the valley in the $\varphi \neq 0$ direction starting from the otherwise-meta-stable minimum, while the red curve shows the same for the valley starting from the true ground state. For sequestered quintessence the slope of the red and green trajectories is the same. The SdSC demands that the slope (or curvature) of the green curve is bounded below by an amount proportional to the effective positive vacuum energy density of the would-be meta-stable state.

Only for truly exponentially small m_q and thus exponentially small explicit breaking of the chiral symmetry can we possibly avoid this catastrophe.[11]

Alternatively the quintessence field φ might be located very close to a local maximum of the potential, in which case this is a form of "hilltop quintessence" [83]. Suppose that the initial displacement of the field φ from the exact maximum is $\delta\varphi$, and again conservatively assume that the initial field velocity $\dot{\varphi} = 0$. One then finds using the same logic as in the previous paragraph that the curvature SdSC condition applied to the meta-stable branch implies for the ground state branch that the dimensionless timescale (fraction of a Hubble time) until evolution to an AdS state is

[11]It is amusing to contemplate that there is an interplay between this exponentially small value of explicit chiral symmetry breaking, the quantitative lower bounds on explicit global symmetry violation imposed by the Swampland Global Symmetry Conjecture [52, 82], and the size of the vacuum energy V_0.

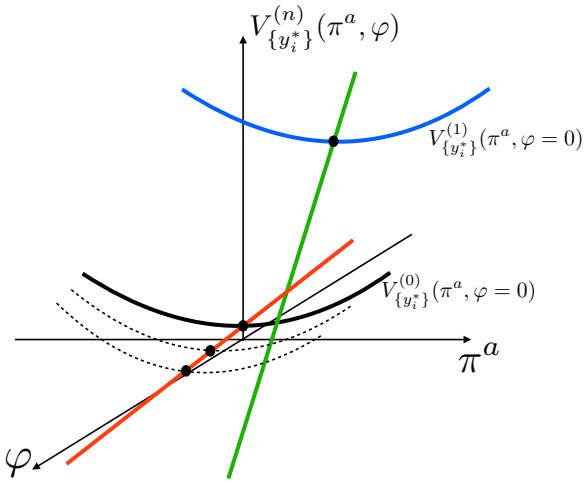

Figure 2.10: Same as figure 2.9 except for coupled quintessence. In this case the slope and curvature of the quintessence valley sloping away from the ground state of QCD differs from that of the meta-stable valley. In principle this could allow the green curve valley bottom to satisfy the SdSC while the red valley bottom is not so steep as to lead to immediate evolution to an AdS state. However such a large change in slope between the two valleys implies a large coupling between the SM and φ giving an extreme fine-tuning in the quintessence sector.

now set by

$$\tau_{AdS} \sim \frac{V_0}{m_q \Lambda_{qcd}^3} \log\left(\frac{V_0 M_{\rm pl}^2}{(\delta\varphi)^2 m_q \Lambda_{qcd}^3}\right). \tag{2.36}$$

This is also an extremely short timescale unless the initial displacement $\delta\varphi$ from the maximum of the potential is tuned to be super-exponentially small. (Moreover, in a cosmological context, there are automatically fluctuations in φ entering the horizon, displacing the value of the quintessence field from the maximum of the potential.)

Thus no matter which of the SdSC conditions applies, the presence of a sequestered quintessence sector does not allow one to evade the SdSC constraint on SM parameter values $\{y_\alpha^*\}$ coming from the presence of meta-stable QCD-sector states. The fundamental reason for this is of course that the difference in effective vacuum energy between the ground state and the meta-stable state(s) at a particular value of the SM parameters $\{y_\alpha^*\}$ is large, and it is impossible to satisfy the constraint on the potential in the quintessence field direction for the meta-stable state without leading to catastrophic evolution of the ground state.

2.3.2 Coupled quintessence

One can see that this is not just a feature of the sequestered quintessence potential: To simultaneously satisfy the SdSC constraint in the meta-stable state and avoid the far-too-steep or curved potential in the ground state requires that the form of the potential in the φ-direction very significantly changes as one moves from the meta-stable branch at $\{y_\alpha^*\}$ to the ground state branch at the same $\{y_\alpha^*\}$ (see figure 2.10). But the only difference between these two branches is the presence of pNGB vacuum expectation values of typical size $\sim f_\pi$. For the quintessence potential function to change very greatly in slope or curvature in response to the switching on of these pion vev's then requires that the quintessence field couples *significantly* to QCD. Parametrically one needs

$$\partial_{\pi^a}^2 \partial_\varphi V^{(n)}_{\{y_\alpha\},\rm QCD}(\pi^a, \varphi) \sim \frac{m_q \Lambda_{qcd}^3}{M_{\rm pl} f_\pi^2}\ , \tag{2.37}$$

which then implies that the effective cubic $\epsilon\varphi(\pi^a)^2$ coupling is $\epsilon \sim m_q\Lambda_{qcd}^3/M_{\rm pl}f_\pi^2 \sim m_q\Lambda_{qcd}/M_{\rm pl}$. Similarly the quartic coupling $\lambda\varphi^2(\pi^a)^2$ is given by $\lambda \sim m_q\Lambda_{qcd}^3/M_{\rm pl}^2 f_\pi^2 \sim m_q\Lambda_{qcd}/M_{\rm pl}^2$. There are also of course couplings to higher powers of the pNGB fields as implied by the non-linearly realised approximate chiral symmetry. These couplings between the SM and φ imply that even in the ground state branch of QCD there are, upon integrating out the pions (with mass $m_p i^2 \sim m_q f_\pi$), radiative corrections to,

eg, the mass-squared of φ of size $\delta m_\varphi^2 \sim (m_q \Lambda_{qcd})^2/16\pi^2 M_{\rm pl}^2$. These are enormous compared to the mass $m_\varphi \sim H_0 \sim \sqrt{V_0}/M_{\rm pl}$ required of a successful quintessence field. Similarly other parameters of the quintessence potential get very large correction. In other words, one must exponentially tune by an amount $\sim (m_q \Lambda_{qcd})^2/16\pi^2 V_0$ (in our Universe roughly a 1 part in 10^{39} tuning) m_φ^2, as well as other parameters, to get the coupled quintessence model not to again evolve very quickly to AdS and a big crunch.

Thus the presence of a quintessence field does not obviously invalidate the arguments concerning the inconsistency of meta-stable QCD states with the SdSC. I emphasise that in these arguments I have not at all used the observational or experimental constraints on quintessence fields, such the equation of state parameter bounds, or the limits on fifth-forces or equivalence-principle violation, which of course only apply to our Universe. I have only used the fact that the SdSC must, by assumption, be satisfied for the meta-stable states, together with the necessity of having the putative Universe in a QCD ground state (at the same values of the SM parameters) survive longer than an exponentially short period of time before entering an AdS big crunch phase.

Chapter 3

The Higgs Landscape

In this chapter I will explore the Standard Model landscape as a function of perhaps its most emblematic parameter: the Higgs mass-squared term.

3.1 Useful Theorems

3.2 Negative Higgs Mass-Squared

Let us first consider the extreme limit of the SM where the EW vev, $v \to \infty$, with all Yukawa and gauge couplings kept fixed as well as the higgs quartic coupling. In this limit the IR theory is of course a pure $SU(3) \times U(1)_{EM}$ gauge theory with no matter, as all quarks, leptons, weak gauge bosons, and the higgs boson itself have become super massive. The question is if this theory has meta-stable states.

Because there is no matter, the color and EM gauge groups are completely decoupled from each other, so the question becomes do either, or both, of pure $U(1)$ and $SU(3)$ theories have meta-stable states. There is no argument that we are aware of that indicates that $U(1)$ has meta-stable states, but the situation is plausibly different for $SU(3)$.

3.2.1 meta-stable states of pure $SU(N_c)$ gauge theories

Following early suggestions [61], Witten [84] and Shifman [85] argued that for large N_c, non-supersymmetric pure $SU(N_c)$ possesses $N_c - 1$ meta-stable vacua, as reviewed in Ref. [86].[1]

Why do these pure glue meta-stable states exist, and what characterises them? Roughly speaking the argument is that the vacuum energy density $V(\theta)$ must be, for

[1] We particularly thank Mike Teper for discussions of the status of meta-stable states in $SU(N_c)$ theories.

all N_c, both a 2π periodic function of the topological parameter θ, $V(\theta) = V(\theta + 2\pi)$, *and* in the large-$N_c$ limit have the form $V(\theta) = N_c^2 f(\theta/N_c)$ with $f(x)$ a 2π-periodic function, and no other factors of N_c appearing [84]. (We emphasise that here it is being assumed that there is no light QCD axion in the spectrum to relax the CP-violating θ-term.) But these demands seem to be contradictory as the second condition says the period of V should be $2\pi N_c$. The resolution, similarly to the case of the chiral Lagrangian, is that $V(\theta)$ must be a *multi-branched function*. The true ground state energy density is then given by

$$V(\theta) = \min_n V^{(n)}(\theta) \quad \text{with} \quad V^{(n)}(\theta) = N_c^2 f\left(\frac{\theta + 2\pi n}{N_c}\right), \tag{3.1}$$

where $n = 0, \ldots, N_c - 1$. Namely each branch has periodicity $2\pi N_c$, but because of level crossings the true ground state energy density is correctly 2π-periodic. This multi-branch structure leads at every value of θ to a total of N_c potential vacua, including at $\theta = 0$, as illustrated schematically in figure 3.1 for $SU(6)$. In fact Witten [84] argued that in the formal $N_c \to \infty$ limit the function $f(x) = x^2$ and that all states were local minima. However at finite N_c as the various branches evolve and cross the character of the local critical point can change from absolutely stable, to meta-stable, to saddle point to local maximum. So to really enumerate the number of locally stable states in a finite N_c theory at a given θ one needs a finer classification.

Before turning to this it is worth mentioning that there is a simple expression for the gap in energy density at $\theta = 0$ between the low-lying states, $n \ll N_c$, in the $N_c \to \infty$ limit:

$$V^{(n)}(0) - V^{(0)}(0) \simeq \frac{(2\pi n)^2}{2}\chi \tag{3.2}$$

where χ is the so-called topological susceptibility defined by

$$\chi = \int d^4x \langle Q(x)Q(0)\rangle \quad \text{where} \quad Q = \frac{1}{8\pi^2}\mathrm{Tr}(G^{\mu\nu}\tilde{G}_{\mu\nu}) \ . \tag{3.3}$$

Moreover, in the large-N_c limit an order parameter distinguishing the N_c different states at a given value of θ is [87]

$$\langle Q\rangle_n = (\theta + 2\pi n)\chi \ . \tag{3.4}$$

(There are other possible order parameters, for example the QCD string tension in each n-state.) Related to this, the $n \neq 0$ states are not invariant under CP transformations even if $\theta = 0, \pi$, the two CP-invariant values of the topological angle. For the SM the topological susceptibility has a value that depends on the η' mass as $\chi \sim (f_{\eta'} m_{\eta'})^2/6$, at least in the large-$N_c$ limit [88, 89], while for pure $SU(3)$

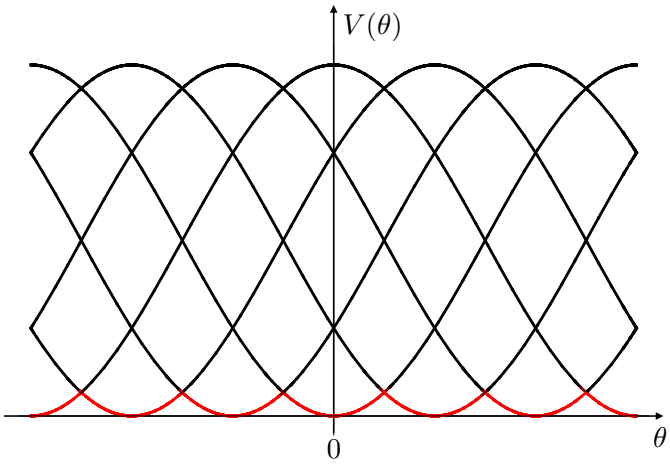

Figure 3.1: Sketch of branches of $V(\theta)$ for pure $SU(6)$ YM theory according to a large-N_c analysis. The red portions of the curves give the true stable ground state energy density as a function of the parameter θ. A refined analysis is necessary to determine if the black sections of the curves include meta-stable states at finite N_c, and if so how many at each value of θ.

gauge theory lattice simulations indicate $\chi \sim (190\,\mathrm{MeV})^4$ [90] (though this depends somewhat on how the lattice scale is set).

Importantly in the large-N_c limit an $\mathcal{O}(N_c)$ subset of these states become highly meta-stable. They are both locally stable, and have false vacuum tunnelling rates to lower states which have been argued, using an approach based on softly-broken supersymmetric QCD, to behave as $\Gamma_n/\mathrm{Volume} \sim \exp(-bN_c^4)$ for some constant $b > 0$ and so become absolutely stable in the formal $N_c \to \infty$ limit [85]. (We caution the reader that the computation of these decay rates in the far-from-supersymmetric limit is not under good control, so numerical factors and, in our opinion, even the N_c^4 scaling are not reliably established.[2] In addition there has been only a very limited study of this large-N_c physics using lattice techniques [92, 93].)

In recent work [94] arguments have been presented that, depending on the value of θ, the number of locally stable vacua, N_s (excluding the true ground state), is by

[2]See also the discussion of Ref. [91].

a particular semiclassical analysis given by

$$N_s = \begin{cases} 2\left[\frac{N_c}{4}\right] & \theta = 0 \\ \left[\frac{N_c}{4}\right] + \left[\frac{N_c+3}{4}\right] - 1 & 0 < \theta < \pi/2 \\ \left[\frac{N_c+1}{2}\right] - 1 & \theta = \pi/2 \\ \left[\frac{N_c+1}{4}\right] + \left[\frac{N_c+2}{4}\right] - 1 & \pi/2 < \theta < \pi \\ 2\left[\frac{N_c+2}{4}\right] - 1 & \theta = \pi \end{cases}$$

where $[x]$ denotes the largest integer $\leq x$. So if we take this analysis as a guide then, naively, at $N_c = 3$ there are predicted to be, respectively, $(0, 0, 1, 1, 1)$ meta-stable states as θ varies in the given ranges, while for $N_c = 4$ there would be $(2, 1, 1, 1, 1)$ meta-stable states.[3] It is particularly interesting that in this case there are meta-stable states predicted at $\theta = 0$.

However, at small N_c, all the semiclassical arguments that we are aware of break down, and it is not clear from the analysis that has so far been performed if there are meta-stable states at low N_c, in particular for $SU(3)_c$. There are (yet) no reliable lattice studies of this question, so strictly speaking the situation regarding pure $SU(3)_c$ YM theory is unknown.

3.2.2 Possible relation to the hierarchy problem

If we boldly assume that there are meta-stable states in pure $SU(3)_c$ at $\theta = 0$ split from the true ground state by an energy density $\Delta V \sim \Lambda_{qcd}^4$ the refined Swampland de Sitter Conjecture, together with the results on quintessence in section 2.3 (which equally apply to this case), then plausibly tells us that the SM with electroweak symmetry breaking scale $v \gg 50\,\text{TeV}$ is in the swampland. In other words, *there are no solutions of the full UV gravitational theory (including all possible consistent compactifications if it is higher dimensional) that lead to the SM with an electroweak vev* $v \gg 50\,\text{TeV}$. This would be a partial resolution to the hierarchy problem and shares some features with previous attempts to link the hierarchy problem with the swampland program [96, 97]. In particular there is a failure of effective field theory reasoning, in that apparently innocuous parameter regions of otherwise consistent quantum field theories are inconsistent when coupled to gravity.[4]

[3] In Ref. [95] the large-N_c effective Lagrangian was modified by including $1/N_c$ effects, possibly enabling an improved discussion of the meta-stable states of $SU(N_c)$ at finite N_c. A richer structure of meta-stable states was found in this analysis, with new meta-stable states being argued to exist both for pure $SU(3)_c$ Yang-Mills theory, and for $SU(3)_c$ coupled to N light quarks. If correct this would strengthen our results. We emphasise that no calculations that are fully under control have yet been performed in the interesting region of small N_c.

[4] One of the most studied of the Swampland constraints is the Weak Gravity Conjecture which, among other things, states that QED with a single Dirac fermion of mass m and gauge charge e

Of course there are caveats to this statement, even if the SdSC is accepted as fact, and pure $SU(3)_c$ at $\theta = 0$ has meta-stable states. First, we have taken the Yukawa couplings to be fixed as $v \to \infty$, but if, instead, these couplings were reduced so as to keep the "hard" quark masses coming from EWSB fixed at their observed values, then the QCD sector of the theory would not possess meta-stable states, and there apparently would be no constraint on v. We do not have a strong argument against this reasoning. However, we note that the limit where all the quark Yukawa couplings vanish is forbidden by the claimed absence of exact global symmetries in theories coupled to gravity, which is one of the best supported of all Swampland Program conjectures. In fact the quantitative Swampland Global Symmetry Conjecture [52,82] mentioned in the Introduction declares that there is a bound on how small more than one of the Yukawa couplings can simultaneously be, $y \gtrsim \exp(-M_{\rm pl}^2/\Lambda^2)$, so if the cutoff Λ of the effective 4d quantum field theory is close to the Planck scale the option of scaling all the Yukawa couplings to close to zero is forbidden. This illustrates how the web of swampland conjectures might intertwine to limit the allowed SM parameter values.

Second the arguments above have not constrained the case where the Higgs mass-squared parameter is large and positive so there is no traditional electroweak symmetry breaking. This is the subject of the next subsection and future paper.

Third, we presently have poor understanding of the non-perturbative physics of QCD-like theories, especially as regards "exotic" phenomena such as meta-stable states. It is logically possible that there are different features of full non-perturbative QCD (and the SM!) that are constrained by present, or future, swampland program conjectures/results, and that these constraints are more powerful than the SdSC in limiting the available SM parameter values.

3.3 Positive Higgs Mass-Squared

I will now discuss the opposite limit in the Higgs mass parameter, that is the large positive direction $m_H^2 \to +M_{\rm pl}^2$. My motivation will again be to explore whether this part of the SM landscape may also lie in the swampland by virtue of SdSC and TPCC-like criteria. The goal is thus to understand the vacuum structure of the theory in this limit and in particular test for the presence of meta- stable states.

is inconsistent with gravity if $|e| \leq m/\sqrt{2}M_{\rm pl}$ [53]. This and the magnetic form of the conjecture have been suggested to possibly provide an explanation of the weak-to-Planck scale hierarchy in extensions of the SM [96, 97].

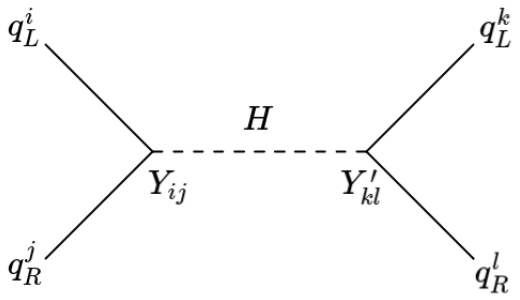

Figure 3.2: Schematically, effective four quark vertices are sourced by integrating out a Higgs field with positive mass squared. Y and Y' are up or down type Yukawa matrices, depending on the type of external quark lines.

If the Higgs mass-squared parameter is taken to be large and positive compared to the QCD scale, $m_H^2 \gg +(1\,\mathrm{GeV})^2$, the Higgs doublet decouples from the low-energy physics of the remaining Higgs-less theory, and there is (naively) no EWSB. The IR theory is simply the SM gauge group coupled to naively massless quarks and leptons. The leptons do not immediately play a central role in what follows; I shall mention their potential indirect effect at the very end. Thus, the relevant part of the leading-order effective Lagrangian I will focus on is

$$\mathcal{L} = -\sum_I \frac{1}{4} F^I_{\mu\nu} F^{I,\mu\nu} + \overline{q}^i_L \gamma^\mu D_\mu q^i_L + \overline{q}^i_R \gamma^\mu D_\mu q^i_R \ . \tag{3.5}$$

Here the covariant derivative D_μ includes all standard model $SU(3) \times SU(2)_L \times U(1)_Y$ gauge fields, $q_L = (u_L, d_L, c_L, s_L, t_L, b_L)$ is a left-handed quark flavor multiplet and similarly for the right-handed quarks. The presence of the heavy Higgs doublet lingers in the form of operators of the low-energy Higgs-less effective theory suppressed by powers of $1/m_H^2$. The most important of these for our purposes are the dimension six 4-quark terms, of schematic form

$$\Delta\mathcal{L} = \frac{C^{ijkl}_{XYZW}}{m_H^2} \overline{q}^i_X q^j_Y \overline{q}^k_Z q^l_W \ . \tag{3.6}$$

These dimension 6 operators are obtained upon integrating out the Higgs through tree diagrams as in fig. 3.2 so that the constants C^{ijkl}_{XYZW} are linked to the Yukawa matrices in a straightforward way. Of course, the $q_{L,R}$ are ultimately not the proper degrees of freedom in the IR as the theory is confining and chiral symmetry breaking occurs with a vacuum expectation value of the chiral condensate $\langle \overline{q}_L q_R \rangle \sim \Lambda^3_{\mathrm{QCD}} \mathbb{1}$.

It has been known for a long time that this chiral condensate itself, even without a Higgs doublet, breaks electroweak symmetry, meaning that pions can act as a

substitute for the Higgs boson, giving mass to the electroweak gauge bosons. This formed the initial motivation for the development of technicolor models [98–102]. More recently the SM in this phase has been studied in [103, 104] with a focus on particle spectrum and interactions. No proper study of the full pion potential exists in this regime however.

Of course the EW SSB would occur at the significantly smaller energy scale of Λ'_{QCD} however. Moreover, $\Lambda'_{\text{QCD}} \ll \Lambda_{\text{QCD}}$ as all 6 quarks are massless and contribute to the running of the QCD beta function eq. (1.24). Despite a vacuum existing with the usual pattern of $W^{\pm}$, Z^0 bosons acquiring mass alongside a surviving $U(1)_{EM}$, the IR phenomenology unsurprisingly turns out to be quite different. In section 3.3.1 we describe in detail the unfolding of the resulting low energy EFT. In brief, the weakly coupled electroweak gauge interactions act as a perturbation on the strong dynamics of confining QCD with all 6 quarks massless, while the Higgs induced vertices are a perturbation weaker still that we can ignore initially. As shown schematically in fig. 3.3, at the $U(1)_{EM}$ preserving vacuum the chiral symmetry spontaneous breaking $SU(6)_L \times SU(6)_R \to SU(6)_V$ produces 35 Nambu-Goldstone bosons, three of which are eaten by the electroweak gauge bosons and 16 of which acquire mass of order $\mathcal{O}(g^2 g'^2)$ due to the *explicit* breaking of chiral symmetry by the electroweak gauge interactions.

I then set out to investigate the full IR potential of pNGBs. Its critical points turn out to be determined by the pseudo-potential

$$\Delta \propto -\frac{1}{16}\sum_{i}^{3} \text{Tr}^2\left(U^\dagger(\mathbb{1}_3 \otimes \sigma^i)U(\mathbb{1}_3 \otimes \sigma^3)\right) \ , \tag{3.7}$$

where U describes the pions as per eq. (3.10). I prove the stability of the $U(1)_{EM}$ preserving vacuum manifold and its connectedness. I then classify and explicitly construct a possibly exhaustive set of further extrema and prove them to be saddle points. It is still possible that there are other critical points and I describe how they would be constructed. I do not however in this thesis definitely prove their existence or lack thereof, leaving it to future work. I conclude by discussing further effects complicating the structure of the potential.

3.3.1 Electroweak symmetry breaking via QCD chiral condensate

Ignoring the electroweak sector, QCD is an $SU(3)_c$ gauge theory with 6 massless quarks

$$\mathcal{L}_{\rm QCD} = i\,\overline{q}_L \not{D}_c q_L + i\,\overline{q}_R \not{D}_c q_R\ , \tag{3.8}$$

where $\not{D}_c$ here includes only gluon gauge fields, $q_L = (u_L, d_L, c_L, s_L, t_L, b_L)$ is a left-handed flavor multiplet and similarly for the right-handed multiplet. As their is no quark mass matrix, eq. (3.8) has a global $G = SU(6)_L \times SU(6)_R$ chiral symmetry which is spontaneously broken down to the vector $H = SU(6)_V$ group by the chiral condensate

$$\langle \overline{q}_L q_R \rangle = C_0' \mathbb{1}_6, \tag{3.9}$$

where C_0' is expected to be of order $\Lambda_{\rm QCD}'^3$. In the absence of anything else, this would give rise to 35 exactly massless NGB fields $\pi^\alpha(x) = f_\pi' \Pi^\alpha(x)$, the generalization of pions, reflecting the number of broken generators of G, as in fig. 3.3(a). These perturbative fields can be parametrized as usual in the CCWZ formalism in terms of the $SU(6)$ matrix

$$\langle \overline{q}_L q_R \rangle = C_0' U, \qquad U = e^{i\Pi^\alpha T^\alpha}, \tag{3.10}$$

where I will take the T^α to be a particular basis of the $\mathfrak{su}(6)$ Lie algebra with $\mathrm{Tr}\left(T^\alpha T^\beta\right) = 2\delta^{\alpha\beta}$. As usual U transforms non-linearly under G as

$$U \to L^\dagger U R, \qquad L, R \in SU(6)\ . \tag{3.11}$$

A convenient basis of $\mathfrak{su}(6)$ for our application is $T^\alpha = \{T_2^i, T_3^a, T^{jb}\}$, where

$$\begin{aligned} T_2^i &= \frac{1}{\sqrt{3}} \mathbb{1}_3 \otimes \sigma^i, \\ T_3^a &= \frac{1}{\sqrt{3}} \lambda^a \otimes \mathbb{1}_2, \\ T^{ia} &= \frac{1}{\sqrt{2}} \lambda^a \otimes \sigma^i, \end{aligned} \tag{3.12}$$

with $i = 1, 2, 3$ and $a = 1...8$. λ^j (σ^i) are the Gell-Mann (Pauli) matrices and $\otimes$ stands for the Kronecker matrix product. The 3×3 part of the matrices acts on the space of generations while the 2×2 part acts within a generation.

The gauging of a subgroup $G_w \subset G$ explicitly breaks G down to S, which is made of G_w itself plus whatever generators of G that commute with all of G_w. This

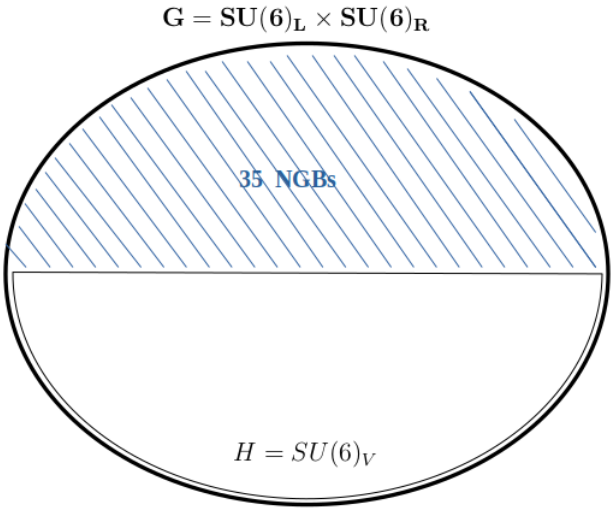

(a) *Chiral SSB*

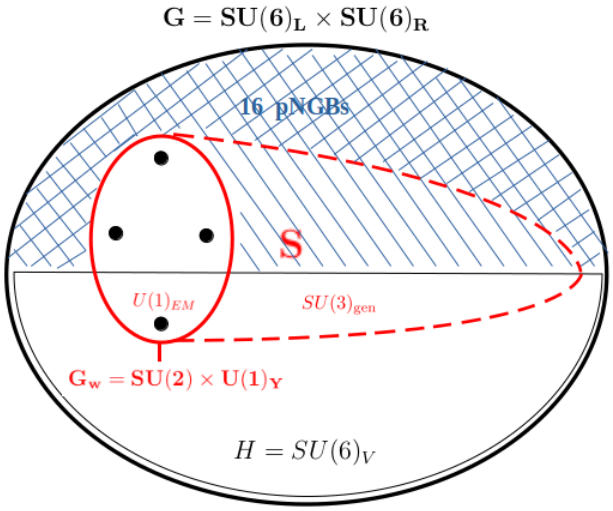

(b) *EW gauging effect*

Figure 3.3: Chiral symmetry breaking $G \to H$ in $SU(3)$ Yang-Mills theory with 6 massless quark flavors results in 35 exactly massless NGBs, as shown in (a). The pattern is complicated in (b) by the explicit breaking of G by the weakly coupled EW gauge group G_w. At the $U = \mathbb{1}_6$ vacuum, three of 4 generators spanning G_w correspond to fictitious NGBs eaten by the $W^\pm$ and Z through the Higgs mechanism; the 4th generates $U(1)_{EM}$ in the low energy theory. The surviving global exact symmetry is S, which trivially includes G_w, plus the inter-generation mixing $SU(3)_L \times SU(3)_{R,u} \times SU(3)_{R,d}$, acting respectively on left-handed doublets, right handed up-type and down-type quarks separately. This spontaneously breaks down to the vectorial doublet mixing symmetry $SU(3)_{\text{gen}} \subset H$, giving 16 exactly massless GBs - single dashed region in (b). Finally, there remain 16 explicitly broken generators of G to which correspond pNGBs with masses proportional to the EW gauge couplings - double dashed region in (b).

complicates the symmetry breaking pattern. If the gauge couplings of G_w are weak however one can assume chiral symmetry breaking and eq. (3.10) to still hold. One expects however corrections to the effect of

1. pNGBs with mass proportional to the weak gauge couplings for symmetry generators of G/H not in S,

2. gauge boson masses through the Higgs mechanism for generators in $G_w \cap G/H$,

3. NGBs remaining exactly massless for generators in $S/(G_w \cup H)$.

We are of course interested in the details of the case of electroweak gauge group $G_w = SU(2)_L \times U(1)_Y$, for which the above regions are displayed in fig. 3.3. Such dynamical symmetry breaking of gauge symmetries has been extensively studied in the context of technicolor and composite Higgs theories[5] [100–102, 105].

In practice, gauged subgroups of G acting on the flavor multiplets $q_{L,R}$ in their fundamental representation enter as

$$\delta\mathcal{L}_w = \overline{q}_L \gamma^\mu \mathbb{A}^I_\mu P^I_L q_L + \overline{q}_R \gamma^\mu \mathbb{A}^I_\mu P^I_R q_R. \tag{3.13}$$

where the $P^a_{L,R} \in \mathfrak{su}(6)$ are generators of the left/right action of G_w, here defined to also absorb any coupling constants. $\mathbb{A}^a_\mu(x)$ are the gauge bosons. For the case of the SM electroweak interactions we have the three $SU(2)_L$ gauge bosons $W^{i=1,2,3}_\mu$ as well as the B^Y_μ for the abelian hypercharge, with

$$\begin{aligned} &P^i_L = g\frac{1}{2}(\mathbb{1}_3 \otimes \sigma^i)\ , \quad P^i_R = 0\ , \\ &P^Y_L = g'\frac{1}{6}\mathbb{1}_6\ , \quad P^Y_R = g'\mathbb{1}_3 \otimes \begin{pmatrix} 2/3 & 0 \\ 0 & -1/3 \end{pmatrix} = g'\left[\frac{1}{6}\mathbb{1}_6 + \frac{1}{2}(\mathbb{1}_3 \otimes \sigma^3)\right]\ , \end{aligned} \tag{3.14}$$

which can be read off from fig. 1.1.

To leading order, the effective IR Lagrangian is uniquely constrained by gauge invariance to be

$$\mathcal{L} = \frac{f'^2}{4}\mathrm{Tr}\left((\mathcal{D}_\mu U)^\dagger \mathcal{D}^\mu U\right), \tag{3.15}$$

where the covariant derivative

$$\mathcal{D}_\mu U = \partial_\mu U - iA^a_\mu\left(P^I_L U - U P^I_R\right). \tag{3.16}$$

[5]The problem of how exactly the gauged group G_w divides itself between H and G/H is known as the 'vacuum alignment problem'.

ensures said invariance under the non-linear action of eq. (3.11) of gauge transformations. Notice of course that for $A^a_\mu \to 0$ this reduces to the usual chiral Lagrangian leading term. Expanding eq. (3.15) out more explicitly

$$\begin{aligned}\mathcal{L} = \frac{f'^2}{4}\mathrm{Tr}\left(\partial_\mu U^\dagger \partial^\mu U + 2iA^a_\mu\left(\partial^\mu U U^\dagger P^I_L + \partial^\mu U^\dagger U P^I_R\right)\right.\\ \left. + A^a_\mu A^{\mu b}\left(-2U^\dagger P^I_L U P^J_R + P^I_L P^b_L + P^I_R P^J_R\right)\right). \end{aligned} \tag{3.17}$$

Feynman rules for the pNGB fields are obtained by expanding U around its vacuum value. Around $U = \mathbb{1}_6$ these are summarized in fig. 3.4. The field dependent gauge boson mass matrix is defined as

$$(M^2_A)^{ab}(U) = \frac{f^2}{2}\mathrm{Tr}\left(-2U^\dagger P^{\{a}_L U P^{b\}}_R + P^I_L P^b_L + P^I_R P^J_R\right), \tag{3.18}$$

For the SM values in eq. (3.14), diagonalizing $M^{ab}(\mathbb{1}_6)$ gives the normal pattern of weak boson masses $m^2_W = 3g^2f^2/4$, $m^2_Z = 3(g^2+g'^2)f^2/4$ and photon $m_\gamma = 0$. As $g, g' < 1$ the W and Z consistently appear in the effective theory. I emphasise that this pattern of symmetry breaking, as also depicted in fig. 3.3, is not the same at every point in the field space of pNGBs. Infact, at a generic point away from the locus connected to $U = \mathbb{1}_6$ all four EW gauge bosons are massive.

3.3.2 pNGB potential

EW gauge interactions generate an effective potential $\mathbb{V}(\Pi^\alpha)$ for the pNGBs. Having identified the leading term of the confined theory as eq. (3.17), I will now discuss contributions to $\mathbb{V}$. Within the EFT we must write down all pNGB potential terms respecting the symmetries. Gauge symmetry under the full G_W is particularly constraining. It is useful to bear in mind the spurion transformations of the projectors $P^a_{L,R}$

$$P^I_L \to L^\dagger P^I_L L\ , \quad P^I_R \to R^\dagger P^I_R R\ , \tag{3.19}$$

for $L, R \in SU(6)$. Within the EFT, potential terms are also generated perturbatively by means of loop diagrams with internal gauge bosons. I will only consider one loop contributions. Working in Landau gauge allows one to ignore all vertices of the form (c) in fig. 3.4 [6]. While information about the structure of $\mathbb{V}$ can be obtained by EFT considerations, the relative size between 'bare' terms coming from the strong

[6] In fact, in order to not trivially vanish in the limit of all external momenta going to zero and therefore contribute something to the potential, the Π^{α_0} line in vertex (c) has to be internal, forming part of the loop along with the gauge boson line. The propagator for A^a_μ in Landau gauge then vanishes in said limit and the diagram evaluates to zero.

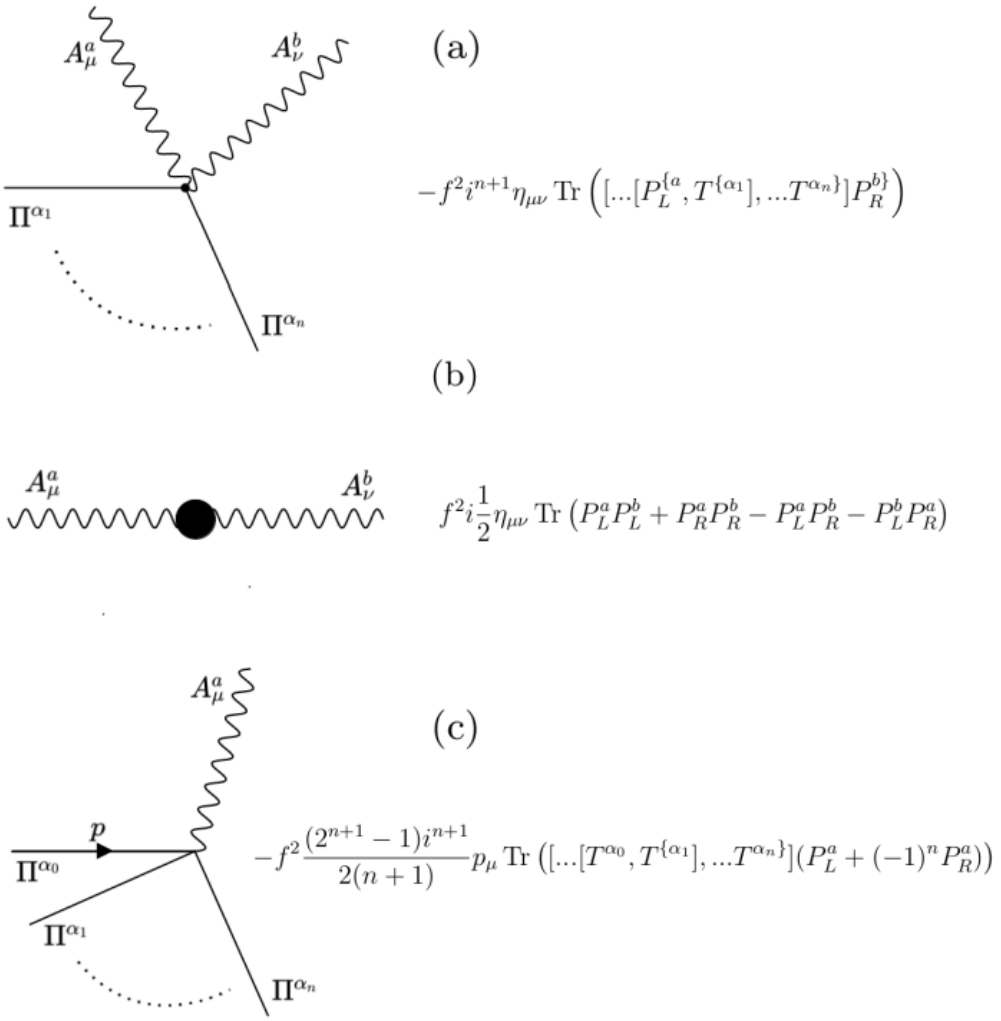

Figure 3.4: Feynman rules for the class of confining theories described by eq. (3.15). The generators of the left (right) action P_L^I (P_R^I) of the gauged subgroup are defined to include couplings, e.g. see the SM case of eq. (3.14). Some gauge bosons become massive through the Higgs mechanism as implied by vertex (b). Their mass matrix is at this point generally not diagonal. For $n = 0$, (c) gives momentum-dependent gauge boson - fictitious pion mixing terms.

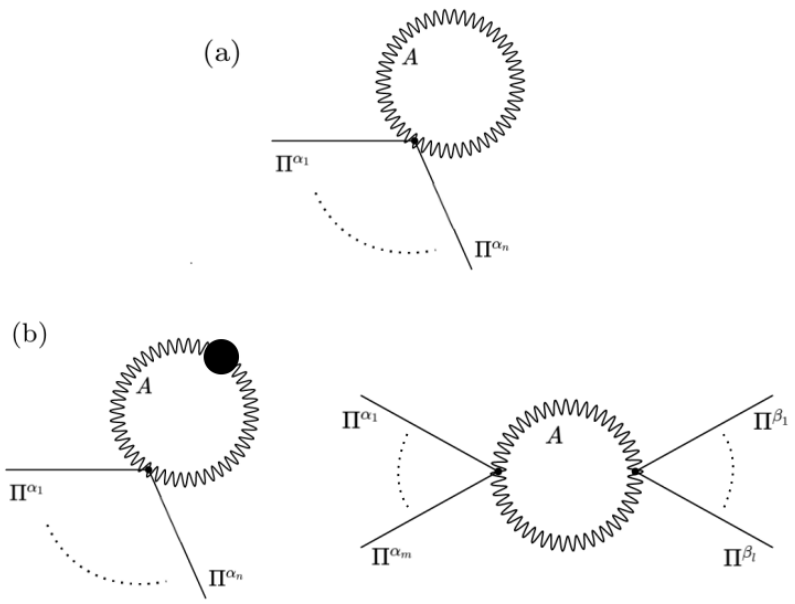

Figure 3.5: One loop diagrams contributing to the pNGB potential at (a) quadratic and (b) quartic order in weak gauge couplings, in Landau gauge. Wavy lines are massless gauge bosons, while their mass matrix is treated as a two point vertex (black blob).

dynamics at energies $\sim \Lambda'_{\rm QCD}$ and corrections from calculable loops in the EFT is not decidable. In section 3.3.3 the potential will be written in terms of current correlators of the full theory and enough information will be extracted to classify critical points with some confidence.

In general, the lowest order - quadratic in gauge couplings - the field dependent contribution to the effective potential is given by

$$\mathbb{V} \supset v_2 \mathrm{Tr}(M_A^2(U)) = v_2 \sum_I \left(-2U^\dagger P_L^I U P_R^I + P_L^I P_L^I + P_R^I P_R^I\right) \ , \tag{3.20}$$

where $v_2 \sim \Lambda^4_{\rm QCD}$ is an unknown coefficient. This is renormalised by all diagrams of the form (a) in fig. 3.5. However, for the SM values of eq. (3.14) this does not give a non-trivial potential for the NGBs as the $SU(2)_L$ action is purely left-handed while the $U(1)_Y$ action is proportional to the identity in its left action, so that $U^\dagger P_L^Y U = P_L^Y$. More generally, the only non-trivial elements of M_A^{ab} are cross terms proportional to $\mathcal{O}(gg')$.

At quartic order in gauge couplings, the potential has a contribution

$$\mathbb{V} \supset v_4 \mathrm{Tr}(M_A^4(U)) = v_4 \left(\frac{27g^4}{16} + \frac{9g'^2}{16} + \frac{9g^2g'^2}{2} \sum_{i=1}^{3} \mathrm{Tr}^2\left(U^\dagger T_2^i U T_2^3\right)\right) \ , \tag{3.21}$$

where v_4 is another unknown coefficient and I have immediately specialised to the SM case. This is renormalised by all diagrams (b) in fig. 3.5. Thus, to lowest order in gauge couplings, the potential has a form $\mathcal{O}(g^2 g'^2)$ and we see the first appearance of the quantity Δ defined in eq. (3.7). Expanding eq. (3.21) around $U = \mathbb{1}_6$ to quadratic order in pion fields one sees 16 degenerate pNGBs with mass $\sim \Lambda'_{\rm QCD} g g'$, associated to the $\lambda^a \otimes \sigma^1$ and $\lambda^a \otimes \sigma^2$ generators of eq. (3.12). Exact NGBs corresponding to the T_3^a and $\lambda^a \otimes \sigma^3$ generators remain massless, although those associated to T_2^i are fictitious, forming the longitudinal part of the $W^\pm$ and Z.

A further term exists at same order in gauge couplings which satisfies all symmetries

$$\mathbb{V} \supset v'_4 \mathrm{Tr}\left(U^\dagger P_L^I U P_R^J U^\dagger P_L^I U P_R^J\right) \ , \tag{3.22}$$

with v'_4 another unknown coefficient. Unlike previous terms, this is not renormalised at one loop but is a pure contact term.

3.3.3 The Potential from First Principles

The full theory[7] can be written as

$$\mathcal{L} = -\sum_I \frac{1}{4} F^I_{\mu\nu} F^{I,\mu\nu} + i\,\overline{q}_L \not{\partial} q_L + i\,\overline{q}_R \not{\partial} q_R + \mathbb{A}^I_\mu J^{I,\mu}_L + \mathbb{A}^I_\mu J^{I,\mu}_R \ , \tag{3.23}$$

where

$$J^{I,\mu}_L = \overline{q}_L \gamma^\mu P^I_L q_L, \qquad J^{I,\mu}_R = \overline{q}_R \gamma^\mu P^I_R q_R \ . \tag{3.24}$$

Then, the effective action to quadratic order in gauge fields in momentum space after integrating out the fluctuations around a fixed classical background U is given by

$$\mathcal{L} = \left(-\frac{1}{2}(\Delta P_T)^{\mu\nu}\, p^2 + \frac{1}{2} i \langle J^{I,\mu}_L J^{J,\nu}_L \rangle_p + \frac{1}{2} i \langle J^{I,\mu}_R J^{J,\nu}_R \rangle_p + i \langle J^{I,\mu}_L J^{J,\nu}_R \rangle_p \right) \mathbb{A}^I_\mu \mathbb{A}^J_\nu \tag{3.25}$$

where

$$(\Delta P_T)^{\mu\nu} = \eta^{\mu\nu} - \frac{p^\mu p^\nu}{p^2} \tag{3.26}$$

is the usual projector onto transverse polarisations, and

$$\langle J^{I,\mu}_X J^{J,\nu}_Y \rangle_p = \int dx^4 e^{-ixp} \langle J^{I,\mu}_X(x) J^{J,\nu}_Y(0) \rangle \tag{3.27}$$

[7] Leaving out leptons and Higgs mass suppressed higher dimensional operators.

are momentum space current correlators, which can be written in terms of self energies and U as

$$i\langle J_L^{I,\mu} J_L^{J,\nu}\rangle_p = (\Delta P_T)^{\mu\nu}\Pi_L(p^2)\mathrm{Tr}\left(P_L^I P_L^J\right) \ , \tag{3.28}$$

$$i\langle J_R^{I,\mu} J_R^{J,\nu}\rangle_p = (\Delta P_T)^{\mu\nu}\Pi_R(p^2)\mathrm{Tr}\left(P_R^I P_R^J\right) \ , \tag{3.29}$$

$$i\langle J_L^{I,\mu} J_R^{J,\nu}\rangle_p = -\frac{1}{2}(\Delta P_T)^{\mu\nu}\Pi_{LR}(p^2)\mathrm{Tr}\left(U^\dagger P_L^I U P_R^J\right) \tag{3.30}$$

For the SM, given eq. (3.14), we have

$$\mathcal{L}_{\text{eff}}^{\mathbb{A}} = \frac{1}{2}(P_T)_{\mu\nu}\ \mathbb{A}^I \mathbb{D}_{IJ}\mathbb{A}^J \ , \tag{3.31}$$

where

$$\mathbb{D}_{IJ} = \begin{pmatrix} -p^2+\frac{3}{2}g^2\Pi_L(p^2) & 0 & 0 & -gg'\frac{F^1}{2}\Pi_{LR} \\ 0 & -p^2+\frac{3}{2}g^2\Pi_L(p^2) & 0 & -gg'\frac{F^2}{2}\Pi_{LR} \\ 0 & 0 & -p^2+\frac{3}{2}g^2\Pi_L(p^2) & -gg'\frac{F^3}{2}\Pi_{LR} \\ -gg'\frac{F^1}{2}\Pi_{LR} & -gg'\frac{F^2}{2}\Pi_{LR} & -gg'\frac{F^3}{2}\Pi_{LR} & -p^2+g'^2\left[\frac{1}{6}(\Pi_L-\Pi_{LR})+\frac{5}{3}\Pi_R\right] \end{pmatrix} .$$

The one-loop effective potential for the pNGBs can now we computed as sum of diagrams in the usual way and is given by

$$\mathbb{V} = \sum_I \int \frac{dp^4}{(2\pi)^4}\ \ln\left(d^I\right) = \pi^2 \int dp^2 p^2 \ln\left(\det(\mathbb{D})\right) \ , \tag{3.32}$$

$$= \pi^2 \int dQ^2 Q^2 \ln\left(1 - F^2 \frac{3g^2 g'^2 \Pi_{LR}^2}{(2Q^2+3g^2\Pi_L^2)(6Q^2+g'^2(\Pi_L-\Pi_{LR}+10\Pi_R))}\right) \ + \ \text{FI} \ , \tag{3.33}$$

where d^I are the eigenvalues of the $\mathbb{D}$ matrix, the integral has become Euclidean $Q^2 = -p^2$ and I have ignored a field independent (FI) piece.

Notice, it is not necessary to know the full form of the potential as what is of main interest is the classification of critical points. Since $\mathbb{V}$ only depends on the fields through Δ, we have

$$\frac{\partial \mathbb{V}}{\partial \Pi^\alpha} = \frac{\partial \mathbb{V}}{\partial \Delta}\frac{\partial \Delta}{\partial \Pi^\alpha} \ \stackrel{!}{=} 0 \qquad \text{(critical points)} \ . \tag{3.34}$$

so by simple chain rule the critical points of the potential are either critical points of Δ, which I will classify in section 2.2.1, or an extremum of $\mathbb{V}(\Delta)$. Furthermore, the Hessian is

$$\frac{\partial^2 \mathbb{V}}{\partial \Pi^\alpha \partial \Pi^\beta} = \frac{\partial^2 \mathbb{V}}{\partial \Delta^2}\frac{\partial \Delta}{\partial \Pi^\alpha}\frac{\partial \Delta}{\partial \Pi^\beta} + \frac{\partial \mathbb{V}}{\partial \Delta}\frac{\partial \Delta}{\partial \Pi^\alpha \partial \Pi^\alpha} \ . \tag{3.35}$$

Thus, for the critical points of Δ, one just needs information about the sign of $\mathbb{V}'(\Delta)$.

$$\frac{\partial \mathbb{V}}{\partial \Delta} \propto \pi^2 \int dQ^2 Q^2 \frac{3g^2 g'^2 \Pi_{LR}^2}{\text{Den}} \ , \tag{3.36}$$

where the denominator is given by

$$\begin{aligned} \text{Den} &= 12Q^4 + 2Q^2 \left(9g^2\Pi_L + g'^2(\Pi_L - \Pi_{LR} + 10\Pi_R)\right) \\ &\quad + 3g^2 g'^2 \left(\Delta\ \Pi_{LR}^2 + \Pi_L^2 - \Pi_L\Pi_{LR} + 10\Pi_L\Pi_R\right) \end{aligned} \tag{3.37}$$

$$\begin{aligned} &= 48Q^4 + 4Q^2 \left(9g^2(\Pi_{AA} + \Pi_{VV}) + g'^2(9\Pi_{AA} + 13\Pi_{VV})\right) \\ &\quad + 3g^2 g'^2 (\underbrace{(4\Delta + 9)}_{\geq 0} \Pi_{AA}^2 + \underbrace{(22 - 8\Delta)}_{> 0} \Pi_{AA}\Pi_{VV} + \underbrace{(4\Delta + 13)}_{> 0} \Pi_{VV}^2) \ , \end{aligned} \tag{3.38}$$

where I have highlighted expressions containing the fields which are always postitive-definite given then range of $\Delta \in (-9/4, 0)$ (see section 3.3.4). In going to the second line I have exchanged left/right correlators for vector/axial ones using the relations [106]

$$\begin{aligned} \Pi_{VV} &= \frac{1}{2}(\Pi_L + \Pi_R - \Pi_{LR}) \\ \Pi_{AA} &= \frac{1}{2}(\Pi_L + \Pi_R + \Pi_{LR}) \\ \Pi_{VA} &= \frac{1}{2}(\Pi_R - \Pi_L) \ , \end{aligned} \tag{3.39}$$

and furthermore I have taken $\Pi_{VA} = 0$ from QCD effects when $\overline{\theta} = 0$ [107]. Accounting for effects that contribute a non-zero Π_{VA}, such as running due to the inclusion of leptons (and a possible $\overline{\theta}$) parameter are important future directions of research. With this assumption however, one can argue for the positivity of the denominator eq. (3.38) and therefore also the sign of $\mathbb{V}'(\Delta)$. For example, by the large-N form of the correlators [106]. The conclusion is thus that the stability of the critical points of $\mathbb{V}$ that are critical points of Δ are the same as if the potential were Δ itself.

3.3.4 Critical Points

I will now investigate the critical points of Δ given in eq. (3.7). First, I rewrite it very slightly to emphasize its geometrical interpretation; it is proportional to the length-squared of the projection of the conjugation orbit of $U(\mathbb{1}_3 \otimes \sigma^3)$ onto the $\mathfrak{su}(2)$ subalgebra.

$$\Delta = -\frac{1}{16} \sum_i^3 \text{Tr}^2 \left((\mathbb{1}_3 \otimes \sigma^i) U (\mathbb{1}_3 \otimes \sigma^3) U^\dagger\right) \ . \tag{3.40}$$

Consider an arbitrary point $\Pi_0 \equiv U_0(\mathbb{1}_3 \otimes \sigma^3)U_0^\dagger = \Pi_0^x T^x$. One can immediately say that

- if $\Pi_0 \in \mathfrak{su}(2) \implies \Pi_0$ is a minimum and $\Delta \sim -9/4$.
- if $\Pi_0 \perp \mathfrak{su}(2) \implies \Pi_0$ is a maximum and $\Delta = 0$. An example of such a point is

$$U_0^{\max} = \frac{1}{\sqrt{2}}\mathbb{1}_6 + i\sqrt{\frac{3}{8}}\left(\lambda^3 \otimes \sigma^1 + \lambda^8 \otimes \sigma^2\right) \ . \tag{3.41}$$

Thus, $U = \mathbb{1}_6$ is indeed a minimum as anticipated already and indeed a global minimum of Δ. In reality of course there is a locus of minima, if nothing else connected to the identity by the remaining exact symmetry group of the theory. The full locus is

$$\begin{aligned} U_\odot &= SU(2)_L \times SU(3)_{R,u} \times SU(3)_{R,d} \\ &= e^{i(\mathbb{1}_3 \otimes \sigma^i)s^i} e^{i(\lambda^a \otimes \sigma^\uparrow)\ell^a_\uparrow} e^{i(\lambda^a \otimes \sigma^\downarrow)\ell^a_\downarrow} \ , \end{aligned} \tag{3.42}$$

where $\sigma^\uparrow, \sigma^\downarrow$ are defined in eq. (3.46). In the following proof I rule out the possibility of their being further global minimum points disconnected from this locus.

Proof: Consider the set for a global minimum

$$U_\odot = \left\{U \in SU(6) \mid U\left(\mathbb{1} \otimes \sigma^3\right)U^\dagger \in \mathfrak{su}(2)\right\} \ . \tag{3.43}$$

Consider now that for any $U \in U_\odot$, there exists a $g \in SU(2)$ such that

$$U\left(\mathbb{1} \otimes \sigma^3\right)U^\dagger = g\left(\mathbb{1} \otimes \sigma^3\right)g^\dagger \ , \tag{3.44}$$

and therefore

$$g^\dagger U\left(\mathbb{1} \otimes \sigma^3\right)U^\dagger g = \left(\mathbb{1} \otimes \sigma^3\right) \ , \tag{3.45}$$

meaning $g^\dagger U \in C$, where C is the centraliser of $\mathbb{1}_3 \otimes \sigma^3$. For a compact Lie group C is connected (see corollary 5 and preceding statements of Chapter IX in [108]) .

End of Proof We conclude by defining shorthand notation for useful matrices.

$$\begin{aligned} \sigma^\uparrow &= \begin{pmatrix} 1 & 0 \\ 0 & 0 \end{pmatrix} \ , \quad \sigma^\downarrow = \begin{pmatrix} 0 & 0 \\ 0 & 1 \end{pmatrix} \ , \\ \sigma^- &= \begin{pmatrix} 0 & 0 \\ 1 & 0 \end{pmatrix} \ , \quad \sigma^+ = \begin{pmatrix} 0 & 1 \\ 0 & 0 \end{pmatrix} \ . \end{aligned} \tag{3.46}$$

3.3.5 Non-global Extrema

What if Π_0 has components both parallel and orthogonal to $\mathfrak{su}(2)$? are there other local extrema? To answer this, consider fluctuations around a point of interest $U(x) = \tilde{U}(x)U_0$ and expand $\tilde{U} = \mathbb{1} + i\tilde{\Pi} + ...$, where $\tilde{\Pi} = \tilde{\Pi}^\alpha T^\alpha$ and demand that the linear term of Δ in $\tilde{\Pi}$ fields vanish. We have

$$\begin{aligned} 16\ \Delta &= -\sum_i^3 \mathrm{Tr}^2\left((\mathbb{1}\otimes\sigma^i)\tilde{U}\Pi_0\tilde{U}^\dagger\right) \\ &= -\sum_i^3 \mathrm{Tr}^2\left((\mathbb{1}\otimes\sigma^i)(\Pi_0 + i[\tilde{\Pi},\Pi_0] + ...)\right) \\ &= -\sum_i^3 \left(\mathrm{Tr}\left((\mathbb{1}\otimes\sigma^i)\Pi_0\right) + i\mathrm{Tr}\left((\mathbb{1}\otimes\sigma^i)[\tilde{\Pi},\Pi_0]\right) + ...\right)^2 \ . \end{aligned} \tag{3.47}$$

Demanding the linear term in $\tilde{\Pi}$ vanish becomes

$$\begin{aligned} 0 &\overset{!}{=} \sum_i^3 \mathrm{Tr}\left((\mathbb{1}\otimes\sigma^i)\Pi_0\right)\mathrm{Tr}\left((\mathbb{1}\otimes\sigma^i)[\tilde{\Pi},\Pi_0]\right)\ , \\ \implies \quad 0 &\overset{!}{=} \Pi_0^i f^{\alpha\beta i}\tilde{\Pi}^\alpha\Pi_0^\beta\ , \end{aligned} \tag{3.48}$$

where $f^{\alpha\beta\gamma}$ are the structure constants in the basis of eq. (3.12). We need this to be true for all possible $\tilde{\Pi}^x$ so that the condition for an extremum becomes

$$\begin{aligned} 0 &\overset{!}{=} f^{\alpha\beta i}\Pi_0^\beta\Pi_0^i \\ &= f^{xi\alpha}\Pi_0^x\Pi_0^i, \quad x = 4, ..., 35 \end{aligned} \tag{3.49}$$

where the index x runs through all basis elements orthogonal to $\mathfrak{su}(2)$ (so everything except T_2^i) and I have used that in the basis eq. (3.12) (as in the generalised Gell-Mann basis) $f^{\alpha\beta\gamma}$ is a totally antisymmetric tensor .

In conclusion we can think of decomposing a general Lie algebra vector Π_0 into its projection onto $\mathfrak{su}(2)$, call it $\Pi_{0,\parallel} = \Pi_0^i T_2^i$, and its orthogonal, $\Pi_{0,\perp} = \Pi_0^x T^x$.

$$\Pi_0 = \Pi_{0,\parallel} + \Pi_{0,\perp}\ , \tag{3.50}$$

and an extremum of Δ corresponds to a point satisfying

$$[\Pi_{0,\parallel}, \Pi_{0,\perp}] = 0\ , \qquad \text{(critical point)}\ . \tag{3.51}$$

Thus, non-trivial critical points are points on the conjugation orbit $U_0(\mathbb{1}_3\otimes\sigma^3)U_0^\dagger$ with components satisfying this commutation.

What is the most general Π_0 to satisfy eq. (3.51)? Consider the most general $\Pi_{0,\|}$ and $\Pi_{0,\perp}$:

$$[\Pi_{0,\|}, \Pi_{0,\perp}] = \left[\frac{1}{\sqrt{3}}\mathbb{1}_3 \otimes \sigma^i \ \Pi^i_{0,\|}, \frac{1}{\sqrt{3}}(\lambda^a \otimes \mathbb{1}_2)\Pi^a_{0,\perp} + \frac{1}{\sqrt{2}}(\lambda^a \otimes \sigma^j)\Pi^{aj}_{0,\perp}\right] \tag{3.52}$$

$$\propto i(\lambda^a \otimes \sigma^k)\Pi^i_{0,\|}\Pi^{aj}\epsilon^{ijk} \stackrel{!}{=} 0 \ , \tag{3.53}$$

so that the condition is $\Pi^{aj} \stackrel{!}{=} \ell^a \Pi^j_{0,\|}$ and in summary the necessary form for a non-trivial extremum is

$$\Pi^e_0 = \left(\frac{1}{\sqrt{6}}\mathbb{1}_3 + \frac{1}{2}\lambda\cdot\ell\right) \otimes \sigma \cdot \Pi_{0,\|} \ + \frac{1}{2}\lambda \cdot k \otimes \mathbb{1}_2 \tag{3.54}$$

where $\Pi_{0,\|}$ and ℓ, k are 3 and 8 dimensional vectors respectively. Both $\Pi_{0,\|}$ and at least one of ℓ, k must be non-zero for a non-trivial extremum. The question is whether such a point can lie on the conjugation orbit of $(\mathbb{1}_3 \otimes \sigma^3)$, i.e. whether

$$U_0(\mathbb{1}_3 \otimes \sigma^3)U_0^\dagger \stackrel{?}{=} \Pi^e_0 \quad \text{for some} \ \ U_0. \tag{3.55}$$

For now I will disregard $k \to 0$ and discuss the more general case later. The answer is then in the affirmative as I will show now. As is well known, an $SU(6)$ matrix can be written in Cayley-Hamilton form as $U_0 = a_0\mathbb{1}_6 + ia_\alpha T^\alpha$.

Statement: A set of non-trivial extrema of Δ correspond to U_0 of the form

$$U_0 = \frac{1}{2}\mathbb{1}_6 + i\left(\frac{1}{\sqrt{6}}\mathbb{1}_3 + \frac{1}{2}\lambda\cdot\ell\right) \otimes (\sigma\cdot\pi) \tag{3.56}$$

with

$$\left(1 + |\ell|^2\right)\frac{|\pi|^2}{3} \stackrel{!}{=} 1, \tag{3.57}$$

$$\left(\frac{1}{\sqrt{6}}\ell^c + \frac{1}{4}\ell^a\ell^b d^{abc}\right) \stackrel{!}{=} 0, \quad \forall\ c = 1, ..., 8 \tag{3.58}$$

$$\pi^3 = 0 \ , \tag{3.59}$$

where d is the totally antisymmetric $SU(3)$ tensor, π is some 3−vector.

Proof: Consider U_0 of the form

$$U_0 = a_0\mathbb{1}_6 + i\left(\frac{1}{\sqrt{6}}\mathbb{1}_3 + \frac{1}{2}\lambda\cdot\ell\right) \otimes (\sigma\cdot\pi) \ . \tag{3.60}$$

Firstly, for U_0 to be indeed unitary we must have

$$U_0^\dagger U_0 = a_0^2\mathbb{1}_6 + \left(\frac{1}{6}\left(1 + |\ell|^2\right)\mathbb{1}_3 + \frac{1}{\sqrt{6}}\ell^c\lambda^c + \frac{1}{4}\ell^a\ell^b d^{abc}\lambda^c\right) \otimes \mathbb{1}_2|\pi|^2 \stackrel{!}{=} \mathbb{1}_6 \tag{3.61}$$

implying the conditions

$$\left(1+|\ell|^2\right)\frac{|\pi|^2}{6}+a_0^2\stackrel{!}{=}1, \tag{3.62}$$

$$\left(\frac{1}{\sqrt{6}}\ell^c+\frac{1}{4}\ell^a\ell^b d^{abc}\right)\stackrel{!}{=}0,\quad \forall\, c=1,...,8 \tag{3.63}$$

$$\pi^3=0\ . \tag{3.64}$$

Then, consider the conjugation action of this U_0

$$\begin{aligned}U_0\left(\mathbb{1}_3\otimes\sigma^3\right)U_0^\dagger=a_0^2\left(\mathbb{1}_3\otimes\sigma^3\right)+ia_0\left(\frac{1}{\sqrt{6}}\mathbb{1}_3+\frac{1}{2}\lambda\cdot\ell\right)\otimes\left[(\sigma\cdot\pi),\sigma^3\right]\\ +\underbrace{\left(\frac{1}{\sqrt{6}}\mathbb{1}_3+\frac{1}{2}\lambda\cdot\ell\right)^2}_{=(1+|\ell|^2)/6}\otimes((\sigma\cdot\pi)\sigma^3(\sigma\cdot\pi))\end{aligned} \tag{3.65}$$

where in evaluating the underbrace I have applied the derived unitarity conditions. Notice that the second term is something of the form of Π_0^e in eq. (3.54), so that we would like for the first and final terms to cancel. Since $\pi^i\pi^j\sigma^i\sigma^3\sigma^j=2\pi\cdot\sigma\pi^3-|\pi|^2\sigma^3$, we see that the correct thing to do is to choose $\pi^3=0$, so that we have

$$U_0\left(\mathbb{1}_3\otimes\sigma^3\right)U_0^\dagger=ia_0\left(\frac{1}{\sqrt{6}}\mathbb{1}_3+\frac{1}{2}\lambda\cdot b\right)\otimes\left[(\sigma\cdot\pi),\sigma^3\right] \tag{3.66}$$

$$+\underbrace{\left(a_0^2-\left(1+|b|^2\right)\frac{|\pi|^2}{6}\right)}_{\stackrel{!}{=}0}\left(\mathbb{1}_3\otimes\sigma^3\right) \tag{3.67}$$

$$=\left(\frac{1}{\sqrt{6}}\mathbb{1}_3+\frac{1}{2}\lambda\cdot b\right)\otimes\left[(\sigma\cdot\pi),\sigma^3\right]\ , \tag{3.68}$$

where we fixe the value of a_0 to cancel. Thus I have proved the statement. Note the choice of $\pi^3=0$ would seem to imply that necessarily $\Pi^3_{0,\|}=0$ in eq. (3.54) but a completely arbitrary $\Pi_{0,\|}$ can be reached via an extra $SU(2)$ conjugation.

End of Proof

All 8 equations of eq. (3.58) are listed in fig. 3.6(a). This set of eight (quadratic) equations in eight unknowns have non-trivial solutions. Notice that the existence of the d^{abc} tensor is crucial for this to happen. For the 2 generation case where $\lambda\to\sigma$ such a term does not exists and one can immediately see that it is impossible to have a non-global extremum. I do not include the explicit solutions here because all these critical points turn out to be saddles, as will be argued in the following section.

It will be important to note that all solutions of eq. (3.58)have the same modulus, given that

$$\ell^c\stackrel{!}{=}-\frac{\sqrt{6}}{4}\ell^a\ell^b d^{abc} \tag{3.69}$$

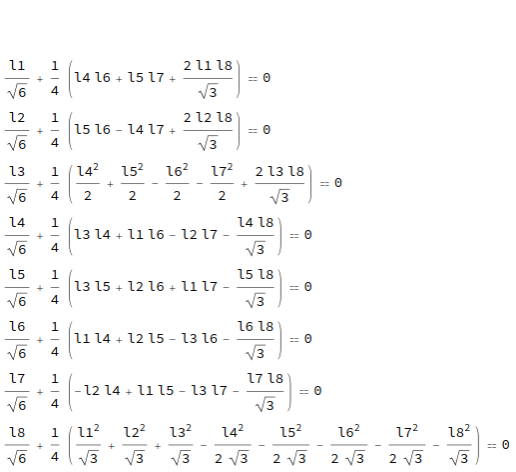

(a) Necessary conditions for an extremum. Alternatively, also $\ell^a \to -\ell^a$, which can give different solutions.

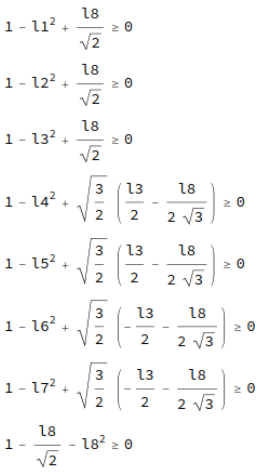

(b) Necessary (but not sufficient) conditions for a minimum

Figure 3.6: Conditions on critical points.

$$\implies |\ell|^2 \stackrel{!}{=} \frac{3}{8}\left(\ell^a \ell^b d^{abc}\right)\left(\ell^{a'} \ell^{b'} d^{a'b'c}\right) = \frac{3}{8}\frac{1}{3}|\ell|^4 \quad \implies \quad |\ell|^2 \stackrel{!}{=} 8 \tag{3.70}$$

where I have made use of identities for the contractions of the d tensor given in [109].

3.3.6 Stability of Critical Points

To explore the stability of the critical points given by the different solutions to eq. (3.58) we must go back to Δ with $U = \tilde{U}U_0$ again, expand and keep terms second order in $\tilde{\Pi}$ fields. Thus one can obtain the requirement for a local minimum to be

$$-\left[\Pi^e_{0,\parallel}, \tilde{\Pi}\right]^{aj}\left[\Pi^e_0, \tilde{\Pi}\right]^{aj} + \left[\Pi^e_{0,\perp}, \tilde{\Pi}\right]^{i}\left[\Pi^e_0, \tilde{\Pi}\right]^{i} \geq 0\ , \quad \forall\ \tilde{\Pi} = \tilde{\Pi}^\alpha T^\alpha\ , \tag{3.71}$$

where as usual $i = 1, 2, 3$ run over $\mathfrak{su}(2)$ subalgebra indices and aj runs through all $\lambda \otimes \sigma$ basis vectors. By inspection, the components $\tilde{\Pi}^i$ and $\tilde{\Pi}^a$ don't appear in the final result, cancelling out. One can thus focus on $\tilde{\Pi} = \tilde{\Pi}^{aj}\lambda^a \otimes \sigma^j$. For simplicity let us consider each direction one at a time and obtain a necessary though not totally sufficient set of conditions for a minimum.

Requiring stability along a single $\lambda^a \otimes \sigma^j$ direction gives

$$\begin{aligned}
&-\operatorname{Tr}\left(\left[\Pi_{0,\parallel}, (\lambda^a \otimes \sigma^j)\right](\lambda^{\bar{b}} \otimes \sigma^{\bar{k}})\right)\operatorname{Tr}\left(\left[\Pi_0, (\lambda^a \otimes \sigma^j)\right](\lambda^{\bar{b}} \otimes \sigma^{\bar{k}})\right) \\
&+\operatorname{Tr}\left(\left[\Pi_{0,\perp}, (\lambda^a \otimes \sigma^j)\right](\mathbb{1}_3 \otimes \sigma^{\bar{k}})\right)\operatorname{Tr}\left(\left[\Pi_0, (\lambda^a \otimes \sigma^j)\right](\mathbb{1}_3 \otimes \sigma^{\bar{k}})\right) \\
&= 4\left(|\Pi_{0,\parallel}|^2 - (\Pi^j_{0,\parallel})^2\right)\left(1 - (\ell^a)^2 + \sqrt{\frac{3}{2}}\ell^{\bar{b}} d^{\bar{b}aa}\right) \stackrel{!}{\geq} 0 \quad \forall\, a = 1, ..., 8 \text{ and } j = 1, 2, 3.
\end{aligned}$$

where only over-lined indices are summed over and I have skipped various steps evaluating. The prefactor is never negative. So the constraint is on the ℓ^a and all 8 inequalities are listed in fig. 3.6(b). For example, the simplest $a = 8$ gives $-\sqrt{2} \leq \ell^8 < \frac{1}{\sqrt{2}}$. Notice that summing up the entire column of inequalities gives

$$\sum_a \left(1 - (\ell^a)^2 + \sqrt{\frac{3}{2}}\ell^{\bar{b}} d^{\bar{b}aa}\right) = 8 - (\ell^a)^2 \stackrel{!}{\geq} 0 \tag{3.72}$$

but we had shown in eq. (3.70) that $\ell^a \ell^a = 8$ at a non-trivial extremum. Therefore in general, in order to sum to zero some of the expressions in fig. 3.6(b) will be negative (implying negative curvature) and others positive (positive curvature). The only way for there to be no negative mass terms is if all expressions in fig. 3.6(b) are exactly zero, corresponding to a point where every single basis vector direction is flat to second order. By inspection, such a point does not exist.

3.3.7 The full conjugation orbit of $(\mathbb{1} \otimes \sigma^3)$

In the previous section we found that the extrema with $k = 0$ identified in section 3.3.5 are all saddle points. It remains to be conclusively proven whether there exist any extrema with $k \neq 0$ and their stability, which I will leave for future work. I will comment however on a necessary feature of such a solution, if it exists.

Consider a general $SU(6)$ matrix in the form

$$U = a\mathbb{1}_6 + it^{\{x\}}T^{\{x\}} \equiv a\mathbb{1}_6 + t^i(\mathbb{1}_3 \otimes \sigma^i) + t^a(\lambda^a \otimes \mathbb{1}_2) + t^{ai}(\lambda^a \otimes \sigma^i), \tag{3.73}$$

with 36 variables a, t^i, t^a, t^{bj}, and $i, j = 1, 2, 3$ and $a, b = 1, ..., 8$ as usual. I have absorbed the normalisation factors of the basis vectors of eq. (3.12) in the variables for simplicity. Unitarity of U requires[8]

$$U^\dagger U \stackrel{!}{=} \mathbb{1}_6$$

$$\begin{aligned}
\implies \quad & a^2 + t^i t^i + \frac{2}{3}t^a t^a + \frac{2}{3}t^{ai}t^{ai} \stackrel{!}{=} 1 \ , && (3.74)\\
& t^a t^{ai} \stackrel{!}{=} 0 \ , && (3.75)\\
& t^a t^b d^{abc} + t^{ai}t^{bi}d^{abc} + 2t^i t^{ci} \stackrel{!}{=} 0 \ , && (3.76)\\
& 2t^i t^c + 2t^a t^{bi} d^{abc} - t^{aj}t^{bk}f^{abc}\epsilon^{jki} \stackrel{!}{=} 0 \ . && (3.77)
\end{aligned}$$

[8]You might ask, how is this compatible with there being 35 d.o.f. The answer is these are not real d.o.f.

Notice for initial simplicity I have taken all coefficients to be real. Applying this most general conjugation now to our starting element

$$\begin{aligned}
U^\dagger(\mathbb{1}_3\otimes\sigma^3)U = a^2(\mathbb{1}_3\otimes\sigma^3) &- 2a\left(t^i\mathbb{1}_3 + t^{ai}\lambda^a\right)\otimes\sigma^k\epsilon^{i3k} \\
&+ \mathbb{1}_3\otimes(2t^3t^i\sigma^i - t^it^i\sigma^3) \\
&+ \left(\frac{2}{3}t^at^a + t^at^b(d^{abc}+if^{abc})\lambda^c\right)\otimes\sigma^3 \\
&+ \left(\frac{2}{3}\delta^{ab}\mathbb{1}_3 + d^{abc}\lambda^c\right)\otimes(2t^{ai}\sigma^it^{b3} - t^{ai}t^{bi}\sigma^3) \\
&+ 2\lambda^a\otimes(t^3t^{aj}\sigma^j + t^{a3}t^i\sigma^i - t^it^{ai}\sigma^3) - 2t^at^{bj}f^{abc}\epsilon^{3jk}\lambda^c\otimes\sigma^k \\
&+ 2f^{abc}t^{ai}t^{bj}\epsilon^{ij3}\lambda^c\otimes\mathbb{1}_2\ ,
\end{aligned}$$

where the d and f tensors are the fully symmetric and antisymmetric tensors of $SU(3)$ respectively. The last term is the only one proportional to the $\mathfrak{su}(3)$ subalgebra and its coefficient is thus the only way to generate k^a in eq. (3.54). This is only non-zero if t^{ai} cannot be written as the direct product of two vectors.

3.3.8 Discussion and Future Work

The theory of the SM at large positive Higgs mass has clearly a rich and complicated structure. In this thesis I have focused on the strongest dynamics, namely that of the confining $SU(3)_c$ sector, treating the EW gauge interactions as a perturbation on top. The ensuing potential for pNGBs from integrating out gauge bosons is non-trivial. I have made significant progress in studying the full potential at one loop. At present I do not find meta-stable states in this theory but I am far from ruling out their presence either and future work will be able to establish the truth.

As argued in section 3.3.3, the calculable extremum points of the potential are the extrema of Δ defined in eq. (3.7). Although it is likely that I have classified all critical points, this statement requires a definitive proof.

Going beyond the analysis of this thesis, two main ingredients were ignored: the leptons and lingering effects from the massive Higgs. In the first approximation of a completely decoupled Higgs the leptons remain massless all the way down to the IR. They thus contribute at all orders to the running of the electromagnetic coupling which runs to zero at the $U(1)_{\rm em}$ preserving locus of vacua of eq. (3.42). It is unlikely that this effect qualitatively changes the potential away from this locus as the photon is massive and no logarithmic running of the $U(1)_{\rm em}$ coupling occurs below the photon mass.

Second, as mentioned already, the leading IR effects of the Higgs are felt through four-Fermi operators. The Yukawa matrices break all remaining symmetries so no flat pNGB direction will survive - apart from those fictitious directions eaten by the gauge bosons - and the vacua go from loci to a single point. Treated as the weakest perturbation, it remains to compute this degeneracy-lifting effect on the vacuum locus of eq. (3.42).[9] This results in a very rich potential of maximum height of order $y_t^2 \Lambda_{\rm QCD}'^6 / m_H^2$ for the 16 previous exactly flat physical field directions on this locus. The details of this potential and its critical points is the subject of future work.

[9]After integrating out the Higgs, the coefficients of the four Fermi operators will change by renormalisation group flow, dominantly by $SU(3)_c$ interactions. But due to the $SU(3)_g^5$ inter-generational symmetry of the SM gauge interactions acting on the SM matter the structure of the relevant flavour spurions remains set by the Yukawa couplings.

Chapter 4

Reflections on Bubble Walls

4.1 Introduction

Cosmological phase transitions in the early Universe that proceed via nucleation of bubbles are a well-motivated possibility in minimal extensions of the Standard Model, as well as in more general scenarios featuring hidden sectors with their own dynamics. Such first order transitions result in the emission of gravitational radiation [23, 110–113] that current and future observatories may be able to detect in the form of a stochastic background of gravitational waves (see e.g. [114, 115] for reviews). An observation of this kind would provide unambiguous evidence for the existence of degrees of freedom beyond the Standard Model. This has spurred significant interest in the gravitational wave signatures of hidden sectors in recent times [41, 42, 116–124].

Despite the abundance of particle physics models susceptible of undergoing an out-of-equilibrium transition, our ability to make use of the resulting gravitational wave signal to extract information about the relevant dynamics is extremely limited. The most revealing features concern the frequency peak of the stochastic background, as well as its spectral shape at high frequencies. The former determines the epoch at which the transition takes place, whereas the latter contains information about the dominant source of gravitational radiation. For example, if most of the energy released during the transition goes into accelerating the bubble walls (as in vacuum [125]), these become relativistic and continue to expand at ever-increasing velocities. In this case, collisions of these "run-away" bubbles constitute the main source of gravitational waves, and the resulting signal falls off as f^{-1} at high frequencies [126]. Alternatively, pressure on the bubble walls due to particles in the thermal plasma may cause the expanding walls to reach a terminal speed. In this case, most of the latent heat gets damped instead into the thermal fluid, and it is its subsequent motion that provides the dominant source of gravitational radiation [39]. The high-frequency fall-off of the

stochastic background is steeper, e.g. decreasing as f^{-4} for radiation sourced by sound waves [127–130]. On the other hand, assuming radiation-domination at the time of gravitational wave production, causal propagation restricts the low frequency shape of the spectrum to grow as f^3, independently of the dominant production channel [131].[1]

Understanding the dynamics of expanding bubble walls in the early Universe is clearly crucial to determine both quantitative and qualitative features of the resulting gravitational wave signal. But given the intrinsic degeneracy present in any stochastic background, it is equally important to explore alternative probes of the relevant dynamics. For example, the upcoming LISA experiment will be sensitive to phase transitions at electroweak to multi-TeV scale temperatures, probing the nature of the electroweak phase transition and potentially shedding light on the dynamics behind baryogenesis and electroweak symmetry breaking. In this range of energies, the complementarity between LISA and current and future colliders will no doubt be key in furthering our understanding of physics at and around the weak scale (see e.g. [114, 115, 135, 136] for reviews and references). Beyond (and below) the electroweak scale, phase transitions within hidden sectors may occur at virtually any temperature, and the corresponding stochastic background could fall anywhere from the low frequency range of PTA observatories [137,138] ($10^{-9} - 10^{-7}$ Hz), to the high frequencies probed by LIGO ($10 - 10^3$ Hz), and beyond. However, vacuum bubbles nucleated in hidden sector transitions may feature very different dynamics to those linked to the weak scale, and the relevant degrees of freedom may be inaccessible at laboratory experiments. Our work is motivated by the goal to more broadly understand the potential behavior of expanding bubbles in the early Universe, as well as to identify alternative predictions that may accompany an observable stochastic background of gravitational waves.

In a first order phase transition, bubbles of true vacuum are nucleated at rest, and begin to expand fueled by the difference in free energy densities at either side of the interface. In vacuum, the velocity of the bubble walls evolves according to [125]

$$\frac{d|\vec{v}|}{dt} = \frac{1}{\gamma^3 R_0} \propto \frac{1}{\gamma^3}\frac{\Delta V}{\sigma} \,, \tag{4.1}$$

with $\gamma = 1/\sqrt{1-\vec{v}^2}$ the usual Lorentz γ-factor, $R_0 \propto \sigma/\Delta V$ the critical bubble radius, and where ΔV and σ refer to the difference in vacuum energy densities and surface tension of the bubble wall. In reality, bubbles do not expand against a sea of

[1] More generally, the low-frequency shape of the stochastic background depends on the equation of state [132, 133] and on the existence of free-streaming particles [133, 134], and could thus provide non-trivial information about the Universe at early times.

false vacuum, but rather within a non-trivial environment that in the early Universe must include the Standard Model plasma as well as, potentially, other ingredients such as dark matter. As the bubble wall speed grows, friction from the surrounding environment can exert a pressure on the interface that opposes the expansion of the bubble walls. Their evolution can still be written as in eq. (4.1), after the replacement [139, 140]:

$$\Delta V \to \Delta V - \mathcal{P} \ , \tag{4.2}$$

where $\mathcal{P}$ refers to the frictional pressure resulting from the interaction between the interface and the surrounding medium, and is in general dependent on the speed of the bubble wall.

Two qualitatively different scenarios are thus possible. If $\Delta V \gg \mathcal{P}$ during the entire evolution of the bubble walls, these effectively behave as if they were in vacuum and most of the energy released as the bubbles grow goes into accelerating the expanding interface. The walls then "run away" – that is, they continue to expand with ever increasing velocities. Alternatively, if $\mathcal{P}$ grows large enough so as to neutralize the difference in vacuum energies, $\Delta V = \mathcal{P}$, the bubble walls reach an equilibrium regime of constant speed. Once in equilibrium, the fraction of the total energy that becomes localized on the interface quickly becomes tiny. Instead, most of the energy gets damped into whatever sector of the surrounding environment is responsible for halting the acceleration of the bubble walls. Calculating the pressure experienced by bubble walls as they expand is a classic problem [139–144] that has received renewed attention in recent times [38, 39, 145–154].

Within a thermal plasma, particles with phase-dependent mass create a pressure on the expanding walls that asymptotes to a constant $\mathcal{P}_\infty \sim \Delta m^2 T^2$ in the ultra-relativistic limit [2], independently of the type of particle [145]. An additional source of friction may be present if the spectrum contains gauge bosons, of the form $\mathcal{P}_\infty \sim \gamma g^2 \Delta m_v T^3$, with g the relevant gauge coupling and Δm_v the change in the mass of the gauge boson at either side of the bubble wall [147, 148, 152]. This effect has its origin in the transition radiation emitted by charged particles as they cross the wall and its γ-dependence can easily render it the most significant source of friction on fast expanding bubbles. Indeed, if the electroweak phase transition were first order, transition radiation would likely cause the bubble walls to reach an equilibrium γ-factor as low as $\gamma_{\rm eq} = \mathcal{O}(10)$ [147].

[2]The ultra-relativistic limit refers to the kinematic regime where the energy of the incident particles in the rest frame of the bubble wall is the largest energy scale. Alternatively, this corresponds to the limit $\gamma \to \infty$ for the γ-factor of the bubble wall.

A crucial aspect of all sources of friction known so far is that the corresponding pressure is a monotonically increasing function of the wall speed. As put forward in [145, 147], this allows for a simple criterion to determine whether bubble walls during a cosmological phase transition become run-away, by comparing the pressure in the ultra-relativistic limit, $\mathcal{P}_\infty$, to the difference in vacuum energy density across the wall:

$$\text{Run-away criterion:} \qquad \Delta V > \mathcal{P}_\infty \qquad [145, 147] \ . \tag{4.3}$$

In this article, we discuss a new physical effect that can qualitatively alter the dynamics of bubble walls during a cosmological phase transition. Namely, the existence of a transient relativistic regime characterized by an approximately constant reflection probability of longitudinal massive vectors off an expanding interface. Effectively, the wall behaves temporarily like an imperfect mirror that reflects a fraction of longitudinal – but not transverse – modes. Two conditions need to be satisfied for this regime to be accessible: (*i*) that the expansion of the bubble walls takes place against a population of massive vectors whose mass changes across the interface; and (*ii*) that the expanding walls are sufficiently "thin". By thin, we mean that the wall thickness (in the rest frame of the bubble wall) be much smaller than the Compton wavelength of the massive vector, i.e.

$$L \ll m^{-1} \ . \tag{4.4}$$

In this case, the regime of constant longitudinal reflection corresponds to Lorentz γ-factors in the range

$$1 \ll \gamma \ll (Lm)^{-1} \ , \tag{4.5}$$

ending when γ is so large that the Lorentz-contracted Compton wavelength of the dark photon becomes smaller than the wall thickness. We will refer to this kinematic regime as the region of "inter-relativistic" motion. Eq.(4.4) ensures that $(Lm)^{-1} \gg 1$, and that this regime is indeed accessible during the evolution of the expanding bubbles. Once γ becomes $\gg (Lm)^{-1}$, reflection probabilities for all polarizations die off exponentially – a well-known feature of the ultra-relativistic limit.

Most notably, the effect described above leads to an additional source of friction on expanding bubble walls. Unlike previously known cases, the corresponding pressure features a characteristic non-monotonic dependence on the relevant γ-factor, reaching a maximum at $\gamma \sim (Lm)^{-1}$ before turning-off at larger values. In (superficial) analogy with the behavior of spacecraft shortly after launch, we will refer to this pressure peak

as Maximum Dynamic Pressure. Its existence can make it much harder for bubble walls to become run-away than previously believed, and we will show that eq. (4.3) can be qualitatively misleading in phase transitions where the bubble walls expand against an existing population of phase-dependent massive dark photons.

This article is dedicated to deriving the claims made in the previous two paragraphs, as well as illustrating some of their phenomenological consequences. We will refer to the temperature of the Standard Model plasma at the epoch of the phase transition as T_*, and denote the phase transition strength via the usual dimensionless quantity [114, 115]:

$$\alpha \equiv \frac{\Delta V}{\rho_{\rm SM}(T_*)} = \frac{\Delta V}{\frac{\pi^2}{30} g_*(T_*) T_*^4} \ . \tag{4.6}$$

We will focus on bubble walls that expand against a population of cold and non-interacting dark photons. Despite its simplicity, this system will be relevant in some physically interesting cases, such as when the dark photons furnish the dark matter [155–160] – a well-motivated benchmark that we often refer to throughout this work. When the bubble walls reach an equilibrium regime as a result of longitudinal reflections, the fraction of the total energy that goes into accelerating the bubble walls becomes increasingly small. Instead, most of the available energy goes into making the reflected dark photons relativistic, turning them into dark radiation. If the dark radiation remains relativistic until late times, an observable contribution to $\Delta N_{\rm eff}$ is possible. In particular, current bounds on $\Delta N_{\rm eff}$ could probe phase transitions with strength $\alpha \gtrsim 10^{-1}$, whereas CMB S-4 measurements could be sensitive to scenarios down to $\alpha \sim 10^{-2}$ for all relevant frequencies.

Extensions of the Standard Model featuring massive vectors are popular both because of their minimality as well as their potential to furnish the dark matter, with a variety of production mechanisms spanning a wide mass range [157–160]. Before we move on, let us summarize why the existence of *massive* dark photons whose mass changes in the course of our cosmological history is not only a well-motivated possibility, but may be an unavoidable feature in a wide class of models. At the renormalizable level, the physical system that we focus on is described by a lagrangian of the form

$$\mathcal{L} \supset \frac{1}{2} \left(\partial_\mu \phi\right)^2 - V(\phi) - \frac{1}{4} F_{\mu\nu} F^{\mu\nu} + \frac{1}{2} m^2 V_\mu V^\mu \ , \tag{4.7}$$

where ϕ is a real scalar field and V_μ is the massive dark photon. By assumption, the potential for ϕ features two non-degenerate vacua such that the scalar sector undergoes a phase transition in the early Universe. Without loss of generality (WLOG) we take the false and the true vacuum to lie at $\langle \phi \rangle = 0$ and $\langle \phi \rangle = v$. $V(\phi)$ may be a finite

temperature effective potential, or it may be a zero-temperature potential in which case the transition proceeds via quantum tunneling. If the scalar sector is in thermal equilibrium with the Standard Model then $T_* \sim v$, whereas $T_* \ll v$ is possible if the transition is 'super-cooled', or if ϕ belongs in a hidden sector that is decoupled from the thermal plasma. At nucleation, the thickness of the bubble walls is determined by the features of the scalar potential, and typically $L \sim (\sqrt{\lambda}\, v)^{-1}$, with λ the typical quartic coupling in $V(\phi)$. The size of the dimensionless combination $T_* L$ will have a quantitative effect on our results, as we will discuss when relevant.

At the level of eq. (4.7), the scalar and dark photon sectors are fully decoupled. Beyond the renormalizable terms of eq. (4.7), this need not remain true. For example, the following operator

$$\mathcal{L} \supset \frac{\kappa}{2} \phi^2 V^\mu V_\mu \ , \tag{4.8}$$

leads to an additional contribution to the vector mass in the true vacuum, of the form $\Delta m^2 = \kappa v^2$. As the scalar vev 'turns on' in the early Universe the dark photon mass will shift accordingly. Of course, the scalar field may be complex instead of real, which can be trivially accommodated by writing $|\phi|^2$ instead. Indeed, an effective interaction $\propto |H|^2 V^\mu V_\mu$, with H the Standard Model Higgs doublet, would lead to a shift in the dark photon mass before and after the electroweak phase transition. We emphasize that eq. (4.8) cannot be forbidden on the basis of symmetry, and its manifest lack of gauge redundancy is a moot point given that the theory under consideration already contains a mass for V^μ. Legalistically, one might object to eq. (4.8) on the basis that it differs from a Stückelberg mass, $\frac{1}{2} m^2 V^\mu V_\mu$, in that the former is not a renormalizable interaction and demands UV-completion. However, upholding the laws of effective field theory, we have no choice but to overrule this objection. Accepting the existence of a finite cutoff in our description of nature, a theory with a massive dark photon and scalar degrees of freedom will in general feature effective interactions as in eq. (4.8).

Indeed, a non-zero κ in eq. (4.8) sets an upper bound on the scale of UV completion. Provided that the term in eq. (4.8) only accounts for a subleading contribution to the overall mass of the dark photon in the true vacuum ($\Delta m^2 \ll m^2$), the upper bound on the UV cutoff can be conveniently written as [161]

$$\Lambda \lesssim \frac{4\pi v}{\sqrt{\Delta m^2 / m^2}} \ . \tag{4.9}$$

Here, we indeed focus on cases where the change in the dark photon mass is tiny. This allows for a separation between the scale of the phase transition, v, and the UV cutoff, allowing us to neglect the effect of heavy degrees of freedom on the dynamics

of the phase transition and focus instead on the consequences of non-zero Δm^2 on the evolution of the bubble walls. As we will see, even when $\Delta m^2/m^2 \ll 1$, the implications for the evolution of cosmological vacuum bubbles can be significant.[3]

An important comment before we proceed. As made clear in the preceding paragraph, the content of this paper is only relevant in the presence of vector bosons that are *massive* at either side of the bubble wall. Our results therefore do not affect the pressure created by *massless* gauge bosons that gain a mass as they cross the wall, and so we have nothing to add to e.g. the pressure created by W and Z bosons during a first order electroweak phase transition.

The rest of this paper is organized as follows. We begin in section 4.2 with a summary of the physical set-up that we will focus on in the remainder of this manuscript. In section 4.3, we present our calculation of the reflection probability for phase-dependent massive vectors. Fig. 4.2 illustrates the main result of this section: the existence of a transient relativistic regime characterized by an approximately constant reflection probability of longitudinally polarized dark photons. Section 4.4 focuses on fleshing out the consequences of our results for the evolution of bubble walls in the early Universe, including the existence of a Maximum Dynamic Pressure in section 4.4.1, as well as a self-consistent determination of the equilibrium γ-factor when this pressure is large enough to halt the acceleration of the bubble walls in section 4.4.2. The fate of the reflected dark photons depends sensitively on a variety of considerations, most notably on whether the sector undergoing the phase transition is hot or cold, as we discuss in section 4.4.3. We summarize our conclusions in section 4.7, and a number of appendices supplement the discussion in the main text.

4.2 Set-up

The rest of this article is dedicated to calculating the pressure on an expanding bubble wall due to an existing population of phase-dependent massive dark photons and to discussing the implications of our results. With this goal, we consider an expanding planar interface, representing a portion of a sufficiently large bubble wall, moving with local velocity $\vec{v}$ and corresponding γ-factor $\gamma \equiv 1/\sqrt{1-\vec{v}^2}$. The wall is not expanding in vacuum, but rather against a population of cold and non-interacting massive vector bosons with number density n_V. WLOG, we take the velocity of the bubble wall in the rest frame of the dark photons to be along the negative z-axis, $\vec{v} = -|\vec{v}|\hat{z}$. At leading

[3] Although most of our subsequent discussion will proceed within the effective theory defined in eq. (4.7)-4.8, we discuss in section 4.5.1 how this effective description can arise from a UV-complete model.

order, to compute the pressure on the wall we need the momentum transfer from particles that either reflect or transmit across the interface. Our assumption that the dark photon sector is non self-interacting allows us to consider the individual interactions of particles with the wall, although this approach is more generally valid whenever the relevant mean free path exceeds the wall thickness.

Like previous work focused on computing pressure on expanding bubbles, we find it convenient to work in the rest frame of the interface. In this frame, the scalar order parameter characterizing the transition varies only as a function of the spatial coordinates, which in our convention will be along the z-axis. A dark photon wind moving from the false to the true vacuum hits the bubble wall with velocity $-\vec{v} = |\vec{v}|\hat{z}$. All particles hit the interface at normal incidence and there are no particles traveling in the opposite direction – both observations follow from our assumption that the dark photon sector is cold [4]. This set-up is depicted in fig. 4.1.

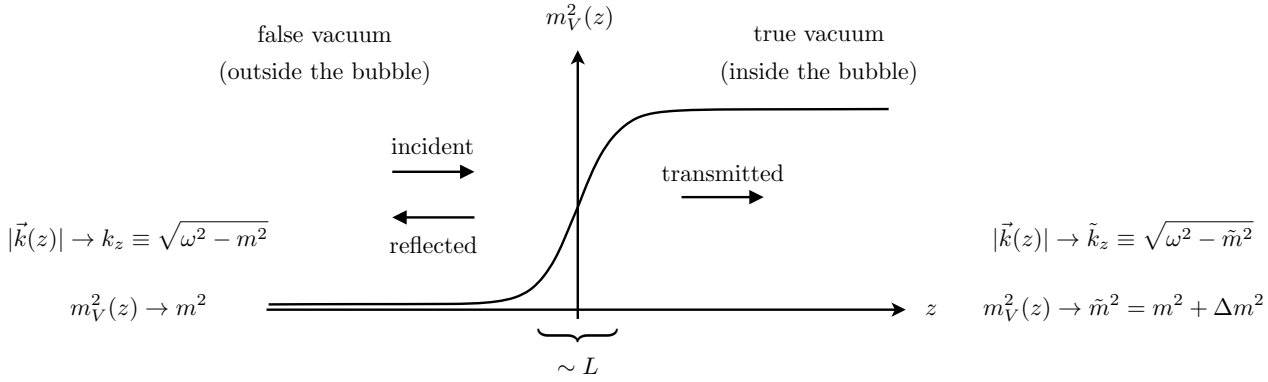

Figure 4.1: In the rest frame of the bubble wall, a dark photon wind hits the interface from the region of false vacuum. The energy of the incident dark photons, $\omega = \gamma m$, remains conserved in the interaction with the wall, whereas momentum along the z-direction changes resulting in a net momentum transfer to the interface. L refers to the wall thickness, i.e. the typical length scale over which the order parameter varies. In this article, we focus on the case where the vector mass changes by a small amount at either side of the bubble wall, i.e. $\Delta m^2 \ll m^2 \simeq \tilde{m}^2$. Much of our work will be concerned with the dynamics of the inter-relativistic kinematic regime of eq. (4.5) where $m \ll \omega \ll L^{-1}$.

By assumption, the dark photon mass depends on the order parameter characterizing the phase transition. As anticipated in the Introduction, and further dis-

[4]Quantitatively, the assumption of normal incidence requires that, in the wall frame, the normal component of the dark photon momentum is much greater than the components along the plane of the bubble wall, i.e. $|\vec{k}_\perp| \gg |\vec{k}_\parallel|$. For a gas of dark photons at temperature $T_{\rm dp} \ll m$ and a relativistic wall, $|\vec{k}_\perp| \sim \gamma m \gg |\vec{k}_\parallel| \sim \sqrt{T_{\rm dr} m}$ provided $\gamma \gg \sqrt{T_{\rm dp}/m}$, which is satisfied trivially. It should be be straightforward to generalize our results beyond these assumptions.

cussed in section 4.5.1, realistic situations often feature a dependence of the form $m_V^2(z) = m^2 + \kappa v(z)^2$, with v the relevant order parameter and κ a constant determined by the underlying model. However, for most of our discussion, it will be sufficient to just assume that the vector mass-squared parameter is z-dependent, with asymptotic values m^2 and $\tilde{m}^2$ for large negative and positive z, as indicated in fig. 4.1. We define the difference in squared masses as $\Delta m^2 \equiv \tilde{m}^2 - m^2 > 0$ and we will always assume that $\Delta m^2 \ll m^2 \simeq \tilde{m}^2$, in keeping with the discussion around eq. (4.9).

Since the wall background is independent of t, the energy of the incident particles, $\omega = \gamma m$, remains conserved in the interaction with the wall, whereas momentum in the z-direction changes in a way that results in a net momentum transfer to the interface. In total, the pressure exerted on the wall as a result of this dark photon wind can be written as

$$\mathcal{P} = \gamma |\vec{v}| n_V \times \frac{1}{3} \sum_{\lambda} \left(R_\lambda \, \Delta k_R + T_\lambda \, \Delta k_T \right) \ . \tag{4.10}$$

The factor $\gamma|\vec{v}|n_V$ corresponds to the flux of incoming massive vectors hitting the wall (in the wall frame), whereas the quantity in parentheses represents the average momentum transfer to the wall from an incoming particle with fixed polarization λ, with R_λ and T_λ the corresponding reflection and transmission probabilities. The momentum transfer from reflected and transmitted particles is given by $\Delta k_R = 2k_z$ and $\Delta k_T = k_z - \tilde{k}_z$, with k_z and $\tilde{k}_z$ the asymptotic transverse momenta at either side of the bubble wall, as defined in fig. 4.1. The sum over λ includes the three physical polarizations of a massive vector, and the lack of mixing between different polarizations in eq. (4.10) follows as a result of normal incidence.

For example, in the regime of ultra-relativistic motion – when ω is the largest energy scale in the problem, $\omega \gg m, L^{-1}$ – reflection and transmission probabilities must asymptote to zero and unity respectively, and eq. (4.10) takes the form,

$$\mathcal{P}_\infty = \lim_{\gamma \to \infty} \mathcal{P} \simeq \gamma n_V \Delta k_T = \rho_V \frac{\Delta m^2}{2m^2} \ , \tag{4.11}$$

where we have used $\Delta k_T \simeq \Delta m^2/(2\gamma m)$, and $\rho_V = m n_V$ is the energy density of dark photons. If the massive vector population outside of the bubble wall was instead described in terms of a fully thermal distribution, with $T \gg m$, we would have $\omega \sim \gamma T$ and $n_V \sim T^3$, and therefore $\mathcal{P}_\infty \sim T^2 \Delta m^2$ as is well known [145]. As seen in eq. (4.11), the frictional pressure reaches a constant (independent of the wall velocity) in this limit.

A comment is in order before we move on. Comparing the asymptotic pressure in eq. (4.11) to the difference in vacuum energy densities, one finds

$$\frac{\mathcal{P}_\infty}{\Delta V} \simeq \frac{\Delta m^2}{2m^2}\,\frac{\rho_V}{\Delta V} \sim \alpha\,\frac{\Delta m^2}{m^2}\,\frac{\rho_V(T_*)}{\rho_{\rm dm}(T_*)}\,\frac{\rho_{\rm dm}(T_*)}{\rho_{\rm SM}(T_*)}\,, \tag{4.12}$$

where α is defined in eq. (4.6) and in the last step we have made it explicit that all the relevant energy densities are to be evaluated at the phase transition epoch. The ratio $\rho_V/\rho_{\rm dm}$ in eq. (4.12) is 1 if the dark photons account for all of the dark matter, whereas α and $\Delta m^2/m^2$ are $\ll 1$ as discussed previously. The ratio of dark matter to Standard Model radiation in the early Universe is $\rho_{\rm dm}/\rho_{\rm SM} \lll 1$, making eq. (4.12) correspondingly tiny. As per the run-away criterion of eq. (4.3), one would be tempted to conclude that a small change in the dark matter mass would have a negligible effect on the evolution of cosmological bubble walls. Our results will show that – in general – this expectation can be mistaken.

To proceed, we must obtain reflection and transmission probabilities, as a function of γ, for massive vectors interacting with the non-trivial background of the bubble wall. This problem reduces to solving the equations of motion for massive electromagnetism with a spatially varying photon mass, as we discuss next.

4.3 Reflection and transmission probabilities

We begin in section 4.3.1 with a brief discussion regarding massive electromagnetism with a spatially varying vector mass. In 4.3.2, we obtain reflection and transmission probabilities in one the of the few non-trivial cases where an analytic solution is accessible: a step function change in the mass of the dark photon. This corresponds to the limit of vanishing wall thickness, and it provides an accurate description of the system in the regime $\omega \ll L^{-1}$, where ω is the incoming particle's energy as shown in fig. 4.1. Considering a step wall allows us to illustrate one of our main results: that the reflection probability for longitudinal modes asymptotes to a constant in the inter-relativistic regime of eq. (4.5). In 4.3.3 we turn to the realistic situation of finite width, and show that the existence of a relativistic regime of near-constant longitudinal reflection is a generic feature of thin walls with finite thickness.

4.3.1 Massive electromagnetism

In the absence of charged sources, Maxwell's equations in the presence of a varying vector mass read

$$\partial_\mu F^{\mu\nu} + m_V^2(x) V^\nu = 0\,, \tag{4.13}$$

which, in turn, imply the consistency condition

$$\partial_\mu \left(m_V^2(x) V^\mu \right) = 0 \ . \tag{4.14}$$

As is well known, when the vector mass is constant, $m_V^2(x) = m^2$, eq. (4.14) reduces to the familiar requirement that $\partial_\mu V^\mu = 0$, and Maxwell's equations admit plane-wave solutions of the form

$$V^\mu(x) = v^\mu e^{-ik\cdot x} \qquad \text{(constant vector mass)} \ , \tag{4.15}$$

for all k^μ such that $k^2 = m^2$, and the v^μ are momentum-dependent complex coefficients satisfying $k_\mu v^\mu = 0$.[5] As usual, the v^μ can be written as a sum over unit-normalized polarization vectors, one for each of the three physical degrees of freedom of a massive spin-1 particle. For $\vec{k} = \pm|\vec{k}|\hat{z}$, a convenient basis is given by

$$\varepsilon_x^\mu = (0,1,0,0) \ , \qquad \varepsilon_y^\mu = (0,0,1,0) \qquad \text{and} \qquad \varepsilon_l^\mu = \left(\frac{|\vec{k}|}{m}, 0, 0, \pm\frac{\omega}{m} \right) \ . \tag{4.16}$$

When the photon mass has a non-trivial profile, analytic solutions to eq. (4.13)-(4.14) only exist in some special cases. Assuming the vector mass-squared features no time dependence, as appropriate in the rest frame of the bubble wall, eq. (4.14) can be written as

$$\partial_\mu V^\mu = -\left(\vec{\nabla} \log m_V^2(\vec{x}) \right) \cdot \vec{V} \ . \tag{4.17}$$

If $\vec{k} \parallel \vec{\nabla} m_V^2$, as in the case of normal incidence, eq. (4.17) is non-vanishing for the longitudinal component, whereas $\partial_\mu V^\mu = 0$ for the transverse modes. As summarized around fig. 4.1, this is indeed the set-up that we focus on in this work.

4.3.2 A step wall

We will first consider a step-function change in the vector mass:

$$m_V^2(z) = m^2 + \Delta m_V^2(z) \qquad \text{with} \qquad \Delta m_V^2(z) = \Delta m^2 \, \Theta(z) \ , \tag{4.18}$$

where $\Delta m^2 = \tilde{m}^2 - m^2 > 0$ and $\Theta(z)$ is the Heaviside step function. With this mass profile, the equations of motion feature plane-wave solutions on either side of the wall localized at $z = 0$. These can be written as

$$V_\perp^\mu(t,z) = e^{-i\omega t} \begin{cases} (0,1,1,0) e^{ik_z z} + r_\perp (0,1,1,0) e^{-ik_z z} & z < 0 \\ t_\perp (0,1,1,0) e^{i\tilde{k}_z z} & z > 0 \end{cases} \tag{4.19}$$

[5] The field V^μ is of course real-valued. It is implicitly assumed that only the real part of eq. (4.15) has physical significance. The same applies to all other expressions of this form in the remainder of this paper.

for the transverse modes, [6] and

$$V_l^\mu(t,z) = e^{-i\omega t}\begin{cases} \left(\frac{k_z}{m},0,0,\frac{\omega}{m}\right)e^{ik_z z} + r_l\left(\frac{k_z}{m},0,0,-\frac{\omega}{m}\right)e^{-ik_z z} & z<0 \\ t_l\left(\frac{\tilde{k}_z}{\tilde{m}},0,0,\frac{\omega}{\tilde{m}}\right)e^{i\tilde{k}_z z} & z>0 \end{cases} \tag{4.20}$$

for the longitudinal component, with $k_z = \sqrt{\omega^2 - m^2}$ and $\tilde{k}_z = \sqrt{\omega^2 - \tilde{m}^2}$ as defined in fig. 4.1. The overall normalization of eq. (4.19)-(4.20) is arbitrary, and with this choice the reflection and transmission probabilities are given by

$$R_\alpha = |r_\alpha|^2 \qquad \text{and} \qquad T_\alpha = \frac{\tilde{k}_z}{k_z}|t_\alpha|^2 \ , \tag{4.21}$$

with $\alpha = \perp, l$ for transverse and longitudinal modes respectively.

We can now obtain analytic solutions for both reflection and transmission probabilities by integrating the equations of motion across the interface. Let us discuss the transverse modes first. As discussed below eq. (4.17), the transverse modes satisfy $\partial_\mu V_\perp^\mu = 0$, and eq. (4.13) reads $(\Box + m_V^2(z))V_\perp^\mu = 0$. We then have:

$$\lim_{\epsilon\to 0}\int_{-\epsilon}^{+\epsilon} dz\, \left(\Box + m_V^2(z)\right) V_\perp^\mu = 0 \qquad \Rightarrow \qquad \partial_z V_\perp^\mu \text{ is continuous at } z=0\ . \tag{4.22}$$

Combined with the requirement that $V_\perp^\mu$ itself remains continuous, we can solve for $r_\perp$ and $t_\perp$. In particular, the reflection probability is given by

$$R_\perp = |r_\perp|^2 = \left|\frac{k_z - \tilde{k}_z}{k_z + \tilde{k}_z}\right|^2 \xrightarrow{\omega \gg m,\tilde{m}} \left(\frac{\Delta m^2}{4\omega^2}\right)^2 = \gamma^{-4}\left(\frac{\Delta m^2}{4m^2}\right)^2 \ . \tag{4.23}$$

Unsurprisingly, $R_\perp$ falls off rapidly in the regime of relativistic motion.

The behavior of the longitudinal mode is starkly different. We can obtain a first matching condition by integrating eq. (4.14) across the wall:

$$\lim_{\epsilon\to 0}\int_{-\epsilon}^{+\epsilon} dz\, \partial_\mu\left(m_V^2(z)V_l^\mu\right) = 0 \qquad \Rightarrow \qquad m_V^2(z)V_l^3 \text{ is continuous at } z=0\ . \tag{4.24}$$

Integrating eq. (4.13) provides the second condition we need. Since $\partial_\mu V_l^\mu$ no longer vanishes, expanding Eq.(4.13) we now have $(\Box + m_V^2(z))V_l^\mu - \partial^\mu(\partial_\nu V_l^\nu) = 0$. The matching condition arising from the $\mu = 0$ equation is degenerate with eq. (4.24). Instead, focusing on $\mu = 3$, we find

$$\lim_{\epsilon\to 0}\int_{-\epsilon}^{+\epsilon} dz\, \left((\Box + m_V^2(z))V_l^3 + \partial_z(\partial_\nu V_l^\nu)\right) = 0 \qquad \Rightarrow \qquad \partial_t V_l^0 \text{ is continuous at } z=0\,. \tag{4.25}$$

[6] We have taken advantage of rotational invariance in the $x-y$ plane to set $t_x = t_y \equiv t_\perp$ and $r_x = r_y \equiv r_\perp$.

Given that the time dependence of V^μ is of the form $e^{-i\omega t}$ for all z, the previous requirement is equivalent to demanding that V_l^0 itself remains continuous. The corresponding reflection probability now reads

$$R_l = |r_l|^2 = \left| \frac{\tilde{m}^2\, k_z - m^2\, \tilde{k}_z}{\tilde{m}^2\, k_z + m^2\, \tilde{k}_z} \right|^2 \xrightarrow{\omega \gg m, \tilde{m}} \left(\frac{\tilde{m}^2 - m^2}{\tilde{m}^2 + m^2} \right)^2 \simeq \left(\frac{\Delta m^2}{2m^2} \right)^2 , \tag{4.26}$$

where the last step assumes $\Delta m^2 \ll m^2 \simeq \tilde{m}^2$. As advertised in the Introduction, in the regime of relativistic motion the longitudinal reflection probability approaches a constant, independent of γ.[7] [8]

4.3.3 A smooth wall

In a realistic situation where the wall thickness is finite and the vector mass varies smoothly, the analytic results of the previous subsection only provide an accurate approximation to the reflection and transmission probabilities in the regime $\omega \ll L^{-1}$. In what follows, we perform a more general analysis of the case of finite width. We parametrize the dark photon mass as in eq. (4.18), except now

$$\Delta m_V^2(z) = \Delta m^2 \Theta_L(z) , \tag{4.27}$$

where $\Theta_L(z)$ is no longer a step function, but rather some smooth function that approaches 0 and 1 for large negative and positive z respectively, and with an appropriate step-function limit as $L \to 0$. We will discuss a specific choice of mass profile at the end of this subsection, but will otherwise keep things general.

Let us start by building some intuition behind the radically different behavior exhibited by the transverse and longitudinal components discussed in 4.3.2 by taking a closer look at the corresponding field equations. It will be helpful to factor out the time dependence of V^μ, as follows

$$V^\mu(t, z) = v^\mu(z) e^{-i\omega t} , \tag{4.28}$$

[7] At the level of a Stückelberg theory, a discontinuity in the number of degrees of freedom (dof) occurs in the limit $m \to 0$, with 2 vs 3 physical polarizations at either side of the interface. The fact that $R_l \to 1$ as $m \to 0$ in eq. (4.26) reflects the observation that the longitudinal mode would be unphysical in the region $z < 0$, and therefore must not propagate into the region $z > 0$. In an Abelian Higgs UV-completion, the number of dof of course stays continuous, with the would-be longitudinal accounted for by the appropriate linear combination of the two real dof of the complex Higgs. The physical dof are two transverse modes and the suitable combination of the real scalars, and therefore the treatment presented in this section is not applicable in the massless regime. Scattering with $m = 0$ has been studied long ago, e.g. [162]. As emphasized in the Introduction, and in section 4.5.1, we instead focus on cases where (in the Abelian Higgs language) the Higgs vev is 'on' on both sides of the wall.

[8] See section 4.6.3 for an alternative derivation of eq. (4.26) making use the of Goldstone nature of longitudinals at high energies.

and instead focus on the behavior of the $v^\mu(z)$. As we discussed previously, the equations of motion for the transverse modes read $(\Box + m_V^2(z))V_\perp^\mu = 0$. In terms of the v^μ, this can be written as

$$\left(\partial_z^2 + k_z^2\right) v_\perp^\mu(z) = \Delta m_V^2(z)\, v_\perp^\mu(z) \ , \tag{4.29}$$

with $k_z^2 = \omega^2 - m^2$. The transverse components obey a Schrödinger-like equation for a particle moving in one dimension with "energy" k_z^2 in the presence of a potential $U_\perp(z) = \Delta m_V^2(z)$. In the $L \to 0$ limit, our problem reduces to one-dimensional quantum mechanical scattering on a step potential, with energies above the step. Indeed, eq. (4.23) is just the reflection probability for this classic problem.

On the other hand, the Schrödinger equation governing the behavior of the longitudinal component reads

$$\begin{aligned} \left(\partial_z^2 + k_z^2\right) \lambda(z) &= U_l(z)\lambda(z) \\ \text{with} \qquad U_l(z) &= \Delta m_V^2(z) + \frac{3}{4}\left(\frac{\partial_z m_V^2(z)}{m_V^2(z)}\right)^2 - \frac{1}{2}\frac{\partial_z^2 m_V^2(z)}{m_V^2(z)} \ , \end{aligned} \tag{4.30}$$

where we have defined

$$\lambda(z) \equiv \frac{m_V(z)}{\omega} v_l^3(z) \qquad \text{such that} \qquad \lambda(z) \to \begin{cases} e^{ik_z z} + r_l e^{-ik_z z} & \text{for} \quad z \ll -L \\ t_l e^{i\tilde{k}_z z} & \text{for} \quad z \gg +L \end{cases} . \tag{4.31}$$

The effective scattering potential for the longitudinal component, $U_l(z)$, depends on the length scale over which the mass changes not just through the choice of mass profile but through its derivatives – much unlike its transverse counterparts. It is this crucial difference that leads to the strikingly different behavior of longitudinal and transverse modes.

In the relativistic limit, $k_z \simeq \omega \gg m$, we might neglect the first term in $U_l(z)$. The derivative terms in the effective potential are localized in a region of thickness $\sim L$, and the second-derivative term is dominant whenever $\Delta m^2/m^2$ is tiny. We then have

$$U_l(z) \simeq -\frac{1}{2}\left(\frac{\partial_z^2 m_V^2(z)}{m_V^2(z)}\right) \simeq -\frac{\Delta m^2}{2m^2}\Theta_L''(z) \ . \tag{4.32}$$

The step-function limit discussed in the previous subsection corresponds to $\Theta_L''(z) \xrightarrow{L\to 0} \delta'(z)$, and eq. (4.30) reduces to the Schrödinger equation in a potential $U_l(z) = -\frac{\Delta m^2}{2m^2}\delta'(z)$. Solving this equation subject to the appropriate boundary conditions, one indeed recovers the result of eq. (4.26) to leading order in the ratio $\Delta m^2/m^2$, as we summarize in appendix 4.6.1.

Since the longitudinal reflection coefficient in the relativistic regime is $R_l \ll 1$ whenever the change in the dark photon mass is tiny, we can go further and leverage the one-dimensional Born approximation familiar from quantum mechanics to obtain an analytic expression for the reflection probability in the case of a smoothly varying mass. As we summarize in appendix 4.6.2, the Born approximation to the longitudinal reflection coefficient can be written in closed form in terms of the effective scattering potential in eq. (4.30) as

$$R_{l,\,\mathrm{Born}} = \frac{1}{4k_z^2}\left|\int_{-\infty}^{\infty} dz\; e^{2ik_z z}\; U_l(z)\right|^2 \;. \tag{4.33}$$

Plugging eq. (4.32) into eq. (4.33) and integrating by parts, we find

$$\begin{aligned} R_{l,\,\mathrm{Born}} &\simeq \frac{1}{4k_z^2}\left(\frac{\Delta m^2}{2m^2}\right)^2 \left|\Big[e^{2ik_z z}\;\Theta_L'(z)\Big]_{-\infty}^{+\infty} - 2ik_z\int_{-\infty}^{\infty} dz\; e^{2ik_z z}\;\Theta_L'(z)\right|^2 && (4.34)\\ &\simeq \left(\frac{\Delta m^2}{2m^2}\right)^2 \left|\int_{-L}^{L} dz\;\left(1+2ik_z z+\mathcal{O}(k_z^2 z^2)\right)\;\Theta_L'(z)\right|^2 && (4.35)\\ &= \left(\frac{\Delta m^2}{2m^2}\right)^2 \left(1+\mathcal{O}(k_z^2 L^2)\right)\;. && (4.36)\end{aligned}$$

To get the second line, we used that Θ_L' quickly vanishes for $|z| \gtrsim L$, and we Taylor expanded the exponential for $|k_z z| \ll 1$. Since Θ_L interpolates between 0 and 1, Θ_L' can be treated as a probability density function. With this interpretation, the integral in the second line is essentially an average of $1+2ik_z z$ over the region $(-L, L)$, weighted by this probability density. The average of $k_z z$ is bounded in magnitude by $k_z L$, giving the final line. Eq. (4.36) coincides with the step-function result of eq. (4.26) provided $k_z \simeq \omega \ll L^{-1}$, as expected. Moreover, it highlights how the existence of a kinematic regime where the longitudinal reflection coefficient stays nearly constant is in fact a generic feature of any smooth mass profile, lasting all the way up to $k_z \simeq \omega \sim L^{-1}$.

Given a specific profile, we can use eq. (4.33) to obtain an analytic approximation to the reflection probability. For example, for a wall profile of the familiar kink form

$$\Theta_L(z) = \frac{1}{4}\left[1+\tanh(z/L)\right]^2 \;, \tag{4.37}$$

one finds

$$R_{l,\,\mathrm{Born}} \simeq \left(\frac{\Delta m^2}{2m^2}\right)^2 \frac{\pi^2 (k_z L)^2\left[1+(k_z L)^2\right]}{\sinh^2(\pi k_z L)} \;. \tag{4.38}$$

Eq. (4.38) reproduces the result of eq. (4.26) in the regime $\omega \simeq k_z \ll L^{-1}$, up to corrections of $\mathcal{O}(k_z^2 L^2)$, whereas in the ultra-relativistic limit it takes the form

$$R_{l,\,\text{Born}} \simeq \left(\frac{\Delta m^2}{2m^2}\right)^2 \times 4\pi^2 \,(k_z L)^4 \, e^{-2\pi k_z L} \qquad \text{for} \qquad k_z \simeq \omega \gg L^{-1} \,. \tag{4.39}$$

Indeed, the longitudinal reflection probability dies off exponentially fast – as expected – in the regime of ultra-relativistic motion.

The results of this subsection are best summarized in fig. 4.2, where we show the reflection probability for longitudinal and transverse vectors for the mass profile in eq. (4.37), obtained by numerically solving the corresponding equations of motion. As advertised, the longitudinal reflection coefficient features a plateau for γ-factors in the regime $1 \ll \gamma \ll (Lm)^{-1}$, which is well-approximated by the step-function result of eq. (4.26). The consequences of this behavior for the evolution of bubble walls are the topic of the next section.

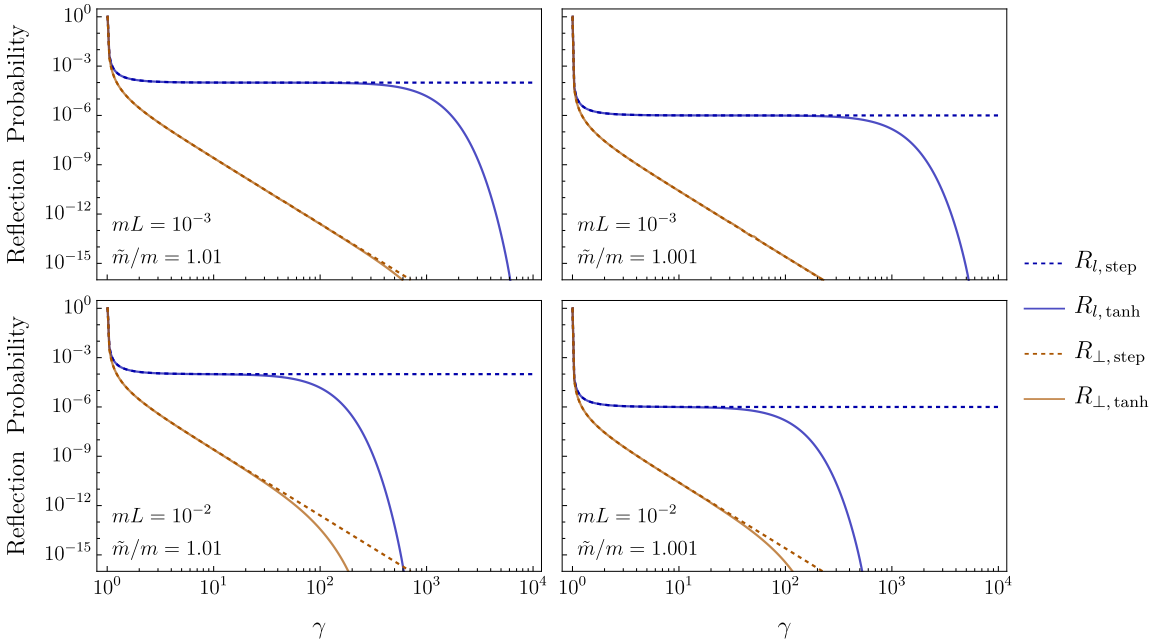

Figure 4.2: Reflection probability for longitudinal (blue) and transverse (orange) massive vectors scattering off a planar wall in the limit of normal incidence, as a function of the Lorentz γ-factor. The change in mass across the interface is 1% and 0.1% for the left and right panels respectively. Solid lines show numerical results for a smooth mass profile of the form $m_V^2(z) = m^2 + \Delta m^2 \Theta_L(z)$, with $\Theta_L(z)$ as in eq. (4.37). Dashed lines correspond to the step function results of eq. (4.23) and (4.26). As anticipated, the step-function analysis provides an excellent approximation up to $\gamma \sim (mL)^{-1}$.

4.4 Dark photon friction on bubble walls

We now discuss the implications of the results presented in section 4.3 for the dynamics of expanding vacuum bubbles in the early Universe. In section 4.4.1, we compute the pressure on an expanding wall due to the presence of dark photons, and argue that the requirement for run-away walls can be much stronger than previously believed. Section 4.4.2 focuses on the dynamics of bubble walls that reach an equilibrium regime as a result of longitudinal friction, including a self-consistent determination of the equilibrium γ-factor. Once in equilibrium, most of the energy released in the transition goes into making a fraction of the dark photons relativistic. The fate of this dark radiation depends sensitively on the size of self-interactions among the dark photons, as well as between the dark photons and particles in the thermal plasma, as we discuss in section 4.4.3. If interaction rates are negligible – an assumption more likely to hold if the sector undergoing vacuum decay is cold – we argue that the reflected dark photons accumulate in a thin "shell" of dark radiation surrounding the expanding bubbles. If they remain relativistic until late times, their contribution to $\Delta N_{\rm eff}$ could be observable for phase transitions with strength $\alpha \sim 10^{-2} - 10^{-1}$. Alternatively, if the scalar sector is in equilibrium with the thermal plasma, interactions between the reflected dark photons and ϕ particles can easily be efficient, in which case the energy density in dark radiation gets transferred instead into the thermal fluid.

4.4.1 Maximum Dynamic Pressure

It is helpful to rearrange eq. (4.10) using the relationship $T_\lambda = 1 - R_\lambda$, as follows:

$$\mathcal{P} = \gamma|\vec{v}|n_V \left\{ \frac{1}{3}R_l(k_z + \tilde{k}_z) + (k_z - \tilde{k}_z) + \frac{2}{3}R_\perp(k_z + \tilde{k}_z) \right\} . \tag{4.40}$$

In the relativistic limit, $k_z + \tilde{k}_z \simeq 2\gamma m$ and $k_z - \tilde{k}_z \simeq \Delta m^2/(2\gamma m)$, and eq. (4.40) reads

$$\mathcal{P} \simeq \frac{2}{3}\gamma^2 \rho_V R_l + \rho_V \frac{\Delta m^2}{2m^2} + \frac{4}{3}\gamma^2 \rho_V R_\perp \qquad \text{for} \qquad \gamma \gg 1 . \tag{4.41}$$

The second term above is just the asymptotic contribution of eq. (4.11). The last term corresponds to reflections of transverse modes. As discussed around eq. (4.23), $R_\perp \propto \gamma^{-4}$ already in the inter-relativistic regime, and therefore this third term falls off as γ^{-2} for large γ. In contrast, the peculiar behavior of the longitudinal reflection probability, R_l, which stays approximately constant in the region of inter-relativistic motion, leads to a contribution to the overall pressure on the expanding interface that

grows $\propto \gamma^2$. In total, neglecting the last term above and substituting the expression for R_l appropriate in the inter-relativistic regime (remember eq. (4.26)), we have:

$$\mathcal{P} \simeq \underbrace{\frac{2}{3}\gamma^2 \rho_V \left(\frac{\Delta m^2}{2m^2}\right)^2}_{\text{longitudinal reflections}} + \underbrace{\rho_V \frac{\Delta m^2}{2m^2}}_{\mathcal{P}_\infty} \qquad \text{for} \qquad 1 \ll \gamma \ll (mL)^{-1} \ . \tag{4.42}$$

We emphasize that this γ^2-growing pressure is a transient phenomenon that is only present for γ-factors within the range indicated in eq. (4.42). Once $\gamma \gg (mL)^{-1}$, the longitudinal reflection probability dies off exponentially fast, leaving the second term above as the sole significant contribution to the overall pressure.

A consequence of our previous discussion is that the pressure exerted on the expanding interface will reach a maximum near the end of the inter-relativistic regime, before dropping down to $\mathcal{P}_\infty \simeq \rho_V \times \Delta m^2/2m^2$ in the ultra-relativistic limit. As advertised in the Introduction, we will refer to this pressure peak as Maximum Dynamic Pressure. Parametrically, it is given by

$$\mathcal{P}_{\rm mdp} \simeq \frac{2}{3}\gamma_{\rm max}^2 \rho_V R_l + \rho_V \frac{\Delta m^2}{2m^2} \sim \frac{\rho_V}{(Lm)^2}\left(\frac{\Delta m^2}{2m^2}\right)^2 + \rho_V \frac{\Delta m^2}{2m^2} \ , \tag{4.43}$$

where $\gamma_{\rm max} \sim (mL)^{-1}$ is the value of γ at Maximum Dynamic Pressure. As a result, for bubble walls to become run-away, the following condition must be satisfied:

$$\text{Run-away criterion:} \qquad \Delta V > \mathcal{P}_{\rm mdp} \qquad \text{(this work)} \ . \tag{4.44}$$

Eq.(4.44) replaces eq. (4.3) as a diagnostic of run-away bubble walls in the presence of phase-dependent massive dark photons in transitions with access to the regime of inter-relativistic motion, and is a primary new result of this work.

If the first term in eq. (4.43) is a small correction on top of the asymptotic pressure, $\mathcal{P}_\infty$, the effect of longitudinal mode reflections will be largely irrelevant to describe the dynamics of the expanding bubbles. However, if the first term dominates then eq. (4.44) can be much stronger than the requirement $\Delta V > \mathcal{P}_\infty$ quoted in eq. (4.3). Parametrically, the effect of longitudinal reflections will dominate the overall pressure on the expanding interface provided

$$mL \ll \sqrt{\frac{\Delta m^2}{m^2}} \ . \tag{4.45}$$

When $\Delta m^2/m^2 \ll 1$, this is a stronger requirement than the condition in eq. (4.5) for the inter-relativistic regime to be accessible, although the main feature in both cases

is that there must be a significant hierarchy between the mass of the dark photon and the energy scale L^{-1} characterizing the thickness of the bubble wall.

Our discussion thus far has only been concerned with the pressure due to a population of cold dark photons. If the sector undergoing the transition is cold, such that vacuum decay proceeds via quantum tunneling and there is no thermal plasma that interacts with the bubble walls, this will be a good approximation to the overall pressure. Alternatively, if the scalar sector is in equilibrium with the thermal fluid, an additional source of pressure will be present due to interactions between the plasma and the wall. As mentioned in the Introduction, particles in the plasma that gain mass across the wall contribute as $\mathcal{P}_\infty \sim \Delta m^2 T^2$ in the relativistic limit [145]. In perturbative theories this source of friction can easily fall below ΔV, and therefore won't be large enough to obstruct the acceleration of the bubble walls. Potentially more significant are those cases where the phase transition sector features gauge bosons that acquire a mass as they cross the wall. As anticipated in section 4.1, this can lead to an additional source of pressure from the transition radiation emitted as charged particles cross the interface, of the form $\mathcal{P}_\infty \sim \gamma g^2 \Delta m_v T^3$ [147, 148, 152]. For this source of friction to be subdominant to that from longitudinal dark photons, one would need

$$\gamma_{\rm eq} g^2 \Delta m_v T_*^3 \lesssim \Delta V \ . \tag{4.46}$$

This condition can be interpreted as an upper bound on T_* relative to the typical energy scale of the phase transition. Parametrically, taking for simplicity $\Delta V \sim v^4$ and $\Delta m_v \sim gv$, we find

$$\frac{T_*}{v} \lesssim \frac{1}{g\,\gamma_{\rm eq}^{1/3}} \tag{4.47}$$

$$\sim 10^{-3} \left(\frac{1}{g}\right) \left(\frac{\Delta m^2/m^2}{10^{-4}}\right)^{1/3} \left(\frac{10^{-2}}{\alpha}\right)^{1/6} \left(\frac{100\ \text{GeV}}{T_*}\right)^{1/6} \left(\frac{\rho_{\rm dm}}{\rho_V}\right)^{1/6} \ . \tag{4.48}$$

If the relevant gauge couplings are $g = \mathcal{O}(1)$ – as in the Standard Model – then neglecting transition radiation would require $T_* \ll v$, i.e. the transition needs to be significantly super-cooled. More generally, in hidden sectors where the relevant gauge couplings are $g \ll 1$, the above condition could be satisfied even within 'standard' thermal transitions where $T_* \sim v$. A more comprehensive analysis of the class of thermal transitions for which this assumption holds is an interesting direction for future investigation.

Fig. 4.3 shows the pressure on an expanding interface due to massive dark photons, relative to its asymptotic value in the limit $\gamma \to \infty$, in cases where the inter-relativistic

kinematic regime identified in eq. (4.5) is accessible during the wall's expansion. The evolution of bubble walls that fail the run-away condition of eq. (4.44) as a result of longitudinal friction is the topic to which we now turn.

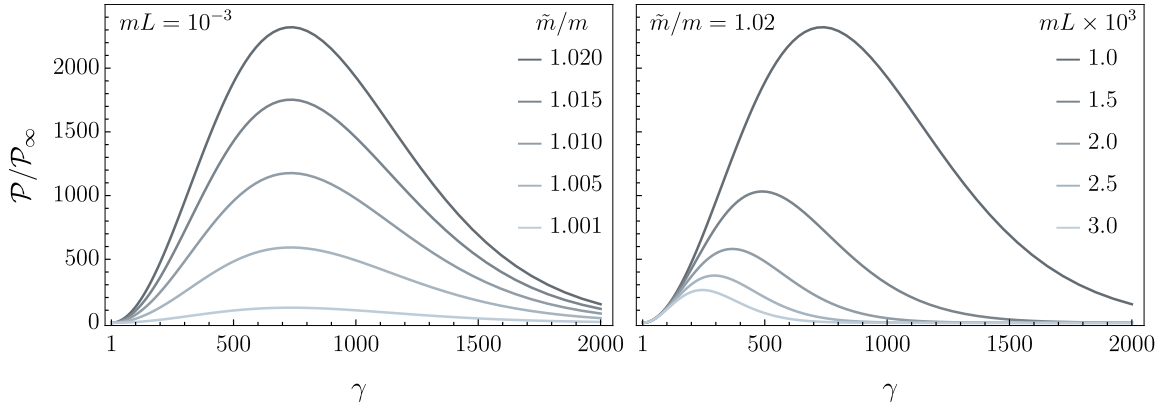

Figure 4.3: The pressure exerted by massive dark photons on an expanding bubble wall can feature a non-monotonic dependence on the wall γ-factor due to reflections of longitudinal modes, reaching a peak at $\gamma \sim (mL)^{-1}$ that is potentially much larger than its asymptotic value in the ultra-relativistic limit. The criterion for run-away bubble walls can therefore be far stronger than simply requiring $\Delta V > \mathcal{P}_\infty$, as discussed around eq. (4.44). **Left:** increasing the relative change in the dark photon mass raises the Maximum Dynamic Pressure without significantly altering its position. **Right:** decreasing the wall thickness increases *both* the height and position of the MDP. This behavior is in qualitative agreement with the discussion in and around eq. (4.43). Both plots have been obtained by evaluating eq. (4.40) after numerically obtaining reflection coefficients corresponding to the smooth wall profile of eq. (4.37).

4.4.2 Equilibrium γ-factor and energy budget

If the Maximum Dynamic Pressure is dominated by the reflection of longitudinal modes, and the run-away criterion of eq. (4.44) is not satisfied, then bubble walls will reach an equilibrium regime once $\mathcal{P}(\gamma_{\rm eq}) \simeq \Delta V$. Parametrically, the equilibrium γ-factor is given by

$$\gamma_{\rm eq} \simeq \left(\frac{3\Delta V}{2\rho_V R_l}\right)^{1/2} \tag{4.49}$$

$$\sim 10^9 \left(\frac{10^{-4}}{\Delta m^2/m^2}\right)\left(\frac{\alpha}{10^{-2}}\right)^{1/2}\left(\frac{T_*}{100\ \text{GeV}}\right)^{1/2}\left(\frac{\rho_{\rm dm}}{\rho_V}\right)^{1/2} . \tag{4.50}$$

How easy is it for bubble walls to reach an equilibrium regime as a result of longitudinal reflections? An obvious self-consistency condition on our determination

of $\gamma_{\rm eq}$ in eq. (4.49) is that it lies below the γ-factor at Maximum Dynamic Pressure, i.e.

$$\gamma_{\rm eq} \lesssim \frac{1}{mL} \ . \tag{4.51}$$

Additionally, a "kinematic" condition is that the expanding walls reach equilibrium *before* the bubble walls collide and the phase transition ends. The bubble radius at collision is set by the Hubble scale at the epoch of the phase transition. Demanding that the size of the expanding bubbles at the onset of the equilibrium regime is a fraction $x < 1$ of the Hubble radius, we find

$$R_{\rm eq} \simeq \gamma_{\rm eq} R_0 \lesssim x H(T_*)^{-1} \qquad \Rightarrow \qquad \gamma_{\rm eq} \lesssim \frac{x}{R_0 H(T_*)} \ , \tag{4.52}$$

where R_0 is the critical bubble radius.

Eq.(4.51) and (4.52) can be interpreted in various ways, but perhaps the most relevant for us is to regard them as *lower bounds* on the fractional change of the dark photon mass for the effect of longitudinal pressure to be large enough to stop the acceleration of the bubble walls, as follows:

$$\frac{\Delta m^2}{m^2} \gtrsim \left(\frac{\Delta m^2}{m^2}\right)_{\rm min} \equiv 2\left(\frac{3\Delta V}{2\rho_V}\right)^{1/2} \times \ {\rm Max}\left\{mL,\, x^{-1} R_0 H(T_*)\right\} \ . \tag{4.53}$$

This is illustrated in fig. 4.4, where we show contours of $\sqrt{(\Delta m^2/m^2)_{\rm min}}$ for various choices of the underlying parameters, as described in the caption. As can be seen in fig. 4.4, even extremely small changes in the mass of the dark photon across the interface can cause enough friction to halt the acceleration of the bubble walls.

After the bubble walls reach an equilibrium speed, they carry a decreasing fraction of the total energy available in the transition:

$$\frac{E_{\rm wall}}{E_{\rm total}} \simeq \frac{4\pi R(t)^2 \gamma_{\rm eq} \sigma}{\frac{4\pi}{3} R(t)^3 \Delta V} \sim \frac{\gamma_{\rm eq}\sigma}{\Delta V \, R(t)} \ , \tag{4.54}$$

where $R(t)$ is the bubble radius at time t. As $R(t)$ grows, $E_{\rm wall}/E_{\rm total}$ quickly becomes tiny. By comparison, the above ratio is identically 1 for transitions in vacuum, where all the available energy goes into accelerating the bubble walls [125]. In thermal transitions where the walls reach an equilibrium speed due to friction from the thermal plasma, most of the available energy goes instead into producing motion in the form of sound waves or hydrodynamic turbulence, as mentioned in the Introduction and summarized in [114,115]. In the case at hand, as we will now show, the energy released in the transition goes instead into accelerating a fraction of the dark photons, turning them into dark radiation.

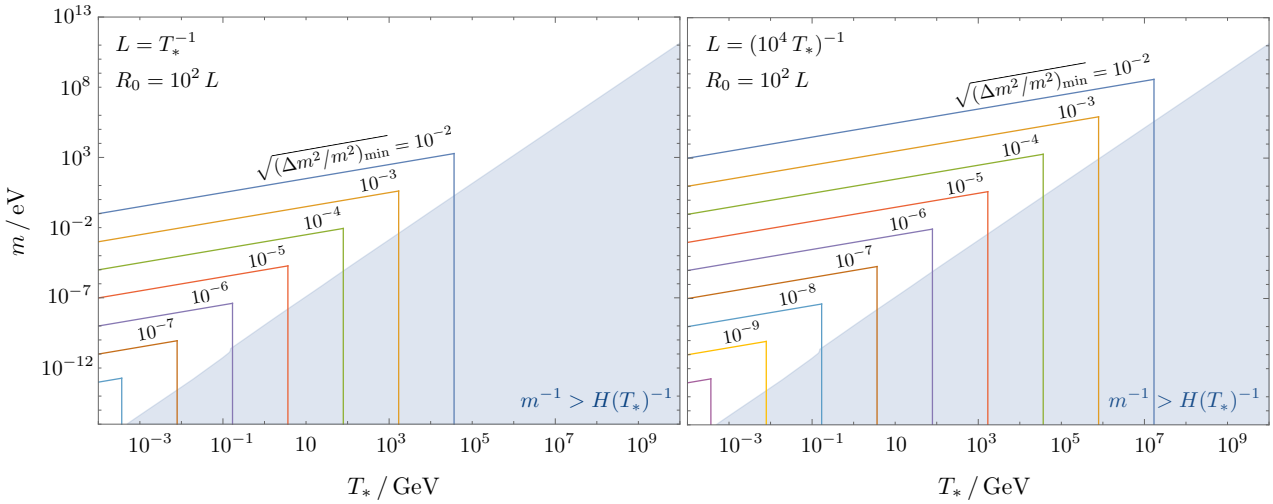

Figure 4.4: Contour lines indicating the lower bound on the fractional change of the dark photon mass for longitudinal reflections to create enough friction to halt the acceleration of the bubble walls. These contours saturate the inequality in eq. (4.53), with the choice $x = 10^{-1}$ for illustration. The energy density in cold dark photons is taken to be that of the dark matter, and the difference in energy densities, ΔV, is taken to be 1% of that in the Standard Model bath (i.e. $\alpha = 10^{-2}$ in eq. (4.6)). The blue shaded area corresponds to dark photon masses such that the corresponding Compton wavelength exceeds the Hubble radius, $m^{-1} > H(T_*)^{-1}$ – a regime that lies outside the validity of our discussion. **Left:** The wall thickness is related to the temperature of the thermal plasma at the phase transition epoch as $L = T_*^{-1}$, as expected in a 'standard' thermal transition. **Right:** $L = (10^4\, T_*)^{-1} \ll T_*^{-1}$, as could be the case if the phase transition took place within a cold hidden sector with a characteristic energy scale $\gg T_*$, or for a thermal transition featuring significant super-cooling (recall discussion below eq. (4.7)).

In the rest frame of the bubble wall, reflected longitudinal modes propagate away from the interface with Lorentz-factor $\gamma_{\rm eq}$, while in the rest frame of the dark photons far away from the wall – loosely, the rest frame of the dark matter – the γ-factor of the reflected dark photons is given by

$$\gamma_{\rm dr} = \frac{1 + |\vec{v}_{\rm eq}|^2}{1 - |\vec{v}_{\rm eq}|^2} \simeq 2\gamma_{\rm eq}^2 \gg \gamma_{\rm eq} \ . \tag{4.55}$$

Within a Hubble volume, the average number density of dark photons that become relativistic as the bubble walls sweep across the dark matter from the onset of the equilibrium regime until the bubbles collide can be approximated by

$$\langle n_{\rm dr} \rangle \simeq \frac{1}{3} R_l n_V \left(1 - \frac{R_{\rm eq}^3}{R_{\rm coll}^3}\right) \ . \tag{4.56}$$

The factor in parenthesis takes care of the fact that we are only interested in keeping track of the fraction of dark matter that gets converted into dark radiation dur-

ing equilibrium (before, most of the energy released as the bubbles grow goes into accelerating the bubble walls). Obviously, if the bubble walls only reach equilibrium right before they collide, $R_{\rm eq} \approx R_{\rm coll}$, then $\langle n_{\rm dr} \rangle$ will be correspondingly tiny. However, provided the onset of equilibrium takes place well before collision, then $\langle n_{\rm dr} \rangle \simeq \frac{1}{3} R_l n_V$. For example, taking $R_{\rm eq} \simeq \gamma_{\rm eq} R_0$ and $R_{\rm eq} \simeq x H(T_*)^{-1}$, we find $R_{\rm eq}^3 / R_{\rm coll}^3 \sim 10^{-15} \ll 1$, where we have evaluated all parameters as in eq. (4.50), and for illustration we have taken $x = 10^{-2}$ as well as $R_0^{-1} = T_* = 100$ GeV. More generally, notice that having $R_{\rm eq} \lesssim R_{\rm coll}$ is a requirement for dark photon reflections to affect significantly the evolution of the bubble walls (as per our discussion around eq. (4.50)), and so we proceed under this assumption.

Right after bubble walls collide, the volume-averaged energy density in dark radiation is therefore

$$\rho_{\rm dr} = \omega_{\rm dr} \langle n_{\rm dr} \rangle \simeq \frac{2}{3} \gamma_{\rm eq}^2 R_l \rho_V \qquad \text{at} \qquad T \sim T_* \,, \tag{4.57}$$

where $\omega_{\rm dr} = \gamma_{\rm dr} m$ and $\gamma_{\rm dr}$ is given in eq. (4.55). Notice the right-hand-side above is equal to ΔV by eq. (4.49) – consistent with energy conservation in the rest frame of the dark matter. Thus, in phase transitions where bubble walls reach an equilibrium regime as a result of friction from the dark photons, most of the difference in vacuum energy densities goes into turning a fraction of the (cold) dark photons into dark radiation.

4.4.3 Fate of the dark radiation

The fate of the reflected dark photons depends sensitively on the values of the various underlying parameters. As a result, general statements about the later evolution of the dark radiation are not possible, and a comprehensive study spanning all available parameter space is well beyond the scope of this work. Instead, we will focus on highlighting the possible outcomes given certain assumptions.

Although sweeping statements are not possible, there are two qualitatively different cases that merit separate consideration, depending on whether the sector undergoing vacuum decay is part of the thermal plasma or belongs in a cold hidden sector such that the transition proceeds via quantum tunneling. We will focus on the cold scenario first. In this case, the absence of a thermal population of particles that will interact with the wall background leaves the dark photons as the sole source of pressure on the expanding interface, and the evolution of the dark radiation as the bubbles grow and after they collide depends primarily on the strength of the self-interactions among the dark photons. As discussed in section 4.5.1, quartic

dark photon self-interactions are generally part of the low energy theory, and in the context of an Abelian Higgs UV-completion the relevant quartic coupling is as given in eq. (4.68). Interactions among the dark radiation and the cold dark photons occur at a center-of-mass energy $\sqrt{s}/2 \simeq \gamma_{\rm eq} m$, which always fall below the cutoff scale of the effective theory. In this kinematic regime, the relevant cross section is as given in eq. (4.72), and one finds that the corresponding interaction rate can be tiny compared to $H(T_*)$ across significant portions of parameter space.

When interactions between the dark matter and the reflected dark photons are negligible, the following picture emerges. Going back to eq. (4.55), notice that (in the dark matter frame) the speed of the dark radiation is ever-so-slightly larger than the speed of the bubble wall:

$$\Delta v_{\rm dr} \equiv |\vec{v}_{\rm dr}| - |\vec{v}_{\rm eq}| = |\vec{v}_{\rm eq}| \frac{1 - |\vec{v}_{\rm eq}|^2}{1 + |\vec{v}_{\rm eq}|^2} \simeq \frac{|\vec{v}_{\rm eq}|}{2\gamma_{\rm eq}^2} \ll 1 \ . \tag{4.58}$$

As a result, from the beginning of the equilibrium regime until the moment of bubble wall collisions, reflected dark photons become uniformly distributed on a shell of thickness ΔL in front of the interface, with

$$\Delta L \sim \Delta v_{\rm dr} \times \Delta t \simeq \frac{|\vec{v}_{\rm eq}| \Delta t}{2\gamma_{\rm eq}^2} \lesssim \frac{R_{\rm coll}}{2\gamma_{\rm eq}^2} \ll R_{\rm coll} \ , \tag{4.59}$$

where Δt refers to the time interval between when equilibrium is reached and collision of the bubble walls, and we have used $|\vec{v}_{\rm eq}| \Delta t \lesssim R_{\rm coll}$. Thus, as the bubbles grow bigger, a shell of dark radiation forms, moving ever-so-slightly in front of the bubble walls. Although the walls move at constant speed, most of the energy density remains localized in a thin layer close to the surface of the expanding bubbles.

The fate of these shells of radiation depends on the interactions between relativistic dark photons as the bubble walls meet. Now, the relevant center-of-mass-energy is $\sqrt{s}/2 \sim \omega_{\rm dr} \simeq 2m\gamma_{\rm eq}^2$, and interactions are often well-described within the high energy Goldstone regime of eq. (4.74). To estimate the interaction rate, notice that although the average number density of dark radiation is well-approximated by $\langle n_{\rm dr} \rangle \simeq \frac{1}{3} R_l n_V$, the distribution of relativistic dark photons is highly inhomogeneous, with $n_{\rm dr} \sim \langle n_{\rm dr} \rangle H^{-1}/\Delta L \gg \langle n_{\rm dr} \rangle$ in a thin shell surrounding the bubble walls and zero elsewhere. This cross section defines a mean-free-path $\lambda_{\rm mfp} = (\sigma n_{\rm dr})^{-1}$. Comparing this length scale to the typical thickness of one of these shells we find, e.g.

$$\frac{\lambda_{\rm mfp}}{\Delta L} \sim \frac{10^8}{\lambda_\Phi^2} \left(\frac{m}{1 \text{ eV}}\right)^3 \left(\frac{10^{-4}}{\Delta m^2/m^2}\right)^6 \left(\frac{T_*}{100 \text{ GeV}}\right) \left(\frac{\alpha}{10^{-2}}\right)^2 \left(\frac{\rho_{\rm dm}}{\rho_V}\right)^3 \ . \tag{4.60}$$

The above expression has a strong dependence on a number of parameters, especially the fractional change in the mass of the dark photon. But interestingly it can remain $\gg 1$ in a large region of the relevant parameter space where longitudinal reflections are relevant to the evolution of the bubble walls. In this case, the shells of dark radiation will pass each other without significant dissipation, a process that could last for much longer than the usual duration of a cosmological phase transitions. The long-lasting motion of these shells could greatly enhance the strength of the gravitational wave signal, a possibility that motivates more careful exploration of this potential new source of gravitational waves. We will return to this topic in future work.

Moreover, it is interesting to consider the limiting possibility that the reflected dark photons remain relativistic long after the phase transition is over, leading to a dark radiation signal. Making the optimistic assumption that significant losses to gravitational radiation and other "inelastic" processes can be ignored, the requirement that the reflected dark photons remain relativistic at temperatures $T \leq T_*$ can be written as:

$$\gamma_{\rm dr}(T \leq T_*) \simeq 2\gamma_{\rm eq}^2 \frac{a(T_*)}{a(T)} \approx 2 \times 10^{13} \left(\frac{10^{-4}}{\Delta m^2/m^2}\right)^2 \left(\frac{\alpha}{10^{-2}}\right) \left(\frac{\rho_{\rm dm}}{\rho_V}\right) \left(\frac{T}{1\ {\rm MeV}}\right) \gtrsim 1\ . \tag{4.61}$$

Of particular interest are the temperatures of Big Bang Nucleusynthesis ($T_{\rm BBN} \sim$ 1 MeV) and recombination ($T_{\rm rec} \sim 1$ eV), when $\Delta N_{\rm eff}$ bounds exist. As can be inferred from eq. (4.61), this is easily the case provided α is not too tiny. When this is the case, the corresponding contribution to $\Delta N_{\rm eff}$ can be written as

$$\Delta N_{\rm eff} = \frac{8}{7}\left(\frac{11}{4}\right)^{4/3} \left(\frac{\rho_{\rm dr}(T_*)}{\rho_{\gamma,0}}\right) \left(\frac{a(T_*)}{a(T_0)}\right)^4 \tag{4.62}$$

$$\simeq 1.4 \left(\frac{\alpha}{0.1}\right) \frac{g_*(T_*)}{g_{*,s}(T_*)^{4/3}} \tag{4.63}$$

$$\simeq 0.3 \left(\frac{\alpha}{0.1}\right) \left(\frac{g_*(100\ {\rm GeV})}{g_*(T_*)}\right)^{1/3}\ , \tag{4.64}$$

where $\rho_{\gamma,0}$ refers to the current energy density in (Standard Model) photons. In the first step above we have used $\rho_{\rm dr}(T_*) \simeq \Delta V$, as discussed around eq. (4.56)-(4.57), and in the final step we have ignored the difference between $g_{*,s}(T_*)$ and $g_*(T_*)$. Interestingly, phase transitions with $\alpha \sim 10^{-1}$ would already be probed by current $\Delta N_{\rm eff}$ constraints – though we emphasize that this is under the assumption that the highly relativistic dark photons suffer no significant energy loss since the time of the

phase transition other than redshift due to Hubble expansion. Under this assumption, fig. 4.5 shows the prediction for $\Delta N_{\rm eff}$ as a function of the characteristic temperature of the phase transition, for various values of α. Strong phase transitions with $\alpha > 0.1$ would be probed by current measurements, while weaker transitions with $\alpha \gtrsim 10^{-2}$ could be probed by CMB-Stage 4 observations [163]. Because bubble acceleration is

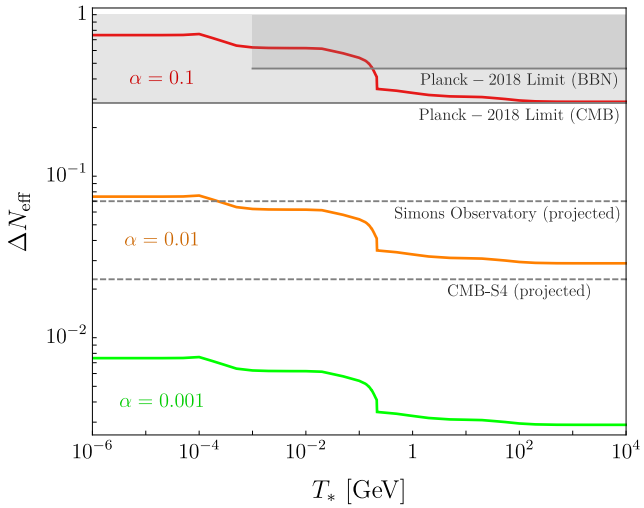

Figure 4.5: In phase transitions where bubble walls reach an equilibrium regime as a result of dark photon reflections, most of the difference in vacuum energy densities goes into turning a fraction of the (cold) dark photons into dark radiation. If the dark radiation remains relativistic until late times, an observable contribution to $\Delta N_{\rm eff}$ is possible. Plotted are the maximum possible contributions to $\Delta N_{\rm eff}$, as discussed in the main text, as a function of the thermal plasma at the epoch of the transition, T_*. Solid gray lines correspond to current bounds [17], and dashed gray lines show the projected sensitivities of upcoming observatories [163, 164].

stalled by the reflection of particles, this effect is a particularly efficient manner of converting the latent heat of the false vacuum to relativistic matter, thus leading to a significant contribution to $\Delta N_{\rm eff}$ if the reflected particles remain relativistic until late times. When instead bubbles of the new phase are run-away or reach a terminal velocity by dispersing energy into the thermal plasma, only the resulting stochastic background of gravitational waves contributes towards dark radiation, and $\Delta N_{\rm eff}$ is a less important observable.

The second scenario highlighted early on in this subsection corresponds to the case where the phase transition sector is in equilibrium with the thermal plasma. In this case, the reflected dark photons will also interact with the population of ϕ's in the thermal fluid via eq. (4.8) (or its UV-complete version, as described in section 4.5.1). Interactions take place at center-of-mass energies $\sqrt{s}/2 \sim \sqrt{2\,T_*\,\omega_{\rm dr}}/2 \simeq \gamma_{\rm eq}\sqrt{m\,T_*}$,

and the corresponding cross section is well-approximated by eq. (4.75) or eq. (4.76) depending on whether $\sqrt{s}$ falls above or below the cutoff scale of the effective theory. As discussed in section 4.5.2, the corresponding interaction rate can be well above $H(T_*)$, although once more this depends sensitively on the values of the underlying parameters. At any rate, interactions between the reflected dark photons and the thermal plasma provide an additional obstacle for the dark radiation to propagate undisturbed. It is therefore more likely that the energy density in the dark radiation gets distributed within the primordial plasma, in which case the main source of gravitational radiation would come from motion within the thermal fluid, similar to the case of phase transitions that reach an equilibrium regime as a result of thermal pressure.

Determining more precisely under what circumstances the reflected dark photons remain relativistic until late times, and therefore contribute to $\Delta N_{\rm eff}$, is an important question worthy of further attention.

4.5 Beyond the effective theory

In this section, we briefly discuss how the effective Lagrangian of eq. (4.7)-(4.8) may arise from a more complete framework. Our goal is not to be exhaustive, but rather to identify the necessary features of underlying models giving rise to our effective theory.

4.5.1 Abelian Higgs UV-completion

The simplest UV-completion of eq. (4.7)-(4.8) can be written in terms of an Abelian Higgs model:

$$\mathcal{L}_{\rm UV} = -\frac{1}{4}F_{\mu\nu}F^{\mu\nu} + |D_\mu\Phi|^2 - V_\Phi(|\Phi|) + \frac{1}{2}(\partial_\mu\phi)^2 - V_\phi(\phi) \,+\, \frac{\eta}{2}\phi^2|\Phi|^2 \,, \qquad (4.65)$$

where $D_\mu\Phi \equiv (\partial_\mu - ig'V_\mu)\Phi$. Assuming a Higgs potential of the usual form: $V_\Phi(|\Phi|) = \lambda_\Phi/2(|\Phi^2| - v'^2/2)^2$, the corresponding radial mode gets a mass $m_\rho = \sqrt{\lambda_\Phi}v'$, whereas $m = g'v'$ is the mass of the dark photon. Integrating out the radial mode, one obtains a low energy effective theory featuring additional interactions among the light degrees of freedom. In particular, a term such as eq. (4.8) – repeated here for convenience – is generated at tree-level:

$$\mathcal{L} \supset \frac{\kappa}{2}\phi^2 V^\mu V_\mu \qquad \text{with} \qquad \kappa = \frac{\eta\, m^2}{m_\rho^2} = \frac{\eta g'^2}{\lambda_\Phi} \,. \qquad (4.66)$$

Notice in particular that the ratio $\Delta m^2/m^2$ is independent of g', and it is therefore controlled by a different set of parameters of the underlying model compared to the overall mass of the dark photon. In this context, the scale of UV-completion is $\Lambda = m_\rho$, which can be written as

$$m_\rho = \frac{\sqrt{\eta} v}{\sqrt{\Delta m^2/m^2}} \lesssim \frac{4\pi v}{\sqrt{\Delta m^2/m^2}} \ . \tag{4.67}$$

This reproduces our EFT expectation for the upper bound on the cutoff scale in eq. (4.9) subject to the perturbativity requirement $\eta \lesssim 16\pi^2$.

Of course, the low energy effective theory contains interactions among the light degrees of freedom beyond eq. (4.8). Of particular interest are self-interactions among the dark photons. Indeed, a quartic interaction is generated at tree-level, of the form

$$\mathcal{L} \supset \lambda_V (V_\mu V^\mu)^2 \qquad \text{with} \qquad \lambda_V \sim \frac{g'^4}{\lambda_\Phi} = \lambda_\Phi \frac{m^4}{m_\rho^4} \lll 1 \ . \tag{4.68}$$

Interactions among the dark photons, as well as between the dark photons and a potential population of ϕ particles in the thermal plasma, are relevant (i) to assess the extent to which our assumptions that the dark matter is cold and non-interacting are self-consistent, and (ii) to determine the evolution of the reflected dark photons, which is the topic of section 4.4.3. For convenience, we summarize the relevant interaction rates in the next section.

4.5.2 Interaction rates

At low momenta, eq. (4.68) leads to a self-interaction among the dark photons of the form

$$\sigma_{VV} \sim \frac{\lambda_V^2}{8\pi m^2} = \frac{\lambda_\Phi^2}{8\pi m_\rho^2} \left(\frac{m}{m_\rho}\right)^6 \qquad \text{for} \qquad |\vec{k}| \ll m \ . \tag{4.69}$$

The corresponding dark matter self-interaction rate is always tiny compared to the Hubble rate in the early Universe in the region of parameter space relevant to this work. Potentially more relevant are interactions between the dark photons and ϕ particles in the thermal fluid. In particular, processes of the form $V\phi \to V\phi$ could be efficient at transferring energy from the plasma to the dark matter, unless the corresponding interaction rates are tiny. The relevant cross section is of the form, parametrically:

$$\sigma_{V\phi} \sim \frac{\kappa^2}{8\pi T_*^2} \sim \frac{1}{8\pi T_*^2} \left(\frac{\Delta m^2}{m^2}\right)^2 \frac{m^4}{T_*^4} \ , \tag{4.70}$$

where $\kappa \simeq \Delta m^2/v^2$, as discussed below eq. (4.8), and we've taken $m_\phi \sim v \sim T_*$, which should be a good approximation at the epoch of the phase transition (barring a tiny quartic coupling for ϕ). Assuming a thermal population of ϕ particles, with number density $n_\phi \sim T_*^3$, we find

$$\frac{\Gamma_{V\phi}}{H(T_*)} \sim 10^{-39} \left(\frac{\Delta m^2/m^2}{10^{-4}}\right)^2 \left(\frac{m}{1\text{ eV}}\right)^4 \left(\frac{100\text{ GeV}}{T_*}\right)^5 . \tag{4.71}$$

Clearly, this ratio can be very small in much of the parameter space of interest (see left panel in fig. 4.4).

Let us know discuss interactions involving the (highly relativistic) reflected dark photons. These will be relevant in section 4.4.3 when we discuss the fate of the dark radiation, and for convenience we summarize the relevant results here. At large center-of-mass energies, i.e. $\sqrt{s} \gg m$, the two-to-two scattering cross section among the dark photons is dominated by the scattering of longitudinally-polarized vectors, and so it will be sufficient for our purposes to just consider the process $V_l V_l \to V_l V_l$. Two limiting kinematic regimes are of interest. In the region $m \ll \sqrt{s} \ll m_\rho$, the relevant cross section is of the form

$$\sigma_{ll} \sim \frac{\lambda_V^2}{8\pi s}\left(\frac{\sqrt{s}}{m}\right)^8 \sim \frac{\lambda_\Phi^2}{8\pi m_\rho^2}\left(\frac{\sqrt{s}}{m_\rho}\right)^6 \qquad \text{for} \qquad m \ll \sqrt{s} \ll m_\rho . \tag{4.72}$$

This will be relevant for scattering between the dark radiation and the cold dark photons, where the relevant center-mass-energy is given by $\sqrt{s}/2 \simeq \gamma_{\rm eq} m$. Comparing the relevant interaction rate to $H(T_*)$, we find

$$\frac{\Gamma_{ll}}{H(T_*)} \sim 10^{-12}\,\frac{\lambda_\Phi^2}{\eta^4}\left(\frac{m}{1\text{ eV}}\right)^5 \left(\frac{10^{-4}}{\Delta m^2/m^2}\right)^2 \left(\frac{T_*}{v}\right)^8 \left(\frac{100\text{ GeV}}{T_*}\right)^4 \left(\frac{\alpha}{10^{-2}}\right)^3 \left(\frac{\rho_{\rm dm}}{\rho_V}\right)^2 , \tag{4.73}$$

where we have evaluated the cross section at $\sqrt{s}/2 = \gamma_{\rm eq} m$, and substituted m_ρ as given in eq. (4.67). Notice that the ratio T_*/v could be $\ll\ll 1$ if the phase transition sector is cold and decoupled from the thermal plasma, as discussed below eq. (4.7), which would further suppress the above ratio. If instead $\sqrt{s} \gg m_\rho$ then the cross section must be computed in the complete theory of eq. (4.65), and we find

$$\sigma_{ll} \sim \frac{\lambda_\Phi^2}{8\pi s} \qquad \text{for} \qquad \sqrt{s} \gg m_\rho , \tag{4.74}$$

as expected by virtue of Goldstone Equivalence. This is the form of the cross section used in deriving eq. (4.60).

Another important class of interactions are those between the dark radiation and the ϕ particles in the plasma when the phase transition sector is thermal. In particular, if the process $V_l\phi \to V\phi$ happens efficiently, the energy density stored in the dark radiation would quickly become distributed among the thermal fluid, as discussed in section 4.4.3. The typical s-parameter is of the form $s \sim 2T_*\omega_{\rm dr}$. In the regime $\sqrt{s} \ll m_\rho$,

$$\sigma_{l\phi} \sim \frac{\kappa^2}{8\pi s}\left(\frac{\sqrt{s}}{m}\right)^4 \qquad \text{for} \qquad m \ll \sqrt{s} \ll m_\rho \ , \tag{4.75}$$

whereas in the high-energy limit $\sqrt{s} \gg m_\rho$,

$$\sigma_{l\phi} \sim \frac{\eta^2}{8\pi s} \qquad \text{for} \qquad \sqrt{s} \gg m_\rho \ . \tag{4.76}$$

As an example, if the there's a full thermal distribution of ϕ particles with $n_\phi \sim T_*^3$, then the relevant interaction rate, relative to $H(T_*)$ is given by

$$\frac{\Gamma_{l\phi}}{H(T_*)} \sim 10^8\,\eta^2\left(\frac{\Delta m^2}{m^2}\right)^2\left(\frac{1\text{ eV}}{m}\right)^2\left(\frac{100\text{ GeV}}{T_*}\right)^2\left(\frac{10^{-2}}{\alpha}\right)^2\left(\frac{\rho_V}{\rho_{\rm dm}}\right)^2 \ , \tag{4.77}$$

where we have used eq. (4.76) in obtaining $\Gamma_{l\phi}$, as appropriate given our choice of parameters on the right-hand-side. Clearly, interactions between the dark radiation and the thermal plasma can be very efficient in parts of the relevant parameter space but – again – this conclusion depends strongly on the choices of the various scales and couplings.

4.6 Reflection probability: supplemental material

In these sections additional details supplementing the discussion of 4.3 are included.

4.6.1 Scattering on a δ' potential

As anticipated in 4.3.3, the effective scattering potential for the longitudinal component in the limit of vanishing wall thickness takes the form

$$U_l(z) \xrightarrow{L\to 0} \kappa\,\delta'(z) \qquad \text{with} \qquad \kappa \equiv -\frac{\Delta m^2}{2m^2} \ , \tag{4.78}$$

and eq. (4.30) reads

$$(\partial_z^2 + k_z^2)\lambda(z) = \kappa\,\delta'(z)\lambda(z) \ . \tag{4.79}$$

We can obtain matching conditions for λ and λ' by integrating (twice) over this equation. First, integrating eq. (4.79) from $z_0 < 0$ to z, we find

$$\int_{z_0}^{z} d\hat{z}\, \left[(\partial_{\hat{z}}^2 + k_z^2)\lambda(\hat{z})\right] = \int_{z_0}^{z} d\hat{z}\, \kappa\, \delta'(\hat{z})\lambda(\hat{z}) \tag{4.80}$$

$$\Rightarrow \qquad \lambda'(z) - \lambda'(z_0) + k_z^2 \int_{z_0}^{z} d\hat{z}\, \lambda(\hat{z}) = \kappa\, \lambda(z)\delta(z) - \frac{\kappa}{2}\left[\lambda'(0^+) + \lambda'(0^-)\right]\Theta(z)\ . \tag{4.81}$$

Integrating eq. (4.81) from $z = -\epsilon$ to $z = +\epsilon$ and taking the limit $\epsilon \to 0$, we find:

$$\lambda(0^+) - \lambda(0^-) = -\frac{\kappa}{2}\left[\lambda(0^+) + \lambda(0^-)\right]\ . \tag{4.82}$$

Similarly, taking $z_0 = -\epsilon$ and $z = +\epsilon$ in eq. (4.81), with $\epsilon \to 0$, one finds:

$$\lambda'(0^+) - \lambda'(0^-) \simeq \frac{\kappa}{2}\left[\lambda'(0^+) + \lambda'(0^-)\right]\ , \tag{4.83}$$

where in the right-hand-side we have only kept terms of $\mathcal{O}(\kappa)$. From the last two equations, one finds $r_l \simeq \kappa$, and therefore

$$R_l \simeq \kappa^2 = \left(\frac{\Delta m^2}{2m^2}\right)^2\ , \tag{4.84}$$

in agreement with eq. (4.26) at leading order in $\kappa \ll 1$.

4.6.2 The Born approximation

In section 4.3.3, we found it convenient to recast the equations of motion for both transverse and longitudinal components as a one-dimensional Schrödinger equation, of the form

$$(\partial_z^2 + k_z^2)\psi(z) = U(z)\psi(z)\ , \tag{4.85}$$

with $U(z) \to U_l(z)$ and $\psi \to \xi$ for the longitudinal component (c.f. eq. (4.30)), and $U(z) \to U_\perp(z)$ and $\psi \to v_\perp^\mu$ for the transverse modes (c.f. eq. (4.29)). It is an important feature that the effective scattering potential vanishses in the limit $z \to -\infty$, as will become clear in due time.

As is well-known, it is possible to recast eq. (4.85) as an integral equation, as follows

$$\psi(z) = \psi_0(z) + \int_{-\infty}^{\infty} dz'\, G(z - z')U(z')\psi(z')\ , \tag{4.86}$$

where ψ_0 is any function satisfying the free particle equation, $\left(\partial_z^2 + k_z^2\right)\psi_0 = 0$, and $G(z)$ is a Green's function for the differential operator on the right-hand-side of eq. (4.85), i.e.

$$\left(\partial_z^2 + k_z^2\right)G(z) = \delta(z)\ . \tag{4.87}$$

It is straightforward to check that eq. (4.86) is equivalent to eq. (4.85) by applying $(\partial_z^2 + k_z^2)$ to both sides and using eq. (4.87). In order to solve for $G(z)$, note that for $z \neq 0$ eq. (4.87) is just the free particle equation. The matching conditions at $z = 0$ are that G must be continuous and G' must have unit jump. Putting this together, the solutions are

$$G(z) = \pm \frac{1}{2ik_z} e^{\pm ik_z|z|} \ , \tag{4.88}$$

up to addition of functions that satisfy the free particle equation. It turns out that we only need one of these two solutions: the one with the + sign.

To represent an incoming plane wave, we take $\psi_0(z) = e^{ik_z z}$. Then our integral equation is

$$\psi(z) = e^{ik_z z} + \frac{1}{2ik_z} \int_{-\infty}^{\infty} dz' \ e^{ik_z|z-z'|} \ U(z')\psi(z') \ . \tag{4.89}$$

So far, we have made no approximations. However, if the correction to the incoming wavefunction ψ_0 is small (meaning the reflection coefficient is tiny), then we can plug this equation for ψ into itself in the integral and truncate higher order terms, leaving

$$\psi(z) \simeq e^{ik_z z} + \frac{1}{2ik_z} \int_{-\infty}^{\infty} dz' \ e^{ik_z|z-z'|} \ U(z') e^{ik_z z'} \tag{4.90}$$

$$= e^{ik_z z} + \frac{e^{ik_z z}}{2ik_z} \int_{-\infty}^{z} dz' \ U(z') + \frac{e^{-ik_z z}}{2ik_z} \int_{z}^{\infty} dz' \ e^{2ik_z z'} \ U(z') \ . \tag{4.91}$$

We wish to extract a reflection probability from this 'first Born approximation'. To this end, consider the limit $z \to -\infty$. The second term above clearly vanishes, given that $U(z') \to 0$ as $z' \to -\infty$ as emphasized below eq. (4.85). Furthermore, the third term can be identified as the reflected plane wave piece, with associated probability

$$R_{l,\,\text{Born}} = \frac{1}{4k_z^2} \left| \int_{-\infty}^{\infty} dz \ e^{2ik_z z} \ U(z) \right|^2 \ . \tag{4.92}$$

Keep in mind that $R_l \simeq R_{l,\,\text{Born}}$ only when $R_l \ll 1$.

4.6.3 Longitudinal reflection from Goldstone Equivalence

In the main text we described the theory of a massive vector in eqs. (4.7) and (4.13) in terms of the Proca Lagrangian, featuring three degrees of freedom for the three physical polarizations of a massive spin-1 particle. However, this is often understood as a particular choice of gauge, after gauge redundancy is restored via $V_\mu \longrightarrow V_\mu - \partial_\mu \theta$. Although $\theta = 0$ (unitary gauge) is naively simplest, often it is convenient to keep the 'Goldstone' θ. The Goldstone Equivalence Theorem (GET) states that in the relativistic limit $\omega \gg m$ correct amplitudes can be obtained by identifying the physical

longitudinal vector with the scalar θ, with an error of order $\mathcal{O}\left(m^2/\omega^2\right)$. Using the usual gauge-fixing parameter ξ, the theory is described by

$$\mathcal{L} = -\frac{1}{4}F^{\mu\nu}F_{\mu\nu} + \frac{1}{2}m_V^2(z)(V_\mu - \partial_\mu\theta)^2 - \frac{1}{2\xi}\left(\partial_\mu V^\mu + m^2\xi\theta\right)^2 \ . \tag{4.93}$$

Proceeding with the equation of motion for θ:

$$\partial_\mu\left(m_V^2(z)\partial^\mu\theta\right) + \xi m^4\theta = 0 \ , \tag{4.94}$$

where we have neglected mixing with V^μ in order to test the spirit of the GET in our context. Working in the step function limit, the scattering solution is simple for $z \neq 0$:

$$\theta = e^{-i\omega t}\begin{cases} e^{ik_z} + r\ e^{-ik_z}, & z < 0 \\ t\ e^{i\tilde{k}_z}, & z > 0 \end{cases} , \tag{4.95}$$

$$k_z = \sqrt{\omega^2 - \xi m^2} \ , \quad \tilde{k}_z = \sqrt{\omega^2 - \xi m^4/\tilde{m}^2} \ , \tag{4.96}$$

and need only be supplemented by the matching conditions:

$$m_V^2(z)\partial_z\theta \qquad \text{and} \qquad \theta \qquad \text{are continuous at } z = 0 \ , \tag{4.97}$$

derived by integrating eq. (4.94) once and twice respectively. A little algebra gives the reflection probability as

$$R = |r|^2 = \left(\frac{\tilde{k}_z\tilde{m}^2 - k_z m^2}{\tilde{k}_z\tilde{m}^2 + k_z m^2}\right)^2 \xrightarrow{\omega \gg m,\tilde{m}} \left(\frac{\tilde{m}^2 - m^2}{\tilde{m}^2 + m^2}\right)^2 + \mathcal{O}\left(\tilde{m}^2/\omega^2\right) \tag{4.98}$$

which is ξ (gauge) independent and matches the leading order result derived in the main text eq. (4.26) consistent with the spirit of the GET. This result suggests that the enhanced reflection of the inter-relativistic limit described in this work might fundamentally be a property of Nambu-Goldstone bosons more generally, a topic that we will return to in future work.

4.7 Summary and discussion

In this chapter, we have discussed a new physical effect that can affect the evolution of cosmological vacuum bubbles expanding against a population of phase-dependent massive dark photons, with a special focus on the case where the dark photons furnish the dark matter. Namely, the existence of a transient relativistic regime, for sufficiently thin walls, characterized by a constant reflection probability of longitudinal

dark photons. The reflection of longitudinal modes creates a pressure on the expanding interface that features a characteristic non-monotonic dependence on the γ-factor of the bubble wall, reaching a peak at intermediate values of γ that we have dubbed Maximum Dynamic Pressure. The existence of a MDP that exceeds the asymptotic value of the pressure in the ultra-relativistic limit can make it much harder for bubble walls to become run-away, even in the absence of a thermal plasma that interacts with the wall background.

Our work opens a number of avenues for future exploration. In phase transitions where bubble walls reach an equilibrium regime as a result of this effect, the later evolution of the reflected dark photons could modify the features of the resulting gravitational wave signal and, in some cases, lead to an observable contribution to $\Delta N_{\rm eff}$ if the reflected dark photons remain relativistic until late times. As discussed in section 4.4 (specially 4.4.3), the extent to which this happens depends on a variety of considerations, most importantly on whether the sector undergoing vacuum decay is cold or, instead, is in thermal equilibrium with the primordial plasma surrounding the expanding bubbles. Understanding more generally the possible implications of the dark radiation for these two broad classes of models is clearly an important topic that deserves further attention.

Moreover, although we have focused exclusively on the case of phase-dependent massive dark photons, it is possible that the phenomenon of MDP on expanding bubble walls could be realized in scenarios beyond this example. Given the impact this can have on the dynamics of bubble walls, which in turn largely determine the features of the resulting gravitational wave signal, this is an important question worthy of further investigation.

Chapter 5

Conclusions

One of the most striking features of our current, most compelling picture of physics at the highest energy scales is the existence of vast landscapes of countless vacua with different infrared physics, all theoretically realizable, with some subset anthropically favorable. By contrast, the laws of nature inferred so far and codified in the Standard Model of particle physics, despite all their complexity and apparently arbitrary features, imply a unique vacuum, to the best of our knowledge. Furthermore, the uniqueness of the vacuum persists at all temperatures, with the QCD and Electroweak 'phase transitions' now established as smooth crossovers. These facts are particularly interesting in light of conjectures regarding obstructions to having positive energy vacua, as described in chapters 1 and 2.

In this thesis, I explored aspects of this contrast. In chapters 2 and 3, I defined and studied regions of the 'Standard Model landscape,' allowing for SM input parameters to vary in the neighborhood of their experimentally determined values. I explored whether these neighboring worlds were characterized by the presence of positive energy meta-stable vacua or not. Non-surprisingly, QCD dynamics play a central role in this story. I mapped the parameter space where meta-stable states exist as a function of Yukawa couplings and the vacuum angle $\overline{\theta}$. These states typically exist more easily in the limit of (flavor) global symmetries being restored and/or when $\overline{\theta}$ is increased. The Higgs hierarchy problem was also examined in this context. I described the structure of the SM in the two natural limits of a large mass term $m_H^2 \longrightarrow \pm\infty$. In one case, the IR of the SM becomes a pure gauge theory, and we find that the presence of meta-stable states is a question that requires future dedicated lattice studies. In the other case, progress can be made by the use of chiral perturbation theory, and I classified most (possibly all) critical points of the non-trivial 35-'pion' potential. There, the vacuum appears to be unique, although the current proof does not completely rule out a more complex class of critical points. Moreover, several effects remain to

be studied which can very plausibly lead to new vacua. These possible loopholes are left for future work.

Back in our own world, although we currently have no evidence for meta-stable vacua, it is possible that a future beyond-the-SM discovery will be made to this effect, as discussed in chapters 1 and 3. The fast development of gravitational wave detectors opens up the possibility of measuring the faint stochastic relic of past vacuum transitions during a first-order phase transition. This gravitational wave signal, along with all other phenomenological consequences of such violent out-of-equilibrium events, is strongly dependent on whether interactions between the bubble walls and the surrounding matter result in a terminal expansion velocity or not. In chapter 4, I showed that longitudinally polarized vectors and Nambu-Goldstone bosons can have uniquely strong reflective properties at leading order when scattering off such domain walls and explored the consequences for phase transitions, finding that they may easily dominate friction. I also showed how this special property generally leads to the reflected particles gaining energy to the extent that they may give a strong dark radiation signal and form a relativistic relic background even today. Fully investigating the physics of first order phase transitions is important to be able to make predictions and discover complementary signals. This is a field still largely under investigation, with much interesting physics still to be discovered.

Bibliography

[1] Valery A. Rubakov and Dmitry S. Gorbunov. *Introduction to the Theory of the Early Universe: Hot big bang theory.* World Scientific, Singapore, 2017.

[2] C. S. Wu, E. Ambler, R. W. Hayward, D. D. Hoppes, and R. P. Hudson. Experimental Test Of Parity Conservation In Beta Decay. *Phys. Rev.*, 105:1413–1414, 1957.

[3] Adam Falkowski and Riccardo Rattazzi. Which EFT. *JHEP*, 10:255, 2019.

[4] Pankaj Agrawal, Debashis Saha, Ling-Xiao Xu, Jiang-Hao Yu, and C. P. Yuan. Determining the shape of the Higgs potential at future colliders. *Phys. Rev. D*, 101(7):075023, 2020.

[5] Gauthier Durieux, Matthew McCullough, and Ennio Salvioni. Charting the Higgs self-coupling boundaries. *JHEP*, 12:148, 2022.

[6] R. L. Workman et al. Review of Particle Physics. *PTEP*, 2022:083C01, 2022.

[7] M. Cepeda et al. Report from Working Group 2: Higgs Physics at the HL-LHC and HE-LHC. *CERN Yellow Rep. Monogr.*, 7:221–584, 2019.

[8] Wojciech Bizoń, Ulrich Haisch, and Luca Rottoli. Constraints on the quartic Higgs self-coupling from double-Higgs production at future hadron colliders. *JHEP*, 10:267, 2019.

[9] Dario Buttazzo, Giuseppe Degrassi, Pier Paolo Giardino, Gian F. Giudice, Filippo Sala, Alberto Salvio, and Alessandro Strumia. Investigating the near-criticality of the Higgs boson. *JHEP*, 12:089, 2013.

[10] Shahida Dar. The Neutron EDM in the SM: A Review. 8 2000.

[11] R.P. Feynman, R.B. Leighton, M. Sands, and EM Hafner. *The Feynman Lectures on Physics; Vol. I*, volume 33. AAPT, 1965.

[12] S. Weinberg. *Gravitation and cosmology.* John Wiley and Sons, New York, 1972.

[13] D. Lovelock. The Einstein tensor and its generalizations. *J. Math. Phys.*, 12:498–501, 1971.

[14] Lars Husdal. On Effective Degrees of Freedom in the Early Universe. *Galaxies*, 4(4):78, 2016.

[15] C. W. Misner, K. S. Thorne, and J. A. Wheeler. *Gravitation.* 1973.

[16] M. Tanabashi et al. Review of Particle Physics. *Phys. Rev. D*, 98(3):030001, 2018.

[17] N. Aghanim et al. Planck 2018 results. VI. Cosmological parameters. *Astron. Astrophys.*, 641:A6, 2020.

[18] Andrei D. Linde. *Particle physics and inflationary cosmology*, volume 5. 1990.

[19] Dmitry S. Gorbunov and Valery A. Rubakov. *Introduction to the theory of the early universe: Cosmological perturbations and inflationary theory.* 2011.

[20] Mariano Quiros. Finite temperature field theory and phase transitions. In *ICTP Summer School in High-Energy Physics and Cosmology*, pages 187–259, 1 1999.

[21] D A Kirzhnits and A D Linde. Macroscopic consequences of the weinberg model. *Phys. Lett. 42B: No. 4, 471-4(25 Dec 1972).*, 1 1972.

[22] Steven Weinberg. Gauge and global symmetries at high temperature. *Phys. Rev. D*, 9:3357–3378, Jun 1974.

[23] Edward Witten. Cosmic Separation of Phases. *Phys. Rev. D*, 30:272–285, 1984.

[24] Claudio Bonati, Massimo D'Elia, Philippe de Forcrand, Owe Philipsen, and Francesco Sanfilippo. The chiral phase transition for two-flavour QCD at imaginary and zero chemical potential. *PoS*, LATTICE2013:219, 2014.

[25] M. Laine and K. Rummukainen. What's new with the electroweak phase transition? *Nucl. Phys. B Proc. Suppl.*, 73:180–185, 1999.

[26] Giuseppe Degrassi, Stefano Di Vita, Joan Elias-Miro, Jose R. Espinosa, Gian F. Giudice, Gino Isidori, and Alessandro Strumia. Higgs mass and vacuum stability in the Standard Model at NNLO. *JHEP*, 08:098, 2012.

[27] Christophe Grojean, Geraldine Servant, and James D. Wells. First-order electroweak phase transition in the standard model with a low cutoff. *Phys. Rev. D*, 71:036001, 2005.

[28] Cedric Delaunay, Christophe Grojean, and James D. Wells. Dynamics of Non-renormalizable Electroweak Symmetry Breaking. *JHEP*, 04:029, 2008.

[29] John Ellis, Marek Lewicki, and Jos Miguel No. On the Maximal Strength of a First-Order Electroweak Phase Transition and its Gravitational Wave Signal. 2018. [JCAP1904,003(2019)].

[30] John Ellis, Marek Lewicki, Jos Miguel No, and Ville Vaskonen. Gravitational wave energy budget in strongly supercooled phase transitions. *JCAP*, 1906(06):024, 2019.

[31] Sebastian Bruggisser, Benedict Von Harling, Oleksii Matsedonskyi, and Géraldine Servant. Baryon Asymmetry from a Composite Higgs Boson. *Phys. Rev. Lett.*, 121(13):131801, 2018.

[32] Jose Ramon Espinosa and Mariano Quiros. Novel Effects in Electroweak Breaking from a Hidden Sector. *Phys. Rev. D*, 76:076004, 2007.

[33] Ankit Beniwal, Marek Lewicki, James D. Wells, Martin White, and Anthony G. Williams. Gravitational wave, collider and dark matter signals from a scalar singlet electroweak baryogenesis. *JHEP*, 08:108, 2017.

[34] Vernon Barger, Paul Langacker, Mathew McCaskey, Michael J. Ramsey-Musolf, and Gabe Shaughnessy. LHC Phenomenology of an Extended Standard Model with a Real Scalar Singlet. *Phys. Rev. D*, 77:035005, 2008.

[35] Jose R. Espinosa, Thomas Konstandin, and Francesco Riva. Strong Electroweak Phase Transitions in the Standard Model with a Singlet. *Nucl. Phys. B*, 854:592–630, 2012.

[36] Jonathan Kozaczuk, Michael J. Ramsey-Musolf, and Jessie Shelton. Exotic Higgs boson decays and the electroweak phase transition. *Phys. Rev. D*, 101(11):115035, 2020.

[37] Gowri Kurup and Maxim Perelstein. Dynamics of Electroweak Phase Transition In Singlet-Scalar Extension of the Standard Model. *Phys. Rev. D*, 96(1):015036, 2017.

[38] Aleksandr Azatov, Giulio Barni, Sabyasachi Chakraborty, Miguel Vanvlasselaer, and Wen Yin. Ultra-relativistic bubbles from the simplest Higgs portal and their cosmological consequences. *JHEP*, 10:017, 2022.

[39] Jose R. Espinosa, Thomas Konstandin, Jose M. No, and Geraldine Servant. Energy Budget of Cosmological First-order Phase Transitions. *JCAP*, 06:028, 2010.

[40] Ryusuke Jinno and Masahiro Takimoto. Gravitational waves from bubble collisions: An analytic derivation. *Phys. Rev. D*, 95(2):024009, 2017.

[41] Malcolm Fairbairn, Edward Hardy, and Alastair Wickens. Hearing without seeing: gravitational waves from hot and cold hidden sectors. *JHEP*, 07:044, 2019.

[42] Moritz Breitbach, Joachim Kopp, Eric Madge, Toby Opferkuch, and Pedro Schwaller. Dark, Cold, and Noisy: Constraining Secluded Hidden Sectors with Gravitational Waves. *JCAP*, 07:007, 2019.

[43] Michael S. Turner, Erick J. Weinberg, and Lawrence M. Widrow. Bubble nucleation in first order inflation and other cosmological phase transitions. *Phys. Rev. D*, 46:2384–2403, 1992.

[44] David J. Gross, Jeffrey A. Harvey, Emil J. Martinec, and Ryan Rohm. Heterotic String Theory. 1. The Free Heterotic String. *Nucl. Phys. B*, 256:253, 1985.

[45] Cumrun Vafa. The String landscape and the swampland. 9 2005.

[46] T. Daniel Brennan, Federico Carta, and Cumrun Vafa. The String Landscape, the Swampland, and the Missing Corner. *PoS*, TASI2017:015, 2017.

[47] Eran Palti. The Swampland: Introduction and Review. *Fortsch. Phys.*, 67(6):1900037, 2019.

[48] J. Polchinski. *String theory. Vol. 1: An introduction to the bosonic string*. Cambridge Monographs on Mathematical Physics. Cambridge University Press, 12 2007.

[49] J. Polchinski. *String theory. Vol. 2: Superstring theory and beyond*. Cambridge Monographs on Mathematical Physics. Cambridge University Press, 12 2007.

[50] Tom Banks and Lance J. Dixon. Constraints on String Vacua with Space-Time Supersymmetry. *Nucl. Phys. B*, 307:93–108, 1988.

[51] Daniel Harlow and Hirosi Ooguri. Symmetries in quantum field theory and quantum gravity. *Commun. Math. Phys.*, 383(3):1669–1804, 2021.

[52] Tristan Daus, Arthur Hebecker, Sascha Leonhardt, and John March-Russell. Towards a Swampland Global Symmetry Conjecture using Weak Gravity. 2020.

[53] Nima Arkani-Hamed, Lubos Motl, Alberto Nicolis, and Cumrun Vafa. The String landscape, black holes and gravity as the weakest force. *JHEP*, 06:060, 2007.

[54] Georges Obied, Hirosi Ooguri, Lev Spodyneiko, and Cumrun Vafa. De Sitter Space and the Swampland. 2018.

[55] David Andriot. On the de Sitter swampland criterion. *Phys. Lett. B*, 785:570–573, 2018.

[56] Sumit K. Garg and Chethan Krishnan. Bounds on Slow Roll and the de Sitter Swampland. *JHEP*, 11:075, 2019.

[57] Hirosi Ooguri, Eran Palti, Gary Shiu, and Cumrun Vafa. Distance and de Sitter Conjectures on the Swampland. *Phys. Lett.*, B788:180–184, 2019.

[58] Prateek Agrawal, Georges Obied, Paul J. Steinhardt, and Cumrun Vafa. On the Cosmological Implications of the String Swampland. *Phys. Lett.*, B784:271–276, 2018.

[59] Alek Bedroya and Cumrun Vafa. Trans-planckian censorship and the swampland, 2019.

[60] Arthur Hebecker and Pablo Soler. The Weak Gravity Conjecture and the Axionic Black Hole Paradox. *JHEP*, 09:036, 2017.

[61] Edward Witten. Large N Chiral Dynamics. *Annals Phys.*, 128:363, 1980.

[62] Michael Creutz. Quark masses and chiral symmetry. *Phys. Rev.*, D52:2951–2959, 1995.

[63] Andrei V. Smilga. QCD at theta similar to pi. *Phys. Rev.*, D59:114021, 1999.

[64] Roger F. Dashen. Some features of chiral symmetry breaking. *Phys. Rev.*, D3:1879–1889, 1971.

[65] L. F. Abbott. A Mechanism for Reducing the Value of the Cosmological Constant. *Phys. Lett.*, 150B:427–430, 1985.

[66] J. David Brown and C. Teitelboim. Neutralization of the Cosmological Constant by Membrane Creation. *Nucl. Phys.*, B297:787–836, 1988.

[67] Raphael Bousso and Joseph Polchinski. Quantization of four form fluxes and dynamical neutralization of the cosmological constant. *JHEP*, 06:006, 2000.

[68] Jonathan L. Feng, John March-Russell, Savdeep Sethi, and Frank Wilczek. Saltatory relaxation of the cosmological constant. *Nucl. Phys.*, B602:307–328, 2001.

[69] Peter W. Graham, David E. Kaplan, and Surjeet Rajendran. Relaxation of the Cosmological Constant. *Phys. Rev.*, D100(1):015048, 2019.

[70] A. Deur, S. J. Brodsky, and G. F. de Teramond. Determination of $\Lambda_{\overline{MS}}$ at five loops from holographic QCD. *J. Phys. G*, 44(10):105005, 2017.

[71] Edward Hardy and Susha Parameswaran. Thermal Dark Energy. *Phys. Rev.*, D101(2):023503, 2020.

[72] R. D. Peccei and Helen R. Quinn. CP Conservation in the Presence of Instantons. *Phys. Rev. Lett.*, 38:1440–1443, 1977. [,328(1977)].

[73] Steven Weinberg. A new light boson? *Phys. Rev. Lett.*, 40:223–226, Jan 1978.

[74] F. Wilczek. Problem of strong p and t invariance in the presence of instantons. *Phys. Rev. Lett.*, 40:279–282, Jan 1978.

[75] Ann E. Nelson. Naturally Weak CP Violation. *Phys. Lett.*, 136B:387–391, 1984.

[76] Stephen M. Barr. Solving the Strong CP Problem Without the Peccei-Quinn Symmetry. *Phys. Rev. Lett.*, 53:329, 1984.

[77] K. S. Babu and Rabindra N. Mohapatra. A Solution to the Strong CP Problem Without an Axion. *Phys. Rev.*, D41:1286, 1990.

[78] Stephen M. Barr, D. Chang, and G. Senjanovic. Strong CP problem and parity. *Phys. Rev. Lett.*, 67:2765–2768, 1991.

[79] K. S. Babu, Bhaskar Dutta, and R. N. Mohapatra. Solving the strong CP and the SUSY phase problems with parity symmetry. *Phys. Rev.*, D65:016005, 2002.

[80] Sergei Dubovsky and Victor Gorbenko. Black Hole Portal into Hidden Valleys. *Phys. Rev.*, D83:106002, 2011.

[81] Hirosi Ooguri and Cumrun Vafa. On the geometry of the string landscape and the swampland. *Nuclear Physics B*, 766(1-3):2133, Mar 2007.

[82] Sylvain Fichet and Prashant Saraswat. Approximate Symmetries and Gravity. *JHEP*, 01:088, 2020.

[83] Sourish Dutta and Robert J. Scherrer. Hilltop quintessence. *Physical Review D*, 78(12), Dec 2008.

[84] Edward Witten. Theta dependence in the large N limit of four-dimensional gauge theories. *Phys. Rev. Lett.*, 81:2862–2865, 1998.

[85] Mikhail A. Shifman. Domain walls and decay rate of the excited vacua in the large N Yang-Mills theory. *Phys. Rev.*, D59:021501, 1999.

[86] Michael Teper. Large N. *PoS*, LATTICE2008:022, 2008.

[87] Gregory Gabadadze and M. Shifman. QCD vacuum and axions: What's happening? *Int. J. Mod. Phys.*, A17:3689–3728, 2002. [,521(2002)].

[88] Edward Witten. Current Algebra Theorems for the U(1) Goldstone Boson. *Nucl. Phys. B*, 156:269–283, 1979.

[89] G. Veneziano. U(1) Without Instantons. *Nucl. Phys. B*, 159:213–224, 1979.

[90] Luigi Del Debbio, Leonardo Giusti, and Claudio Pica. Topological susceptibility in su(3) gauge theory. *Physical Review Letters*, 94(3), Jan 2005.

[91] Michael Dine, Patrick Draper, Laurel Stephenson-Haskins, and Di Xu. θ and the η' in Large N Supersymmetric QCD. *JHEP*, 05:122, 2017.

[92] Luigi Del Debbio, Gian Mario Manca, Haralambos Panagopoulos, Apostolos Skouroupathis, and Ettore Vicari. Theta-dependence of the spectrum of SU(N) gauge theories. *JHEP*, 06:005, 2006.

[93] Claudio Bonati, Massimo D'Elia, Paolo Rossi, and Ettore Vicari. θ dependence of 4D $SU(N)$ gauge theories in the large-N limit. *Phys. Rev.*, D94(8):085017, 2016.

[94] Kyle Aitken, Aleksey Cherman, and Mithat Unsal. Vacuum structure of Yang-Mills theory as a function of theta. *JHEP*, 09:030, 2018.

[95] Igor E. Halperin and Ariel Zhitnitsky. Anomalous effective Lagrangian and theta dependence in QCD at finite N(c). *Phys. Rev. Lett.*, 81:4071–4074, 1998.

[96] Clifford Cheung and Grant N. Remmen. Naturalness and the Weak Gravity Conjecture. *Phys. Rev. Lett.*, 113:051601, 2014.

[97] Nathaniel Craig, Isabel Garcia Garcia, and Seth Koren. The Weak Scale from Weak Gravity. *JHEP*, 09:081, 2019.

[98] S. Weinberg. Implications of dynamical symmetry breaking: An addendum. *Phys. Rev. D*, 19:1277–1280, Feb 1979.

[99] Leonard Susskind. Dynamics of spontaneous symmetry breaking in the weinberg-salam theory. *Phys. Rev. D*, 20:2619–2625, Nov 1979.

[100] S. Chadha and Michael E. Peskin. Implications of Chiral Dynamics in Theories of Technicolor. 1. Elementary Couplings. *Nucl. Phys. B*, 185:61–88, 1981.

[101] S. Chadha and Michael E. Peskin. Implications of Chiral Dynamics in Theories of Technicolor. 2. The Mass of the P^+. *Nucl. Phys. B*, 187:541–562, 1981.

[102] John Preskill. Subgroup Alignment in Hypercolor Theories. *Nucl. Phys. B*, 177:21–59, 1981.

[103] Stuart Samuel. The Standard model in its other phase. *Nucl. Phys. B*, 597:70–88, 2001.

[104] Chris Quigg and Robert Shrock. Gedanken Worlds without Higgs: QCD-Induced Electroweak Symmetry Breaking. *Phys. Rev. D*, 79:096002, 2009.

[105] Steven Weinberg. Implications of Dynamical Symmetry Breaking. *Phys. Rev. D*, 13:974–996, 1976. [Addendum: Phys.Rev.D 19, 1277–1280 (1979)].

[106] Roberto Contino. The Higgs as a Composite Nambu-Goldstone Boson. In *Theoretical Advanced Study Institute in Elementary Particle Physics: Physics of the Large and the Small*, pages 235–306, 2011.

[107] Arkady Vainshtein. Perturbative and nonperturbative renormalization of anomalous quark triangles. *Phys. Lett. B*, 569:187–193, 2003.

[108] Nicolas Bourbaki. *Elements of mathematics.* Hermann, Paris, 1966.

[109] A. J. MacFarlane, Anthony Sudbery, and P. H. Weisz. On Gell-Mann's lambda-matrices, d and f tensors, octets, and parametrizations of SU(3). *Commun. Math. Phys.*, 11:77–90, 1968.

[110] C. J. Hogan. Gravitational radiation from cosmological phase transitions. *Mon. Not. Roy. Astron. Soc.*, 218:629–636, 1986.

[111] Arthur Kosowsky, Michael S. Turner, and Richard Watkins. Gravitational radiation from colliding vacuum bubbles. *Phys. Rev. D*, 45:4514–4535, 1992.

[112] Arthur Kosowsky, Michael S. Turner, and Richard Watkins. Gravitational waves from first order cosmological phase transitions. *Phys. Rev. Lett.*, 69:2026–2029, 1992.

[113] Marc Kamionkowski, Arthur Kosowsky, and Michael S. Turner. Gravitational radiation from first order phase transitions. *Phys. Rev. D*, 49:2837–2851, 1994.

[114] Chiara Caprini et al. Science with the space-based interferometer eLISA. II: Gravitational waves from cosmological phase transitions. *JCAP*, 04:001, 2016.

[115] Chiara Caprini et al. Detecting gravitational waves from cosmological phase transitions with LISA: an update. *JCAP*, 03:024, 2020.

[116] Pedro Schwaller. Gravitational Waves from a Dark Phase Transition. *Phys. Rev. Lett.*, 115(18):181101, 2015.

[117] Alexander J. Helmboldt, Jisuke Kubo, and Susan van der Woude. Observational prospects for gravitational waves from hidden or dark chiral phase transitions. *Phys. Rev. D*, 100(5):055025, 2019.

[118] Ryusuke Jinno, Hyeonseok Seong, Masahiro Takimoto, and Choong Min Um. Gravitational waves from first-order phase transitions: Ultra-supercooled transitions and the fate of relativistic shocks. *JCAP*, 10:033, 2019.

[119] Aleksandr Azatov, Daniele Barducci, and Francesco Sgarlata. Gravitational traces of broken gauge symmetries. *JCAP*, 07:027, 2020.

[120] Yuichiro Nakai, Motoo Suzuki, Fuminobu Takahashi, and Masaki Yamada. Gravitational Waves and Dark Radiation from Dark Phase Transition: Connecting NANOGrav Pulsar Timing Data and Hubble Tension. *Phys. Lett. B*, 816:136238, 2021.

[121] James Halverson, Cody Long, Anindita Maiti, Brent Nelson, and Gustavo Salinas. Gravitational waves from dark Yang-Mills sectors. *JHEP*, 05:154, 2021.

[122] Fei Huang, Veronica Sanz, Jing Shu, and Xiao Xue. LIGO as a probe of dark sectors. *Phys. Rev. D*, 104(9):095001, 2021.

[123] James B. Dent, Bhaskar Dutta, Sumit Ghosh, Jason Kumar, and Jack Runburg. Sensitivity to dark sector scales from gravitational wave signatures. *JHEP*, 08:300, 2022.

[124] Ryusuke Jinno, Bibhushan Shakya, and Jorinde van de Vis. Gravitational Waves from Feebly Interacting Particles in a First Order Phase Transition. 11 2022.

[125] Sidney R. Coleman. The Fate of the False Vacuum. 1. Semiclassical Theory. *Phys. Rev. D*, 15:2929–2936, 1977. [Erratum: Phys.Rev.D 16, 1248 (1977)].

[126] Stephan J. Huber and Thomas Konstandin. Gravitational Wave Production by Collisions: More Bubbles. *JCAP*, 09:022, 2008.

[127] Mark Hindmarsh, Stephan J. Huber, Kari Rummukainen, and David J. Weir. Numerical simulations of acoustically generated gravitational waves at a first order phase transition. *Phys. Rev. D*, 92(12):123009, 2015.

[128] Mark Hindmarsh. Sound shell model for acoustic gravitational wave production at a first-order phase transition in the early Universe. *Phys. Rev. Lett.*, 120(7):071301, 2018.

[129] Mark Hindmarsh, Stephan J. Huber, Kari Rummukainen, and David J. Weir. Shape of the acoustic gravitational wave power spectrum from a first order phase transition. *Phys. Rev. D*, 96(10):103520, 2017. [Erratum: Phys.Rev.D 101, 089902 (2020)].

[130] Mark Hindmarsh and Mulham Hijazi. Gravitational waves from first order cosmological phase transitions in the Sound Shell Model. *JCAP*, 12:062, 2019.

[131] Chiara Caprini, Ruth Durrer, Thomas Konstandin, and Geraldine Servant. General Properties of the Gravitational Wave Spectrum from Phase Transitions. *Phys. Rev. D*, 79:083519, 2009.

[132] Gabriela Barenboim and Wan-Il Park. Gravitational waves from first order phase transitions as a probe of an early matter domination era and its inverse problem. *Phys. Lett. B*, 759:430–438, 2016.

[133] Anson Hook, Gustavo Marques-Tavares, and Davide Racco. Causal gravitational waves as a probe of free streaming particles and the expansion of the Universe. *JHEP*, 02:117, 2021.

[134] Steven Weinberg. Damping of tensor modes in cosmology. *Phys. Rev. D*, 69:023503, 2004.

[135] David E. Morrissey and Michael J. Ramsey-Musolf. Electroweak baryogenesis. *New J. Phys.*, 14:125003, 2012.

[136] Hind Al Ali et al. The muon Smasher's guide. *Rept. Prog. Phys.*, 85(8):084201, 2022.

[137] Z. Arzoumanian et al. The NANOGrav 11-year Data Set: Pulsar-timing Constraints On The Stochastic Gravitational-wave Background. *Astrophys. J.*, 859(1):47, 2018.

[138] L. Lentati et al. European Pulsar Timing Array Limits On An Isotropic Stochastic Gravitational-Wave Background. *Mon. Not. Roy. Astron. Soc.*, 453(3):2576–2598, 2015.

[139] Peter Brockway Arnold. One loop fluctuation - dissipation formula for bubble wall velocity. *Phys. Rev. D*, 48:1539–1545, 1993.

[140] Guy D. Moore and Tomislav Prokopec. How fast can the wall move? A Study of the electroweak phase transition dynamics. *Phys. Rev. D*, 52:7182–7204, 1995.

[141] N. Turok. Electroweak bubbles: Nucleation and growth. *Phys. Rev. Lett.*, 68:1803–1806, 1992.

[142] Michael Dine, Robert G. Leigh, Patrick Y. Huet, Andrei D. Linde, and Dmitri A. Linde. Towards the theory of the electroweak phase transition. *Phys. Rev. D*, 46:550–571, 1992.

[143] Bao-Hua Liu, Larry D. McLerran, and Neil Turok. Bubble nucleation and growth at a baryon number producing electroweak phase transition. *Phys. Rev. D*, 46:2668–2688, 1992.

[144] Guy D. Moore and Tomislav Prokopec. Bubble wall velocity in a first order electroweak phase transition. *Phys. Rev. Lett.*, 75:777–780, 1995.

[145] Dietrich Bodeker and Guy D. Moore. Can electroweak bubble walls run away? *JCAP*, 05:009, 2009.

[146] Leonardo Leitao and Ariel Megevand. Hydrodynamics of ultra-relativistic bubble walls. *Nucl. Phys. B*, 905:45–72, 2016.

[147] Dietrich Bodeker and Guy D. Moore. Electroweak Bubble Wall Speed Limit. *JCAP*, 05:025, 2017.

[148] Aleksandr Azatov and Miguel Vanvlasselaer. Bubble wall velocity: heavy physics effects. *JCAP*, 01:058, 2021.

[149] Wen-Yuan Ai, Bjorn Garbrecht, and Carlos Tamarit. Bubble wall velocities in local equilibrium. *JCAP*, 03(03):015, 2022.

[150] Marc Barroso Mancha, Tomislav Prokopec, and Bogumiła Świeżewska. Field-theoretic derivation of bubble-wall force. *Journal of High Energy Physics*, 2021(1), jan 2021.

[151] Yago Bea, Jorge Casalderrey-Solana, Thanasis Giannakopoulos, David Mateos, Mikel Sanchez-Garitaonandia, and Miguel Zilhão. Bubble wall velocity from holography. *Phys. Rev. D*, 104(12):L121903, 2021.

[152] Yann Gouttenoire, Ryusuke Jinno, and Filippo Sala. Friction pressure on relativistic bubble walls. *JHEP*, 05:004, 2022.

[153] Benoit Laurent and James M. Cline. First principles determination of bubble wall velocity. *Phys. Rev. D*, 106(2):023501, 2022.

[154] Stefania De Curtis, Luigi Delle Rose, Andrea Guiggiani, Ángel Gil Muyor, and Giuliano Panico. Bubble wall dynamics at the electroweak phase transition. *JHEP*, 03:163, 2022.

[155] Wayne Hu, Rennan Barkana, and Andrei Gruzinov. Cold and fuzzy dark matter. *Phys. Rev. Lett.*, 85:1158–1161, 2000.

[156] Lam Hui, Jeremiah P. Ostriker, Scott Tremaine, and Edward Witten. Ultralight scalars as cosmological dark matter. *Phys. Rev. D*, 95(4):043541, 2017.

[157] Ann E. Nelson and Jakub Scholtz. Dark Light, Dark Matter and the Misalignment Mechanism. *Phys. Rev. D*, 84:103501, 2011.

[158] Paola Arias, Davide Cadamuro, Mark Goodsell, Joerg Jaeckel, Javier Redondo, and Andreas Ringwald. WISPy Cold Dark Matter. *JCAP*, 06:013, 2012.

[159] Peter W. Graham, Jeremy Mardon, and Surjeet Rajendran. Vector dark matter from inflationary fluctuations. *Physical Review D*, 93(10), may 2016.

[160] Prateek Agrawal, Naoya Kitajima, Matthew Reece, Toyokazu Sekiguchi, and Fuminobu Takahashi. Relic Abundance of Dark Photon Dark Matter. *Phys. Lett. B*, 801:135136, 2020.

[161] Oleg Lebedev, Hyun Min Lee, and Yann Mambrini. Vector Higgs-portal dark matter and the invisible Higgs. *Phys. Lett. B*, 707:570–576, 2012.

[162] Glennys R. Farrar and John W. McIntosh, Jr. Scattering from a domain wall in a spontaneously broken gauge theory. *Phys. Rev. D*, 51:5889–5904, 1995.

[163] Kevork N. Abazajian, *et al.* CMB-S4 Science Book, First Edition, 2016.

[164] Peter Ade et al. The Simons Observatory: Science goals and forecasts. *JCAP*, 02:056, 2019.